



**GPS-DERIVED PRECIPITABLE WATER  
COMPARED WITH THE AIR FORCE  
WEATHER AGENCY'S MM5 MODEL  
OUTPUT**

THESIS

Patricia A. Vollmer, Captain, USAF

AFIT/GM/ENP/02M-11

**DEPARTMENT OF THE AIR FORCE  
AIR UNIVERSITY**

***AIR FORCE INSTITUTE OF TECHNOLOGY***

---

---

**Wright-Patterson Air Force Base, Ohio**

APPROVED FOR PUBLIC RELEASE; DISTRIBUTION UNLIMITED.

## Report Documentation Page

<b>Report Date</b> 26 Mar 02	<b>Report Type</b> Final	<b>Dates Covered (from... to)</b> Jun 2001 - Mar 2002
<b>Title and Subtitle</b> GPS-Derived Precipitable Water Copared with the Air Force Weather Agency's MM5 Model Output	<b>Contract Number</b>	
	<b>Grant Number</b>	
	<b>Program Element Number</b>	
<b>Author(s)</b> Capt Patricia A. Vollmer, USAF	<b>Project Number</b>	
	<b>Task Number</b>	
	<b>Work Unit Number</b>	
<b>Performing Organization Name(s) and Address(es)</b> Air Force Institute of Technology Graduate School of Engineering and Management (AFIT/EN) 2950 P Street, Bldg 640 WPAFB OH 45433-7765	<b>Performing Organization Report Number</b> AFIT/GM/ENP/02M-11	
<b>Sponsoring/Monitoring Agency Name(s) and Address(es)</b> AFWA/DNXT Attn: Bruce Telfeyan 301 Peacekeeper Dr. Offutt AFB NE	<b>Sponsor/Monitor's Acronym(s)</b>	
	<b>Sponsor/Monitor's Report Number(s)</b>	
<b>Distribution/Availability Statement</b> Approved for public release, distribution unlimited		
<b>Supplementary Notes</b> The original document contains color images.		

**Abstract**

Current moisture initialization sources lack the spatial and temporal resolution required for mesoscale moisture forecast accuracy critical for military operations. The Global Positioning System (GPS) satellite constellation provides an opportunity to extract accurate moisture observations based on the refraction of the GPS signal through the troposphere. GPS-derived precipitable water (PW) from two different research areas was independently compared with the Air Force Weather Agency's (AFWAs) MM5 PW model output. Results were concurrent with similar studies comparing GPS-derived PW with numerical weather models. The mean correlation in CONUS was 92.5%, while in Alaska it was 72.8%. Mean model biases were 1.22 mm in CONUS and 0.69 mm in Alaska. Mean RMSEs were 4.36 mm in CONUS and 2.76 mm in Alaska. In addition, comparisons were made between moist and dry locations, showing a 21.5% difference in correlation and a 17.8% difference in RMSE. The GPS network's superior temporal resolution captured the diurnal variations in PW, while the model consistently failed to take such variations into account as its forecast progressed. This seems it could be the largest source of error between the two data sets. A number of non-meteorological error sources exist that could impact use of GPS-derived PW in operational applications, such as terrain differences between the GPS receiver sites and the model interpolated heights. These error sources need to be further addressed prior to operational assimilation of this data into military weather models.

**Subject Terms**

Meteorology, Global Positioning System, Numerical Methods and Procedures, Satellites, Atmospheric Moisture Content

**Report Classification**

unclassified

**Classification of this page**

unclassified

**Classification of Abstract**

unclassified

**Limitation of Abstract**

UU

**Number of Pages**

108

The views expressed in this thesis are those of the author and do not reflect the official policy or position of the United States Air Force, Department of Defense, or the U. S. Government.

AFIT/GM/ENP/02M-11

GPS-DERIVED PRECIPITABLE WATER COMPARED WITH THE AIR FORCE  
WEATHER AGENCY'S MM5 MODEL OUTPUT

THESIS

Presented to the Faculty

Department of Engineering Physics

Graduate School of Engineering and Management

Air Force Institute of Technology

Air University

Air Education and Training Command

In Partial Fulfillment of the Requirements for the

Degree of Master of Science in Meteorology

Patricia A. Vollmer, BS

Captain, USAF

March 2002

APPROVED FOR PUBLIC RELEASE; DISTRIBUTION UNLIMITED.


GPS-DERIVED PRECIPITABLE WATER COMPARED WITH THE AIR FORCE  
WEATHER AGENCY'S MM5 MODEL OUTPUT

Patricia A. Vollmer, BS  
Captain, USAF

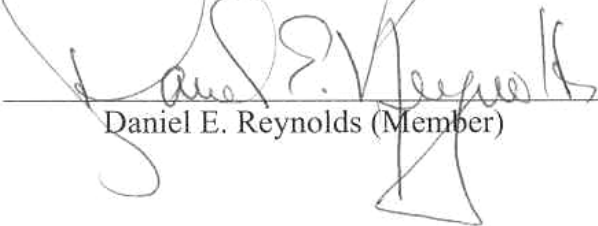
Approved:

  
\_\_\_\_\_  
Gary R. Huffines (Chairperson)

1 March 2002  
date

  
\_\_\_\_\_  
Michael K. Walters (Member)

1 March  
date

  
\_\_\_\_\_  
Daniel E. Reynolds (Member)

1 March  
date

## **Acknowledgements**

First and foremost, I would like to thank the members of my thesis committee, Major Gary Huffines, Lieutenant Colonel Michael Walters and Professor Dan Reynolds. You allowed me to pursue a new, unusual subject that was seemingly in left field. You deserve my thanks for your patience and understanding in my excitement over the many iterations of results, as well as for your continuing to challenge me throughout the thesis process. In addition, Major John Raquet and 2d Lieutenant David Garay from the Electrical Engineering Department receive my gratitude for their expertise in GPS navigation.

My appreciation goes out to the many members of the GPS meteorology community who spent hours educating me on GPS meteorology and then provided me valuable feedback on my results. Seth Gutman, Kirk Holub, and Sher Wagoner at the NOAA Forecast Systems Laboratory provided me with acres of information and access to their American data sets. Also, Jennifer Haase and Eric Calais from the Department of Atmospheric Sciences at Purdue University deserve thanks for courteously providing me feedback and insight into how to interpret my results.

Thanks go to those at the Air Force Weather Agency who took time from their busy real-world obligations to assist me with MM5-related issues. Of note are Captain Rob Swanson, Dr. Scott Applequist and Matthew Sittel.

The members of AFIT ENP GM-02M, especially those colleagues who were also doing MM5-related research, are in my debt for contributing to the free exchange of ideas, criticisms, and opinions that is an example of science at its best.

And finally, I'm eternally grateful to my wonderful husband who provided me valuable feedback even while working on this own Master's thesis. I'll never forget that Friday night when we sat at home on opposite ends of the couch and read each other's theses. He tolerated my constantly sitting in front of the computer, both in the weather lab and at home...as if a keyboard and mouse had grown out of my hands! Please know that it was only temporary.

## Table of Contents

	Page
Acknowledgements .....	iv
List of Figures .....	vii
List of Tables.....	ix
List of Tables.....	ix
Abstract .....	x
I. Introduction.....	1
1.1 Background .....	1
1.2 Problem Statement .....	4
1.3 Research Impact .....	5
1.4 Research Objective.....	6
1.5 Hypotheses .....	7
II. Literature Review .....	8
2.1 The Global Positioning System.....	8
2.2 Use of GPS for Meteorological Research .....	11
2.3 The Fifth-Generation Mesoscale Model .....	14
2.4 Using GPS Meteorology to Validate and Improve Forecast Models.....	17
III. Methodology .....	25
3.1 Data Collection.....	25
3.2 Sources of Error .....	27
3.3 Coding of Processing Programs.....	33
IV. Results and Discussion .....	39
4.1 CONUS .....	39
4.2 Alaska.....	57



V. Conclusions .....	65
5.1 CONUS Conclusions .....	66
5.2 Alaska Conclusions .....	67
5.3 Recommendations for Future Work .....	68
Bibliography .....	70
Appendix A: Geodetic Information .....	73
Appendix B: RAOB Geodetic Information .....	75
Appendix C: Location-Specific Statistics .....	76
Vita .....	95

## List of Figures

	Page
Figure 1. Schematic of the GPS Satellite Vehicle Constellation .....	8
Figure 2. Diagram of the Satellite Coverage Transposed on a Global Map Projection...	9
Figure 3. Visualization of How GPS Determines Precise Location .....	10
Figure 4. The American GPS Precipitable Water Receiver Network .....	26
Figure 5. Area of Influence of a GPS-Derived Precipitable Water Reading. ....	35
Figure 6. Area of Influence in MM5 Grid.....	35
Figure 7. NEXRAD Mosaic Image from 15 UTC 8 July 2001.....	40
Figure 8. NEXRAD Mosaic Image from 09 UTC 25 July 2001.....	41
Figure 9. NEXRAD Mosaic Image from 00 UTC 12 August 2001.....	41
Figure 10. NEXRAD Mosaic Image from 08 UTC 14 September 2001 .....	42
Figure 11. CONUS Domain-Wide Statistical Summaries. ....	43
Figure 12. Mean Correlation of Each GPS Receiver Location: CONUS 06 UTC Initialization, 06-Hour Forecast .....	45
Figure 13. Mean Bias of Each GPS Receiver Location: CONUS 06 UTC Initialization, 06-Hour Forecast.....	46
Figure 14. Mean Normalized RMSE of Each GPS Receiver Location: CONUS 06 UTC Initialization, 06 Hour Forecast.....	47
Figure 15. Mean Normalized Standard Deviation of Each GPS Receiver Location: CONUS 06 UTC Initialization, 06 Hour Forecast.....	48
Figure 16. Mean Correlation of Each GPS Receiver Location: CONUS 18 UTC Initialization, 06-Hour Forecast .....	49

Figure 17. Mean Bias of Each GPS Receiver Location: CONUS 18 UTC Initialization, 06-Hour Forecast.....	49
Figure 18. Mean Normalized RMSE of Each GPS Receiver Location: CONUS 18 UTC Initialization, 06-Hour Forecast .....	50
Figure 19. Mean Normalized Standard Deviation of Each GPS Receiver Location: CONUS 18 UTC Initialization, 06-Hour Forecast.....	51
Figure 20. Number of Observations Available for Calculating the 06 UTC Initialization, 06 Hour Forecast Statistics.....	52
Figure 21. Number of Observations Available for Calculating the 18 UTC Initialization, 06 Hour Forecast Statistics.....	52
Figure 22. Moist Sites vs. Dry Sites Statistical Summaries: CONUS 18 UTC Initialization, 06 Hour Forecast.....	53
Figure 23. Elevation Comparisons: CONUS 06 UTC Initialization, 06 Hour Forecast	54
Figure 24. GPS/RAOB Coastal vs. Inland Statistical Summaries .....	56
Figure 25. Representative Alaska IR Satellite Imagery from 12 UTC 19 July 2001.....	57
Figure 26. Alaska Domain-Wide Statistical Summaries.....	59
Figure 27. Alaska By-Location Statistical Summaries: 00 UTC Initialization, 06 Hour Forecast .....	61
Figure 28. Alaska By-Location Statistical Summaries: 12 UTC Initialization, 06 Hour Forecast .....	62

## List of Tables

	Page
Table 1. AFWA MM5 Physics Packages.....	16
Table 2. Sample GPS-MET Data from Bartlett, NH for 6 July 2001 .....	25
Table 3. Representation of Makes and Models of GPS Receivers .....	28
Table 4. Representation of Makes and Models of GPS Antennas .....	28
Table 5. Comparison of GPS Orbit Calculations Available in GPS-MET Processing..	30
Table 6. Available GPS Processing Software .....	31
Table 7. Sample RAOB-Based Precipitable Water for Charleston, SC.....	36
Table 8. Sample GPS vs. RAOB Comparison File for Slidell, LA.....	36
Table 9. Sample Output File for a 45-Hour Forecast Valid 8 July 2001 03 UTC .....	37
Table 10. Location-specific PW Data for Spokane, WA. ....	37
Table 11. Sample Statistical Summary by DTG .....	38
Table 12. Sample Statistical Summary File by Location.....	38
Table 13. Summary of GPS-RAOB Comparisons in CONUS .....	55
Table 14. Summary Statistics of Fairbanks GPS-PW and RAOB-PW Comparison. ....	64

### **Abstract**

Current moisture initialization sources lack the spatial and temporal resolution required for mesoscale moisture forecast accuracy critical for military operations. The Global Positioning System (GPS) satellite constellation provides an opportunity to extract accurate moisture observations based on the refraction of the GPS signal through the troposphere. GPS-derived precipitable water (PW) from two research areas was independently compared with the Air Force Weather Agency's (AFWA's) MM5 PW model output. Results were concurrent with similar studies comparing GPS-derived PW with numerical weather models. The mean correlation between the GPS-derived PW values and MM5 output in CONUS was 92.5%, while in Alaska it was 72.8%. Mean model biases between the two data sets were  $-1.22$  mm in CONUS and  $0.69$  mm in Alaska, where a positive bias signifies the GPS network having higher PW values. Mean root mean square errors were  $4.36$  mm in CONUS and  $2.76$  mm in Alaska. In addition, comparisons were made between moist and dry locations as well as inland and coastal locations, and a special study was done comparing GPS receiver site elevation and standard deviation.

The GPS network's superior temporal resolution captured the diurnal variations in PW, while the model consistently failed to take such variations into account as its forecast progressed. This difference in diurnal patterns seems to be the largest source of error between the GPS and MM5 data sets. A number of non-meteorological error sources exist that could impact use of GPS-derived PW in operational applications, such

as terrain differences between the GPS receiver sites and the model interpolated heights. These error sources need to be further addressed prior to operational assimilation of this data into military weather models.

# GPS-DERIVED PRECIPITABLE WATER COMPARED WITH THE AIR FORCE WEATHER AGENCY'S MM5 MODEL OUTPUT

## I. Introduction

### 1.1 Background

Global Positioning System (GPS)-derived precipitable water (PW) provides unprecedented spatial and temporal resolution of water vapor, a highly variable parameter that is currently very difficult to initialize accurately. By measuring the “wet delay” of a transmission to a GPS receiver, where the delay is proportional to the integrated water vapor, it is possible to remotely sense a line-of-sight precipitable water amount for a given transmission time and receiver location. This parameter can be normalized into an estimate of a vertically integrated precipitable water value. In order to produce the most accurate water vapor measurement, the GPS receiver must have a means to measure temperature and sea level pressure concurrently.

***1.1.1 Delays in the GPS Signal.*** The Global Positioning System was established by the U.S. government in the early 1980s as a crucial element in navigation and relative positioning. Today, GPS includes a constellation of 24 low-earth-orbit (LEO) satellite vehicles that transmit signals in the L-band (1.2 and 1.6 GHz) to terrestrial users equipped with receivers. These signals are converted into information to aid in

navigation, timing, and positioning, not only for military assets, but also for many civilian uses (Trimble 1996).

Due to the requirement for highly accurate GPS readouts in every transmission, post-processing procedures have been developed to factor out the signal delays from each of these transmissions. These delays are excess path lengths due to the phase shifting between the standing signal and the transmission signal and are factored out of the signal through post-processing at the receiver end of the transmission. There are two major components of the GPS signal delay: the hydrostatic delay and the wet delay.

Hydrostatic delay arises from the nondipole moment of the total atmosphere. This part of the delay factors in all constituents of the neutral atmosphere (to include nitrogen, oxygen, argon, and other trace gases) including a component of water vapor. These constituents have relatively uniform composition in the troposphere. Using a surface pressure measurement, the hydrostatic delay is calculated. With surface pressure measurements, the hydrostatic delay can be measured to better than 1 mm (Businger 1996).

The wet delay arises from the refractivity of the water vapor in the neutral atmosphere. Due to the variability of water vapor in the tropopause, the wet delay can vary from 10 mm in desert regions to more than 400 mm in more humid regions. Not only is there an excellent spatial variability in wet delay, but there also exists a significant temporal variability. When the wet delay is measured in the zenith direction, a simple relationship exists from which precipitable water can be measured.



**1.1.2 Research Efforts in GPS Meteorology.** Exploiting the GPS signal delay for meteorological applications is a relatively young endeavor, with the GPS network only having been in operation since the mid-1980s. GPS meteorology shows considerable promise for both short- and long-term meteorological applications, including climatology. In addition, research is ongoing for the assimilation of GPS water vapor data into larger-scale forecast models, the mapping of global water vapor patterns in a manner similar to computerized axial tomography (CAT scanning), and the measurements of atmospheric refractivity soundings via radio occultation to gather global information about temperature, humidity and ionospheric structures (Ware 2000).

**1.1.3 Precipitable Water in the AFWA MM5.** The Fifth Generation Mesoscale Model (MM5) is a three-dimensional, non-hydrostatic, primitive-equation, nest-grid model with a terrain following sigma ( $\sigma$ ) vertical coordinate system (Grell 1995). It is the Air Force Weather Agency's (AFWA's) weather forecast model of choice. As of this writing, AFWA runs MM5 windows over 29 worldwide mission critical theaters of operations. AFWA maintains 18 parent domains, from which 11 inner nest windows are derived (Applequist 2001).

Kuo (1993) has already shown that precipitable water, despite being a two-dimensional variable, can be aptly assimilated into the MM5. Therefore, it is plausible that with its exceptional temporal and spatial resolution, GPS-derived precipitable water can be a valuable input for modeling tenuous water vapor variables.

Gutman (2001) has offered theories on how GPS PW can be integrated into mesoscale models by using a vertical aliasing technique, similar to the one mentioned by

Kuo (1993). Gutman shows a case study in which GPS PW was assimilated into the National Center for Environmental Prediction's (NCEP's) Rapid Update Cycle 2 (RUC-2) mesoscale forecast model. In addition, he cites previous studies in which it has been shown that the most vertical variability in the integrated vertical moisture profile is in the lower 4000 m.

Currently, AFWA uses the Multivariate Optimal Interpolation (MVOI) scheme to assimilate its data for use by the MM5. MVOI uses point analyses in the vertical to derive vertical profiles of temperature, winds, and moisture. GPS-derived moisture products are currently not assimilated into the MM5 (partly due to the form of assimilation technique). By summer 2002, AFWA's analysis scheme will transition from MVOI to the 3-Dimensional Variational Analysis (3DVAR) system. This method is designed to employ more data sources along with parallelization techniques to compile more information in a comparable amount of time (Ritz et al. 2001). This future transition provides more validity to this research, for 3DVAR will be able to ingest the GPS-derived products for initialization.

## **1.2 Problem Statement**

Currently, GPS-derived PW is not assimilated into any operational weather model, due to a number of factors. Less than 100 sensors are available in the continental United States (CONUS), and less than 100 sensors are available throughout Europe. While the receiver density is currently comparable to the upper-air sounding network, inconsistencies with the GPS receivers and the delay-processing software result in the meteorology community's hesitation to fully implement the network.

AFWA traditionally has been at the leading edge of taking advantage of new data sources for operational use. For example, AFWA was at the forefront of using GOES sounder data as a legitimate data source, long before other operational centers considered such a source as valid. The results of this comparison should demonstrate the utility of GPS-derived PW in numerical weather prediction applications, however, its temporal resolution would make it of best use in a variational assimilation system. Through this research, AFWA may make the decision to assimilate the GPS-derived PW not long after their 3DVAR assimilation scheme becomes operational in 2002.

### **1.3 Research Impact**

For an NWP user to have confidence in a numerical model, it is important for the data being used to initialize the model to be as accurate as possible. Today's numerical models are able to use advanced methods to aptly blend real-world observation data with previously obtained model output. This way, the model is less likely to react to contaminated data.

AFWA is at the forefront of incorporating the best technology to optimize model initialization. It uses the most accurate observation data with the highest temporal and spatial resolution that is computationally possible.

This research will compare GPS-derived precipitable water with the output from AFWA's MM5. GPS-derived precipitable water overcomes the challenges that exist in other moisture observations. For example, radiosonde balloons are only launched every 12 hours from a network of sites that average 500 km between each launch site. Also,

GOES sounder data is only valid in clear-air areas. The presence of cloud water contaminates the data.

Should AFWA begin to ingest GPS-derived PW, the model's moisture output will be nudged towards truer values and will improve the overall quality of the model's output: more valuable forecast data for our nations' warfighters.

#### **1.4 Research Objective**

This research will compare GPS-derived precipitable water (PW) against an operational numerical weather prediction (NWP) forecast model. By doing an independent data comparison in two of AFWA's MM5 theaters of operation, a first-look analysis will be performed that can transition to the next step: experimentally assimilating the new data into the model initialization itself. Studies have already demonstrated the excellent value GPS-derived PW can provide to other forecast models, both by independent data comparisons as well as by legitimate assimilations into the model. This will be the first study involving AFWA's operational MM5 output in GPS-derived PW research.

The objective will be to assess whether GPS-derived PW is a value-added data source, in particular, a recommendation of whether the AFWA MM5 might produce more accurate output should GPS-derived PW be included. With the advent of their 3DVAR initialization scheme in mid-2002, AFWA will be able to ingest the PW values for operational use. Through various statistical analyses, quantitative comparisons will provide the reader with evidence supporting the accomplishment of this objective. Statistics that will make these comparisons include correlation, bias, RMSE, and standard

deviation. These statistics can be partitioned into various categories, such as model initialization time, forecast integration time, and location.

## **1.5 Hypotheses**

Based on other studies that will be detailed in Chapter II, this research is expected to show a reasonable correlation between the GPS-derived PW and the MM5 output. However, the errors that will evolve between the two parameters will concur with errors that already exist between radiosonde-derived PW and MM5 output: the MM5 has a persistent moist bias.

Variations in these results will exist in the different theaters. For example, the data in CONUS will have a continental influence, while the values in Alaska will have a body of water possibly impacting the model results. In addition, the differences in GPS receivers and processing software will cause varying results. Such differences will prevent accurate comparisons between the two theaters.

Finally, the comparisons between the GPS-derived PW and the radiosonde values will show a slight bias, but this bias is expected to be well within the error tolerances of both measurement sensors. This will further substantiate AFWA using these data for model initialization.

## II. Literature Review

### 2.1 The Global Positioning System

**2.1.1 Historical Perspective.** The Global Positioning System was established by the U.S. government in the early 1980s as a crucial element in navigation and relative positioning. Today's GPS network consists of 24 or more low-earth orbit satellite vehicles that transmit signals in the L1 (1228 MHz) and L2 (1575 MHz) bands to terrestrial users that are equipped with receivers (Leick 1990). Until May 2000, the military had the capability to exercise Selective Availability, which would have intentionally degraded the signal for national security purposes. The Clinton administration ended the feature, thus giving the civilian community reliable enhanced capabilities (Leopold 2000). Figures 1 and 2 show diagrams of how the GPS satellite vehicle constellation is arranged and how their ground tracks ensure global coverage.

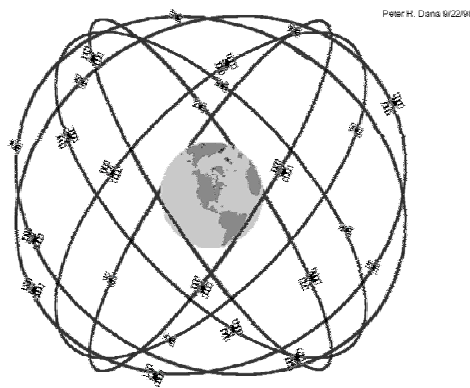


Figure 1. Schematic of the GPS Satellite Vehicle Constellation. The nominal constellation has 24 satellite vehicles distributed among 6 orbital planes. Altitude: 20,200 km. Inclination Angle: 55 degrees. Courtesy of Dana (1999).

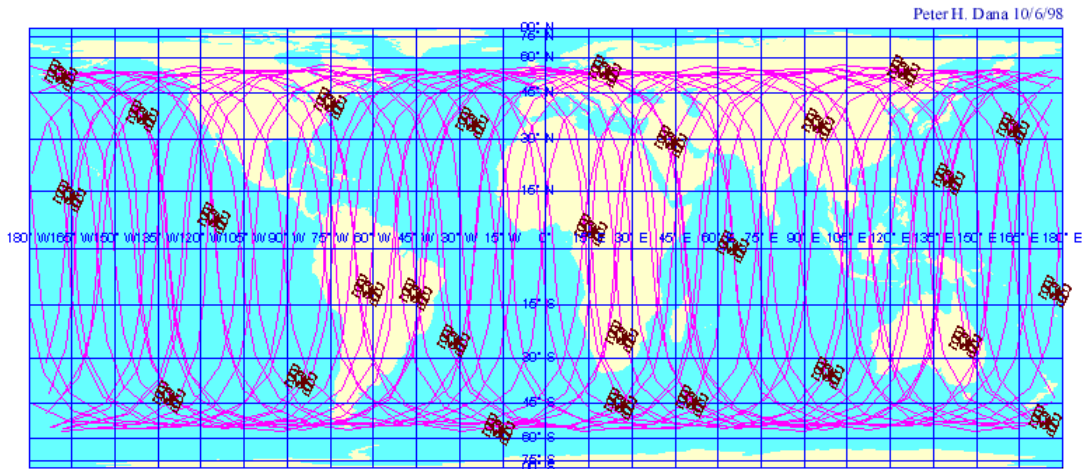


Figure 2. Diagram of the Satellite Coverage Transposed on a Global Map Projection. Ground tracks are shown over a 24-hour period from 29-30 September 1998. Courtesy of Dana (1999).

**2.1.2 Determining Location with GPS.** The signals disseminated from the satellite vehicles are converted into time and distance information. For a GPS location calculation two steps are required: phase shifting of the pseudorandom codes and trilateration.

Phase shifting of the pseudorandom code is the first step in determining ground position. Each satellite vehicle transmits a signal of binary code (ones and zeroes). The ground receiver intercepts this code, and then times its own code to match the satellite vehicle's transmission. The time it takes for the receiver to match up its code, multiplied by the speed of light, gives the ground the receiver the distance it is from the satellite vehicle (Leick 1990).

Trilateration is the process of determining distance from sighting at least four satellite vehicles from any ground positioned receiver on earth. The fourth satellite vehicle is required to resolve receiver clock errors. When a ground receiver is able to determine its distance from the satellite vehicles, the receiver can then use trilateration to

determine its precise location on the earth's geoid (Figure 3). By imagining each satellite's range as a sphere, the intersection of the spheres will constitute the location (Trimble 1996).

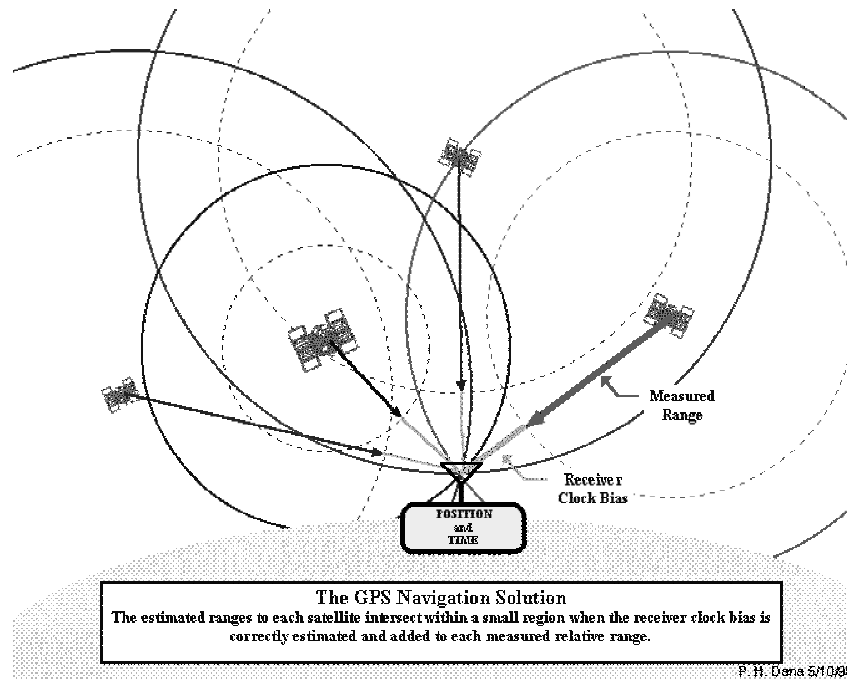


Figure 3. Visualization of How GPS Determines Precise Location. Courtesy of Dana (1999).

**2.1.3 The Current Status and Future of GPS.** Currently, the GPS network satellite vehicles are on the Block IIR build, manufactured by Lockheed-Martin. This constellation was emplaced in 1995, and each satellite is anticipated to have a 10-year design life (Hofmann-Wellenhof 1993). In anticipation of the expiration of the Block IIR systems, Boeing Satellite Systems is expected to begin GPS Block IIF production by the end of 2002, with the first satellite scheduled for a 2005 delivery. In addition, the Department of Defense was expected to request proposals for the Block III design in Fall 2001 (Smith 2001). These plans will ensure reliable coverage.



## 2.2 Use of GPS for Meteorological Research

It has only been in the past decade that geodesists and meteorologists have discovered the relationship between GPS receiver transmissions and the water vapor in the troposphere overlying the receiver site. Meteorologists are interested in taking advantage of this relationship due to its high temporal and spatial resolution, as well as the portability and economy of the measurement devices. Military meteorologists are particularly interested in the passive nature of this remote sensing capability.

Each GPS transmission between a satellite vehicle and ground receiver contains a total delay that must be processed out of the navigation reading. This delay has two parts: the ionospheric delay and the neutral atmosphere delay. Using both the L1 and L2 signals factors the ionospheric delay out, via a dispersion relation relating the two carrier signals. The neutral atmosphere delay (also known as the tropospheric delay) is on the order of 2 m and consists of the hydrostatic delay and the wet delay (Bevis 1992).

Saastamoinen (1972) was among the first to discover the relationship between the refractivity of the atmosphere and the satellite signal delays. The total tropospheric delay consists of the sum of the hydrostatic delay and the wet delay. The hydrostatic delay arises from the dry constituents of the atmosphere. This part of the delay factors in all constituents of the neutral atmosphere (to include nitrogen, oxygen, argon, and other trace gases) *except* the dipole component of water vapor. These constituents have relatively uniform composition in the troposphere. Using a surface pressure measurement, the hydrostatic delay is calculated (Bevis 1992):

$$ZHD = \frac{(2.2779 + 0.0024) \cdot P_s}{(1 - 0.00266 \cdot \cos(2\phi) - 0.00028 \cdot H)} \quad (1)$$

In Equation (1),  $P_s$  is the surface pressure, and the term in the denominator is the variation of the gravitational constant with latitude ( $\phi$ ) and height ( $H$ ). With accurate surface pressure measurements, the hydrostatic delay can be measured to better than 1 mm (Businger 1996).

The wet delay arises from the refractivity of the water vapor in the neutral atmosphere. Due to the variability of water vapor in the troposphere, the wet delay can vary from 10 mm in arid regions to more than 400 mm in more humid regions, such as the tropics. Not only is there a significant spatial variability in wet delay, but there also exists a significant temporal variability.

A simple relationship exists between the zenith wet delay and precipitable water, as seen in Equation (2):

$$PW = \Pi \cdot ZWD \quad (2)$$

where PW is precipitable water in a vertical column, and the zenith wet delay is typically a slant-wise wet delay measurement that has been normalized with a mapping function that is roughly related to the inverse of the sine of the elevation angle (Neill 1996).

The wet delay through the atmosphere is measured in the zenith direction with a simple integration seen in (3):

$$ZWD = 10^{-6} \left[ k_2 \cdot \int \left( \frac{P_v}{T} \right) dz + k_3 \cdot \int \left( \frac{P_v}{T^2} \right) dz \right] \quad (3)$$

where  $P_v$  is the partial pressure of water vapor,  $T$  is the atmospheric temperature and  $k_2$  and  $k_3$  are empirical refractivity constants.

The proportionality constant  $\Pi$  is another simple calculation as seen in (4):

$$\Pi = \frac{10^6}{\rho \cdot R_v \cdot \left[ \left( \frac{k_3}{T_m} \right) + k_2 \right]} \quad (4)$$

where  $R_v$  is the gas constant for water vapor,  $\rho$  is the density of liquid water,  $T_m$  is the mean temperature through a vertical layer (which is further discussed in the next section), and  $k_2$  and  $k_3$  are constants related to the refractivity of water, obtained empirically (Bevis 1994). Therefore, what one sees is a basic relationship, which only requires knowledge of the elevation angle of the satellite vehicle in relation to the ground receiver, the surface pressure to separate the wet delay from the hydrostatic delay, and the mean temperature through the vertical layer.

**2.2.1 Calculation of Mean Temperature.** The calculation of the mean temperature,  $T_m$  (in Kelvins), through the layer has been simplified even further. Bevis (1992) determined a linear relationship between surface and mean temperatures in the continental United States (CONUS) by comparing the mean temperatures from 8718 radiosonde observations with their respective surface temperatures. He determined that the regression equation  $T_m \approx 70.2 \text{ K} + 0.72 T_s$  would yield a precipitable water value with no more than 2% error due to the regression itself. Note that this regression is only good for CONUS and may not apply in other geographic regions. Liou (2001) employed the same technique in Taiwan, using 586 Taipei radiosondes, and empirically derived the relationship  $T_m \approx 1.07T_s - 31.5 \text{ K}$ .

**2.2.2 Calculation of  $\Pi$ .** Emardson and Derks (2000) have taken the regression a step further, by incorporating latitude and time of year into the formula for  $\Pi$ , resulting in a relationship unique to each GPS receiver site:

$$\Pi = 10^{-8} \rho R_v k_2 + 10^{-8} \rho R_v k_3 \theta + a_1 T_s \sin\left(\frac{2\pi t_d}{365}\right) + a_2 \cos\left(\frac{2\pi t_d}{365}\right) \quad (5)$$

In Equation (5),  $k_2$  and  $k_3$  are the same constants as in (4),  $a_1$  and  $a_2$  are empirical constants relating the surface temperature to a mean temperature,  $\theta$  is the latitude of the receiver site in radians, and  $t_d$  is the Julian day (in decimal form). To obtain this relationship, the authors used over 120,000 radiosonde profiles from 38 upper air sites throughout Europe.

Based on these empirical formulae and simplifications, Bevis (1992) has determined that the error still remains within 4%, which is within the tolerance of other existing moisture measurement sets (such as radiosondes).

## **2.3 The Fifth-Generation Mesoscale Model**

The Fifth Generation Pennsylvania State University-National Center for Atmospheric Research Mesoscale Model version 3 (MM5v3) is the Air Force Weather Agency's numerical model of choice for its operational applications.

**2.3.1 Historical Perspective.** The model was first developed by Richard Anthes and T.T. Warner at the Pennsylvania State University (PSU) in 1971, and then was enhanced through cooperation with the National Center for Atmospheric Research (NCAR). Version 3 of the modeling system has been available since July 1999. AFWA has been running the MM5 as its primary operational numerical model since 1997.

**2.3.2 Model Setup.** The MM5 is a limited-area, non-hydrostatic, three-dimensional model that employs primitive equations. The model is in a nested-grid form that calculates output for a parent domain as well as one or more sub-domains. Grell (1995) provides additional information about the model setup.

The MM5 uses a terrain-following sigma ( $\sigma$ ) vertical coordinate, a unitless value defined in Grell (1995) as (6):

$$\sigma = \frac{(p - p_t)}{(p_s - p_t)} \quad (6)$$

where  $p$  is a reference pressure based on user-defined constants and terrain,  $p_s$  is the surface pressure, and  $p_t$  is the specified top pressure. AFWA's MM5 configuration has 41 sigma levels.

The Air Force Weather Agency (AFWA) has taken advantage of the flexibility of this model by allowing variations in nest configurations and physics parameterizations. As of Fall 2001, AFWA runs MM5 windows over 29 worldwide mission critical theaters of operations. They maintain 18 parent domains, from which 11 inner nest windows are derived (Applequist 2001, personal correspondence). In addition, the MM5 has physics packages that AFWA has the option to configure to best take advantage of a particular theater of interest. Theaters that will be addressed in this research all have the same physics packages, as outlined in Table 1 (Craig 2000).

AFWA MM5's parent domains each have 45 km grid resolution, while the inner nest domains have spacings that range from 15 km to 1.67 km. Parent domains are initialized and run twice per day, running 72-hour forecasts in 3-hour intervals. The 15

km inner nest, the domain used for this research, initializes two times per day, 6 hours after the parent domain's run. Inner nests produce 48-hour forecasts, also in 3-hour intervals.

Table 1. AFWA MM5 Physics Packages. Adapted from Craig (2001).

<b>Parameter</b>	<b>Scheme</b>
Atmospheric Radiation	Dudhia Longwave and Shortwave
Cumulus Parameterization	Grell Convective
Explicit Schemes	Reisner Mixed Phase
Planetary Boundary Layer	MRF PBL
Soil Model	Multi-Layer Thermal Diffusion

**2.3.3 Model Initialization.** Until January 2001, the MM5 used synoptic background fields based on the Aviation Model (AVN) or the Navy Operational Global Atmospheric Prediction System (NOGAPS). AFWA's MM5 now initializes its parent domains using a Mesoscale Data Assimilation System / Multivariate Optimal Interpolation (MDAS/MVOI) scheme. The inner nests are not initialized in this way; instead it uses the parent windows. With MDAS/MVOI, the model can now use its own forecast background fields, combined with global analyses, to generate accurate analysis fields that adapted well to the various 45 km resolution parent domain locations (Ritz et al. 2001). With MDAS/MVOI, GPS-derived PW is unable to be of temporal value to the model. A more temporally dynamic assimilation scheme is required to better take advantage of the temporal variability PW values, such as 3DVAR, explained in the next section.

**2.3.5 3DVAR Assimilation Scheme.** By summer 2002, AFWA is expected to have transitioned all of its parent domain initializations to the 3-Dimensional Variational Analysis (3DVAR) system. 3DVAR will accommodate virtually all of the observation types that MDAS/MVOI currently employs, along with some new types, to include wind profiler data. It is expected that GPS-derived precipitable water will be among the data types accommodated by 3DVAR. Parallelization of the data assimilation and interpolation techniques over several processors will also make incorporating GPS-derived PW easier (Ritz 2001).

## **2.4 Using GPS Meteorology to Validate and Improve Forecast Models**

Studies have already shown how GPS-derived precipitable water observations compare with numerical forecast model output. Some studies assimilated the PW values into the model initialization, while others simply conducted an independent data comparison, similar to this research. For further details on these studies, the reader is directed to the references cited in the text. Summaries of a selection of these studies follow.

**2.4.1 High Resolution Limited Area Model (HIRLAM).** The HIRLAM model is a regional NWP system developed by the weather services of the Nordic countries, along with Ireland, Holland, and Spain.

Yang et al. (1999) compared GPS precipitable water data with a  $0.21^\circ$  resolution HIRLAM configuration similar to the operational version at the Danish Meteorological Institute. Comparisons of the 6, 12, and 30-hour forecasts of precipitable water with the

concurrent GPS precipitable water values at 25 sites in Sweden and Finland were conducted. This study was performed between August and November 1995 and over 11,000 observations were compared.

Results of the comparison between the GPS PW values and the HIRLAM analysis were very optimistic. Correlations ranged from 0.91 to 0.96, averaging 0.94, and RMSE ranged between 1.9 and 3.4 mm, with a mean value of 2.4 mm, approximately 18% of the mean PW value. For the 6, 12, and 30-hour forecasts, the correlations were 0.94, 0.93 and 0.93, respectively, and the RMSEs were 2.4, 2.5, and 2.6 mm, respectively.

In Spain, Cucurull et al. (2000) employed the HIRLAM model to compare analysis and forecast precipitable water values with GPS-derived PW values at five GPS sites in the Madrid Sierra region of central Spain. The case was during 2-15 December 1996 and involved two frontal passages. The HIRLAM analyses, when compared with the GPS-derived PW values, resulted in a model moist bias of 0.2 mm and an RMS difference of 2.1 mm. The 24-hour HIRLAM forecast resulted in a bias of  $-1.2$  mm and an RMSE of 3 mm. The higher values were expected of the longer forecast integration time.

Finally, Lenderink and Meijgaard (2001) compared the performance of a modified HIRLAM model, the HIRHAM4, with the Nordic GPS network. The HIRHAM4 is a high-resolution ( $0.167^\circ$ ) version of HIRLAM with a physics package known as ECHAM4. For comparison, the authors also modified the ECHAM4 package with revised cloud and turbulence schemes. At the same time, both the HIRLAM and European Centre for Medium-Range Weather Forecasting (ECMWF) models' analyses



were used in the HIRHAM4 to assess which would handle the high-frequency variation of GPS-derived integrated water vapor (IWV). This setup was run for three frontal passages from 28 August to 5 September 1995.

The study concluded that, in the first 24 hours of forecast, the HIRLAM analyses produced a more accurate depiction of the high variability of the IWV fields, most likely due to the higher resolution ( $0.4^\circ$ ) of the HIRLAM grid compared to the  $1.5^\circ$  ECMWF. After 24 hours, the ECMWF was superior. Regarding the comparison between the two model physics packages, the revised physics package better captured the maxima and minima of IWV during frontal passages, as well as the timing of these peak values.

**2.4.2 Rapid Update Cycle (RUC).** Wolfe and Gutman (2000) have pioneered American efforts to bring GPS meteorology into operational forecasting. In their 2000 study, they assimilated GPS-derived PW into the Mesoscale Analysis and Prediction System (MAPS), which is NOAA's research version of the RUC model. The RUC is a high frequency, state-of-the-art analysis and forecast system run by the National Centers for Environmental Prediction (NCEP). Most operational RUC forecasts are run on 40-km and 20-km resolution grids and seldom exceed 12-hour integration times. In this study, GPS-IPW values were assimilated into the RUC analyses every three hours from 20-29 June 1997 using optimal interpolation.

Output was assessed for the Purcell, OK GPS-receiver site. The analyses showed a mean bias of 1.8 mm (RUC had more moisture) and an error range of 5.5 to  $-6.9$  mm. Only one 12-hour forecast was evaluated in this study, and the preliminary results showed that GPS-IPW in the model better captured variations in convective precipitation.

Smith et al. (2000) provided more detail in the same ongoing RUC assimilation study. In this case, GPS-IPW observations were assimilated every 3 hours into a 60-km resolution, 25-sigma level RUC window over the central United States. Every three hours, a new analysis was produced, using the previous 3-hour forecast as the background field. Parallel runs of the RUC with and without the GPS-IPW have been ongoing since November 1997.

The GPS data provided valuable information at a temporal and spatial resolution that cannot be obtained through a radiosonde network. Because GPS data is available approximately every half hour in the American GPS-MET network, it was possible to ingest the GPS values at every analysis time, while the radiosonde data is only available every 12 hours. In the case presented in Smith et al. (2000), from 16 to 17 April 1998, a cold front crossed eastern Texas. The GPS data moistened the 3-hour forecast of relative humidity fields by 14% ahead of the front, and dried out the fields by 23% behind. This resulted in a 1% improvement of the 850mb RH and a 2% improvement of the 500 mb RH.

Smith et al. (2000) made two other observations that must be considered for future work on assimilation of GPS data into NWP. First, the GPS observations themselves must maintain an accuracy of at least 1.5 mm to be considered a value-added data source. This value has to include errors that could evolve from inaccuracies in orbit, temperature and pressure measurements, and post-processing. It was also concluded that the high variability of IPW limits the value of the data to making improvements in the short-term, especially in the 12-hour forecast timeframe.

Gutman and Benjamin (2001) provided an update to the same experiment, this time with a more populated CONUS GPS-MET network. When Smith et al. (2000) started their work, there were only 18 stations. By late 1999 the number had jumped to 58, including a number of sites on coastlines, where moisture data are often the most variable. Now forecast RH values at both 850 mb and 700 mb were improved by an average of 4.5%. At one model run, the 3-hour forecast was improved by as much as 40%!

Other conclusions found by Gutman and Benjamin (2001) involve the required accuracy and timeliness of the GPS data. In order for the GPS data to be of value to an NWP model, it must be measured at a higher accuracy than the model's error budget. The current convention is for models to analyze the precipitable water fields to within 3 mm accuracy. The Department of Energy has conducted a number of Water Vapor Intensive Observing Periods (WVIOPs), which compares precipitable water from 6 different sources at a facility near Lamont, OK. The results from this period show that GPS-derived precipitable water has an accuracy of about 1 mm, which is well within the tolerances required for a valuable data source for NWP. Concerning the timeliness, observations for initialization into numerical weather models is considered "real-time" if it can be ingested in the current assimilation cycle. This timeline is unique to each model, and the RUC requires 20-30 minutes before an observation is considered late. Currently, for quick post-processing, a "rapid orbit" calculation is required in the processing software. Scripps Institution of Oceanography has the capability to make such orbit calculations with its processing software in 24 hours (compared to 1-2 weeks),

and has done so to well within 1 mm accuracy, which adheres to the tolerances for assimilation into numerical models.

**2.4.3 PSU/NCAR MM5.** De Pondeca and Zou (2001) reported on an assimilation of GPS total zenith delay observations into the MM5 for a precipitation forecast in southern California during an El Nino event. The data was ingested, using a 4DVAR assimilation scheme, into a 6-km resolution domain with 20 sigma levels. A domain based on the 54-km NCEP reanalysis over the western United States was the parent to a 6-km nested grid that served as an initial condition in the 4-DVAR assimilation scheme. After two hours worth of observation ingest, the scheme required a 12-hour spinup, necessary to acquire the dynamic stability and damping of smaller scale gravity waves.

De Pondeca and Zou (2001) compared total zenith delays from MM5 output that was run both with and without the GPS data. The results were remarkable. First, the bias between the model run and the GPS observations was reduced by more than 90% when the GPS data was assimilated. Secondly, the precipitation forecasts were timelier and more accurate, by an average of 33.15%.

Cucurull et al. (2001) also performed a 4DVAR assimilation of simulated GPS-derived PW into a very fine scale MM5 over Spain. Their grid resolutions were 6 km and 2 km, with 5 minute and 30 second terrain resolution, respectively. In this study, simulated values of PW were assimilated using a 4DVAR scheme. First the MM5 was run over the period of interest and PW values were estimated at each grid point at 30 minute intervals. This created an “idealized” fictitious GPS network. This information was then re-introduced to the model using variational assimilation.

Results of this experiment showed the model's high sensitivity to the PW observations. However, no numeric results were available due to the paper's emphasis on assimilation of ZTD into the model.

**2.4.4 Deutsche Wetterdienst (DWD) Models.** Köpken (2001) employed three models derived from the DWD's limited area forecast and analysis system: the Europa Model ( $1/2^\circ$  horizontal resolution and 20 sigma levels), the Deutschland Model ( $1/8^\circ$  horizontal resolution and 30 sigma levels), and the BALTEX Model ( $1/6^\circ$  horizontal resolution and 31 sigma levels).

Köpken's work was conducted with the same Nordic GPS network as Yang (1999) and Lenderink and Meijgaard (2001). The study was conducted over August – October 1995. The GPS data was taken in 30 minute increments and was not assimilated into the models.

The results of Köpken's study were promising, with correlations between the BALTEX model and the GPS data near 90%, and bias of less than 3 mm. The model positive bias was consistent throughout the experiment period at virtually all GPS receiver sites, and for all three of the models. Such a bias was also seen in the HIRLAM model. To further investigate this bias, comparisons between the GPS data and radiosonde data were also performed. Köpken's results for six stations in Sweden and Finland indicated the GPS possessing a slight dry bias of about 1.3 mm. This could indicate that the DWD models have an overall moist bias of approximately 1.5 mm.

**2.4.5 Swedish Meteorological and Hydrological Institute Model.** A Central European GPS meteorology network of 15 sites was analyzed in Borbas (1998). A

numerical model developed by the Swedish Meteorological and Hydrological Institute was used for comparison. This model was a primitive equation model with a 90-km horizontal resolution and 12-sigma levels.

Comparisons were made by linearly interpolating the four nearest gridpoints to GPS-receiver sites in Germany, Switzerland and Poland. The GPS data were processed using two different processing schemes, one at the International GPS Service at the University of Bern, Switzerland, and the other at the Institute of Space Research, Department of Satellite Geodesy in Graz, Austria.

When compared with the NWP, the GPS data was again consistently drier than the model output, with a 5.5 mm RMSE with the Bern processing software, and a 6.3 mm RMSE with the Graz processing software.

**2.4.6 Summary.** Overall, this sample of studies involving GPS-derived precipitable water with NWP has shown the GPS data's reliability, along with its excellent spatial and temporal resolution. For these studies, GPS-derived PW was clearly a value-added data source. Independent data comparisons showed how well GPS compares with radiosonde data, and could reduce consistent biases in many NWP models. Also, assimilation studies have proven on numerous occasions how moisture-related variables are more accurate when GPS data are included.

### III. Methodology

#### 3.1 Data Collection

**3.1.1 GPS-Meteorology Data.** The National Oceanic and Atmospheric Administration Forecast Systems Laboratory (NOAA/FSL) controls the American network of GPS Precipitable Water receivers. Their network of over 50 sites in the CONUS and four sites in Alaska produces precipitable water readings every 30 minutes and posts a comprehensive output file to an FTP site for public viewing and download. Table 2 is an example of the downloaded data from the NOAA/FSL database. Figure 4 shows NOAA's GPS Meteorology network as of May 2001. See Appendix A for terrain, network, and gridding details for each GPS site.

The NOAA/FSL GPS-MET website contains the geodesy and hardware specifications for the sites. Most of the sensors are either Trimble 4000 SSI or Ashtech LP Z-XII3 receivers, and the data is processed with the University of Hawaii/Scripps Institute for Oceanography GAMIT software suite using predicted orbit information.

Table 2. Sample GPS-MET Data from Bartlett, NH for 6 July 2001

ID	Year	Julian Date	IPW (cm)	Press (mb)	Temp (C)	RH (%)	Total Delay (m)	Wet Delay (m)	Hydro Delay (m)	Mean Temp (K)	$\Pi$ (cm)
BARN	2001	187.010	2.512	986.73	19.42	84.7	2.4035	0.1567	2.2468	280.85	6.239
BARN	2001	187.031	2.381	986.95	18.17	89.4	2.3963	0.149	2.2473	279.95	6.259
BARN	2001	187.052	2.385	987.25	17.63	89.7	2.3974	0.1495	2.2479	279.562	6.268
BARN	2001	187.073	2.617	987.65	17.4	89.3	2.413	0.1641	2.2489	279.396	6.271
BARN	2001	187.094	2.62	987.88	17.28	87	2.4138	0.1644	2.2494	279.31	6.273
BARN	2001	187.115	2.539	987.82	17.02	85.2	2.4087	0.1594	2.2492	279.122	6.277



Figure 4. The American GPS Precipitable Water Receiver Network as of 31 May 2001. Courtesy of NOAA/FSL.

**3.1.2 MM5 Data.** The MM5 data for the CONUS and Alaska 15 km grids were obtained from AFWA. The GRIB output was downloaded daily from 06 July 2001 through 31 October 2001. Only four parameters needed to be stripped from the GRIB files: longitude (LUN), latitude (LOT), terrain height (TERHGT), and precipitable water (PWAT). The first three parameters are necessary for properly placing the GPS data on the MM5 grid. Processing of the PWAT data will be discussed later in this chapter.

**3.1.3 RAOB Data.** RAOB sites were chosen based on their proximity to GPS-receiver sites. There was a challenge of finding collocated sites since the NOAA/FSL-controlled GPS network is not concurrent with established WMO weather observation sites. Using guidance from Köpken (2001), the estimated range of atmosphere included in a GPS-derived PW value has 40 km radius. Therefore, only upper air sites within 45



km of GPS sites were chosen for comparison. However, Springfield, MO (SGF)'s RAOB site was also considered, due to its location in the Tornado Alley region of the country, despite it being nearly 70 km from the nearest GPS site, Conway, MO (CNWM).

The radiosonde-based PW values were downloaded from the GPS-MET website (<http://www.gpsmet.noaa.gov>). This website provides radiosonde output in an easy-to-process format. Because this data was pre-formatted, reading it into FORTRAN programs was simple and requires no further discussion in this section.

### **3.2 Sources of Error**

Prior to explaining the data analysis process, it is important to address the sources of error faced in working with GPS data in concert with MM5 and RAOB data. The following is a discussion of possible sources of error. Further details are available in Feng (1998).

**3.2.1 Make and model of GPS equipment.** This is not an explicit source of error that has been measured, but the varying makes and models of GPS equipment provides a lack of consistency in how a GPS-MET sample was taken. Table 3 shows a representation of the makes and models of GPS receiver and antenna equipment, in no particular order.

Table 3. Representation of Makes and Models of GPS Receivers

<b>Receiver Models</b>	<b>Description</b>
Trimble 4000 SSE	Dual frequency P-code on L1 and L2
Trimble 4000 SSI	Dual frequency P-code on L1 and L2
Ashtech LP Z-XII3	12 Channel, L1/L2, P1/P2 w/ continuous reference station capability
Ashtech LP Z12	12 Channel, L1/L2

**3.2.2 Antenna configuration and height.** The type of antenna is a bonafide source of error in processing GPS-MET data. There are two types of GPS antennas well known in the navigation world: the choke ring and the fixed groundplane. Many older antenna models still have a fixed groundplane configuration, and this could be a source of error in GPS calculations. The choke ring antenna is the International GPS Service (IGS) standard for computing phase center corrections (Feng 1998). Table 4 provides information about the various antennas involved in this study.

Table 4. Representation of Makes and Models of GPS Antennas

<b>Antenna Models</b>	<b>Shape</b>
Trimble 33429	Fixed Groundplane
Trimble 29659	Dorne Margolin Choke Ring
Trimble 22020	Fixed Groundplane
Trimble 14532	Fixed Groundplane
Trimble 23903	Fixed Groundplane
Ashtech 700829 "Whopper"	Fixed Groundplane

### **3.2.3 Elevation differences**

#### **3.2.3.1 Differences between GPS site elevation and MM5 TERHGT**

**value.** A significant source of error in the comparisons between GPS and MM5 PW

values is the difference in elevation at each GPS site. The model height of the GPS site was calculated by linear interpolation of the TERHGT value for four surrounding grid points. This was compared with the established height of the GPS receiver, provided by the network administrators. No adjustments were made to correct for the differences in terrain in this study. Elevation residuals are shown in the location data in Appendix A.

**3.2.3.2 Differences between GPS site elevation and RAOB site.** Like the MM5 elevations, the differences between the GPS sites and their nearest RAOB locations can be significant. This elevation difference can be corrected using assumptions of constant relative humidity and a typical lapse rate, but the RAOB sites used in this study had similar enough elevations that such differences were negligible. The elevation residuals between the GPS and RAOB locations are shown with the location data in Appendix A.

**3.2.4 Horizontal differences between GPS site and RAOB site locations.** As discussed in Section 3.1.3, only RAOB sites that were within 45 km of the GPS site were chosen for this study (plus Springfield, MO, as explained in Section 3.1.3). Due to the setup of the GPS network, this resulted in very few RAOB sites being available. The horizontal differences between the GPS sites and RAOB sites are of particular interest due to several of the sites being near coastlines. When a RAOB sites is near a coastline, there is a chance of the balloon drifting over the ocean and being exposed to increased moisture compared to an inland GPS site. These distance differences are shown in Appendix B.

**3.2.5 Orbit calculations.** The orbit calculation methods are another source of error in GPS-MET parameter calculations. Knowledge of ephemeris data is essential to calculate ZHD and ZWD. There are 5 variations on the type of orbit information, outlined in Table 5.

Table 5. Comparison of GPS Orbit Calculations Available in GPS-MET Processing (NASA 2001).

<b>GPS Orbit Calculation</b>	<b>Accuracy</b>	<b>Latency</b>	<b>Update Frequency</b>
Broadcast	~260 cm	real time	--
Scripps Hourly	~20 cm	real time	hourly
Predicted (Ultra Rapid)	~25 cm	real time	twice daily
Rapid	~ 5 cm	17 hours	daily
Final	< 5 cm	~ 13 days	weekly

The NOAA/FSL GPS network uses the Scripps Hourly orbit product, which provides the most up-to-date, real-time orbit information for operational processing of GPS-MET data. Their standard for accuracy is 25 cm, so the Scripps product is within that tolerance.

**3.2.6 Processing software.** This potential for error arises from the varying methods of processing the data. There are several software suites available for calculating tropospheric, hydrostatic and wet delays, from which PW is extracted. A list of the most widely used programs is listed in Table 6. A study was conducted comparing the GPS-MET data from these three software packages with varying orbital calculations. It was concluded that BERNESE and GAMIT had comparable accuracies, and that other factors besides software accuracy can be taken into account to decide on which software package is better (Department of Commerce 1995). The NOAA/FSL network employs the GAMIT software suite.

Table 6. Available GPS Processing Software

Software	Developer
GAMIT	Massachusetts Institute of Technology/Scripps Institute of Oceanography
BERNESE	University of Bern
PAGES	National Geodetic Survey

**3.2.7 Empirical estimates of parameters in GPS-MET calculations.** Many calculations in processing GPS-MET parameters require constants of proportionality. These constants were empirically defined with studies involving thousands of radiosondes.

The mean temperature for  $\Pi$  in Equation (4) is routinely calculated for CONUS and Alaska using Bevis' (1992) empirical correlation based on 8718 radiosonde calculations over 2 years. Other studies have been conducted in Europe and Taiwan that derive other mean temperature correlations. These correlations are sufficient for meteorological use of GPS, and their relative error is less than 1%. Nonetheless, this is still a contribution to the error budget.

The refractivity constants,  $k_2$  and  $k_3$ , in Equations (3) and (4) also are empirically defined. Bevis et al. (1994) provides historical commentary on their derivations. Bevis et al. (1994) also derived his own values for the refractivity constants and assumed them to be within 2 standard deviations of the true values.

Bevis et al. (1994) concluded that the error in mean temperature is much greater than that of the refractivity constants, and that most of the error in the  $\Pi$  calculation is due to the mean temperature.

### ***3.2.8 Differences in PW calculation methods between GPS, RAOB and MM5.***

Another significant source of error is the differences in how PW is calculated among the three data sources.

The GPS PW is calculated using the equations outlined in Chapter II. Note that there is no reference to typical humidity parameters, such as mixing ratio, dew point or specific humidity.

The RAOB PW is calculated using a NOAA algorithm and it integrates mixing ratio over all pressure levels. Mixing ratio is defined as the ratio of water vapor to dry air (Glickman 2000). If the sounding from which mixing ratio is being calculated runs out of data before encountering the highest possible level, then those levels are simply left off; if the top level is less than 5 km elevation, the sounding is thrown out.

MM5 PW is calculated by integrating specific humidity over all pressure levels. For all intents and purposes, it is acceptable to interchange specific humidity and mixing ratio (Glickman 2000). A typical mid-latitude mixing ratio value varies from a specific humidity value by not more than 0.1%. It has been observed that some operational versions of the MM5 may interchange specific humidity and mixing ratio in calculations (Swanson 2001).

### 3.3 Coding of Processing Programs

**3.3.1 Overview.** A number of variables required custom procedures for each of the theaters processed. The following steps needed to be completed: (1) extract relevant information from GPS, MM5 and RAOB input data and read the data from the various sources into FORTRAN arrays, (2) perform linear interpolation of MM5 data to GPS sites, (3) write out arrays of GPS data with RAOB sites, (4) write out the GPS, MM5 and RAOB values by domain and by location, (5) calculate comparative statistics and write them out to delimited text files. These text files were then imported into Microsoft Excel for statistical processing. Now each step will be reviewed in more detail.

**3.3.2 Extract Relevant Information.** Each of the three data sources (GPS, MM5 and RAOB) required unique programs to extract the relevant information. The GPS data came from the FSL FTP site grouped according to location. First, appending all locations' files created a large file. Then a program was developed which brought in the GPS output file and read the columns into arrays according to data type (i.e. year, id, Julian date). A second pass was then performed to conduct several tasks at once. It first threw out the lines with missing PW values. Then it searched through the Julian date arrays to strip out only those values that contained a particular DTG. Those lines were written to a new formatted file named after the Julian DTG.

The MM5 output required more work than the GPS and RAOB data, due to its two-dimensional nature and binary format. The PWAT parameter that was stripped from each GRIB file had to be converted to a binary format and then read into FORTRAN arrays.

The RAOB data was relatively easy to work with. The files were downloaded from the NOAA/FSL website in a long string of formatted soundings with no definitive breaks. To divide the data into separate soundings, an IDL routine was employed. The end result was one file for each of the soundings, named according to sounding location and DTG.

**3.3.3 Perform linear interpolation of MM5 data to GPS sites.** Each GPS site had a grid coordinate corresponding to the MM5 grid position calculated, based on a FORTRAN subroutine from AFWA. The subroutine brought in parameters describing the MM5 grid, along with an array of latitudes and longitudes of the GPS sites, and wrote out an array of IX/JX positions. The interpolation program reads in the MM5 GRIB data and linearly interpolates the values of the sixteen surrounding grid points to the GPS receiver location's IX/JX position.

Sixteen grid points, rather than four, were chosen due to the horizontal extent of a GPS-derived PW observation. Figure 5 shows the trigonometric relationship of the horizontal expanse of an averaged GPS-derived PW reading. The conditions assume a  $7^\circ$  elevation angle (which is the elevation cutoff for the NOAA/FSL network) and that 98% of the column water vapor resides in the lowest 5 km of the atmosphere. This results in a horizontal coverage of approximately  $5200 \text{ km}^2$ .



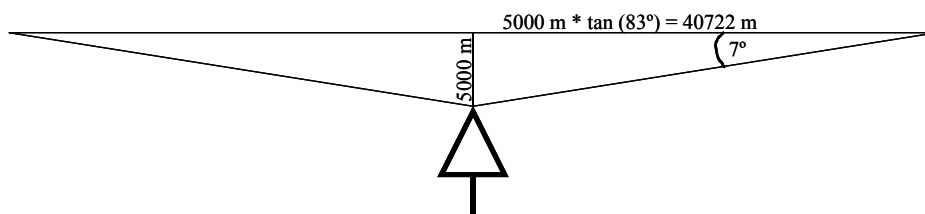


Figure 5. Area of Influence of a GPS-Derived Precipitable Water Reading. Diagram not to scale.

In a 15 km resolution model, the horizontal expanse of sixteen grid points will cover 2025 km<sup>2</sup>. Figure 6 illustrates this. Even though the coverage areas aren't exactly the same, choosing an additional ring of grid points would have resulted in an area much larger than that of the GPS observation. The 7° cutoff will result in a larger area of influence, but expanding the MM5 grid points any farther would cause negligible differences in PWAT values, due to the nature of the interpolation scheme.

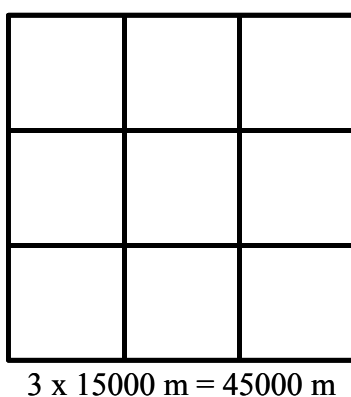


Figure 6. Area of Influence in MM5 Grid. The GPS site is positioned somewhere in the center box.

**3.3.4 Write out arrays of GPS data with RAOB sites.** To calculate precipitable water from each of the RAOB soundings another FORTRAN program was required. The foundation for this program came from Thomas Schlatter and Donald Baker in the PROFS Program Office, NOAA Environmental Research Laboratories, Boulder, Colorado. Schlatter and Baker developed a suite of FORTRAN algorithms in 1981 to

calculate moisture parameters. This suite is the standard throughout NOAA and the National Weather Service. For the precipitable water algorithm, the method of choice was to integrate dimensionless mixing ratios through the pressure levels.

Each sounding was run through the precipitable water algorithm and the output was grouped by location into files. An example of one of these files is in Table 7.

Table 7. Sample RAOB-Based Precipitable Water for Charleston, SC

ID	MO	DY	HR	PW
CHS	7	6	0	5.2679
CHS	7	6	12	4.7164
CHS	7	7	0	4.5271
CHS	7	7	12	4.8938
CHS	7	8	0	3.6750
CHS	7	8	12	4.7439
CHS	7	9	0	6.7243
CHS	7	9	12	6.3339

These data were run through a program to generate files of GPS-derived PW and RAOB-derived PW together, as seen in Table 8.

Table 8. Sample GPS vs. RAOB Comparison File for Slidell, LA

DTG	GPS Site	GPS PW	RAOB Site	RAOB PW
187.01	NDBC	5.2130	SIL	5.8068
187.51	NDBC	4.4710	SIL	5.0915
188.01	NDBC	4.5440	SIL	5.2191
188.51	NDBC	3.7530	SIL	4.3528
189.01	NDBC	3.7390	SIL	4.4593
189.51	NDBC	3.9020	SIL	4.8850
190.01	NDBC	3.8940	SIL	4.3743
190.51	NDBC	5.0740	SIL	5.7159
191.01	NDBC	4.4040	SIL	5.3123
191.51	NDBC	4.6320	SIL	5.3905

**3.3.5 Output by DTG.** Next, the GPS-derived PW and MM5 interpolated PW values were written to a file titled by Julian date/Julian time/forecast integration time. Table 9 is an example of one of these output files.

Table 9. Sample Output File for a 45-Hour Forecast Valid 8 July 2001 03 UTC. PW values are in centimeters.

ID	Lat	Long	IX	JX	GPS PW	MM5 PW
BLRW	43.22	-90.53	218.54	138.78	1.5330	1.8270
DQUA	34.11	-94.29	200.33	72.17	4.2180	5.0045
FBYN	40.08	-97.31	182.79	115.33	3.3970	3.7789
HKLO	35.68	-95.86	190.83	83.49	3.5200	4.5889
JTNT	33.02	-100.98	159.43	65.04	2.8280	2.8529
RWDN	40.09	-100.65	164.43	116.09	2.2000	2.6036
MBWW	41.90	-106.19	135.74	131.80	2.0060	1.8064

**3.3.6 Output by location.** The next task was to group all data together by location. This involved a new program that took the output GPS and MM5 data from a particular DTG and wrote each location's line to a new file, which is shown in Table 10.

Table 10. Location-specific PW Data for Spokane, WA.

DTG	ID	GPS PW	MM5 PW
187.500.06H	SPN1	0.8400	1.2588
187.625.09H	SPN1	1.5220	1.2732
187.750.12H	SPN1	2.0170	1.2030
187.875.15H	SPN1	1.3900	1.0499
188.000.06H	SPN1	1.3970	1.1243
188.000.18H	SPN1	1.3970	1.0859
188.125.09H	SPN1	1.5500	1.1666
188.125.21H	SPN1	1.5500	1.1892

**3.3.7 Comparative statistics calculations.** Summary statistics were calculated from each of the previously described files. A statistics subroutine was developed that calculated the mean values, bias, correlation, root mean square (RMS) error, standard deviation, and n, the number of observations available in each calculation, based on equations from Wilks (1995). Table 11 shows an example of a summary statistics file for a single DTG. The contents of this file can easily be imported into PC-based programs for additional grouping and processing.

Table 11. Sample Statistical Summary by DTG. This file collected all 06H forecasts from the 06 UTC initialization MM5 runs in CONUS. One line of data was generated for each DTG file described above in Table 9.

DTG/Forecast	Init	Corr	Bias	RMSE	StDev	Mean GPS	Mean MM5	n
187.500.06H	06Z	0.9666	-0.2678	0.4472	0.3622	2.9663	3.2341	46
188.500.06H	06Z	0.9485	-0.2737	0.4861	0.4066	3.0918	3.3655	44
189.500.06H	06Z	0.9449	-0.3391	0.5044	0.3782	3.4527	3.7917	42
190.500.06H	06Z	0.9090	-0.3363	0.5912	0.4921	3.3689	3.7052	44
191.500.06H	06Z	0.9568	-0.3813	0.5404	0.3874	3.4713	3.8526	45
192.500.06H	06Z	0.9635	-0.3721	0.5262	0.3765	3.4880	3.8601	45
193.500.06H	06Z	0.9581	-0.1280	0.3958	0.3789	3.3698	3.4978	45
194.500.06H	06Z	0.9674	-0.2316	0.4229	0.3579	3.4582	3.6898	46

By-location files were also run through the statistical summary subroutine to generate data for each location: mean values, residuals, bias, correlation, and regression equation slopes and intercepts. Table 12 shows an example of this combined summary.

Table 12. Sample Statistical Summary File by Location. Each line was generated from stripping off location lines from each of the files listed such as that in Table 10.

ID	Corr	Bias	RMSE	RMSE%	StDev	%Stdev	Mean GPS	Mean MM5	n
ANP1	0.9938	-0.2673	0.2968	11.6236	0.1345	5.2659	2.5538	2.8211	13
ARP3	0.8072	-0.3427	0.5228	12.5932	0.4029	9.7060	4.1512	4.4939	25
AZCN	0.9554	-0.1466	0.2595	15.0628	0.2208	12.8136	1.7229	1.8695	17
BARH	0.9295	-0.0166	0.4668	16.5490	0.5387	19.0971	2.8210	2.8376	4
BARN	0.9474	-0.0101	0.2459	10.9260	0.2509	11.1516	2.2502	2.2603	24
BIL1	0.7005	0.0075	0.2624	15.0918	0.2704	15.5499	1.7388	1.7313	17
BLKV	0.9844	-0.2897	0.3549	11.2416	0.2128	6.7391	3.1574	3.4472	14
BLMM	0.9528	-0.4392	0.5988	21.5478	0.4196	15.0979	2.7789	3.2181	17
BLRW	0.9500	-0.5849	0.6719	28.9181	0.3535	15.2167	2.3234	2.9082	8

## IV. Results and Discussion

### 4.1 CONUS

**4.1.1 Case Studies.** Local storage restrictions limited the amount of MM5 data that could be downloaded from AFWA's FTP site. The MM5 data download was for only 90 days, so the cases available were restricted to a time period during the summer of 2001. Four cases were chosen and are discussed below. Each case was approximately 8 days long, resulting in four independent time periods totaling 30 days. The statistics developed were for a combination of the four cases.

**4.1.1.1 6-14 July 2001 "Ring of Fire".** In this case, strong high pressure centered near Memphis, TN dominated the eastern two-thirds of the country and restricted precipitation to the periphery of the air mass.

The southwest monsoon brought rain to Arizona and New Mexico. The stationary front dropped significant rainfall over Kansas, Missouri and the Ohio River Valley. Over the course of the week, a new system entered the through the Pacific northwest and worked its way across the country. Once it entered the plains, it prompted a strong squall line that worked its way across the country. See Figure 7 for a representative radar mosaic.

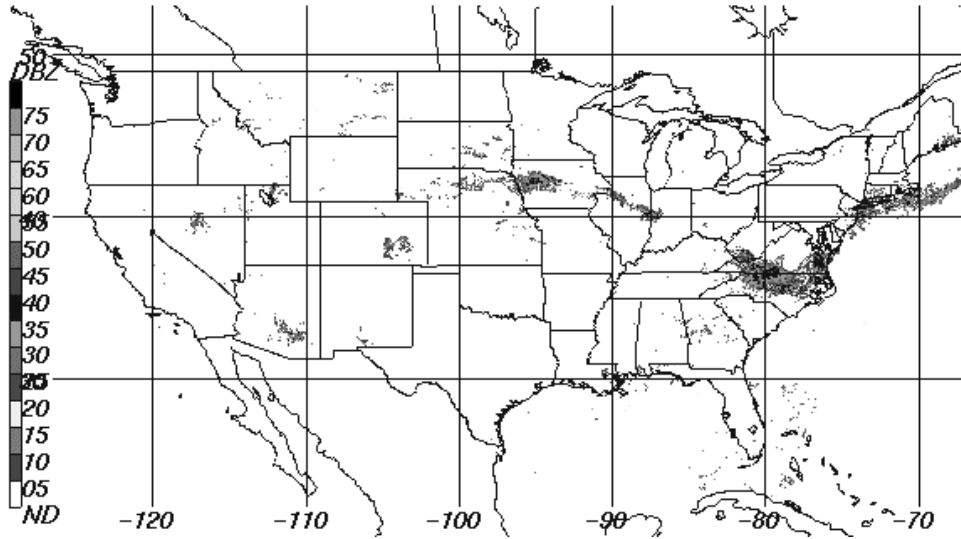


Figure 7. NEXRAD Mosaic Image from 15 UTC 8 July 2001. Note the radar reflectivities arcing across the northern plains and the Midwest. Image courtesy National Oceanic and Atmospheric Administration (NOAA 2002).

**4.1.1.2 25 July – 2 August 2001 “Central Plains Squall Line”.** At the beginning of this time period, the Bermuda high was dominating the southeast quadrant of the nation, while a stationary front draped across the central plains. The southwest monsoon was bringing rain to Arizona and New Mexico. The stationary front was sending significant rainfall over Kansas, Missouri, and the Ohio River Valley. Over the course of the week, a new system entered the country through the Pacific Northwest and worked its way across the country. Once it entered the plains, it prompted a strong squall line. Figure 8 shows a representative radar mosaic.

**4.1.1.3 11 - 18 August 2001 “Dirty Subtropical High”.** During this time period, the Bermuda high was the primary influence east of the Rockies. As seen in Figure 9, scattered showers and garden-variety thunderstorms erupted every afternoon. The monsoon was continuing to influence the desert southwest.

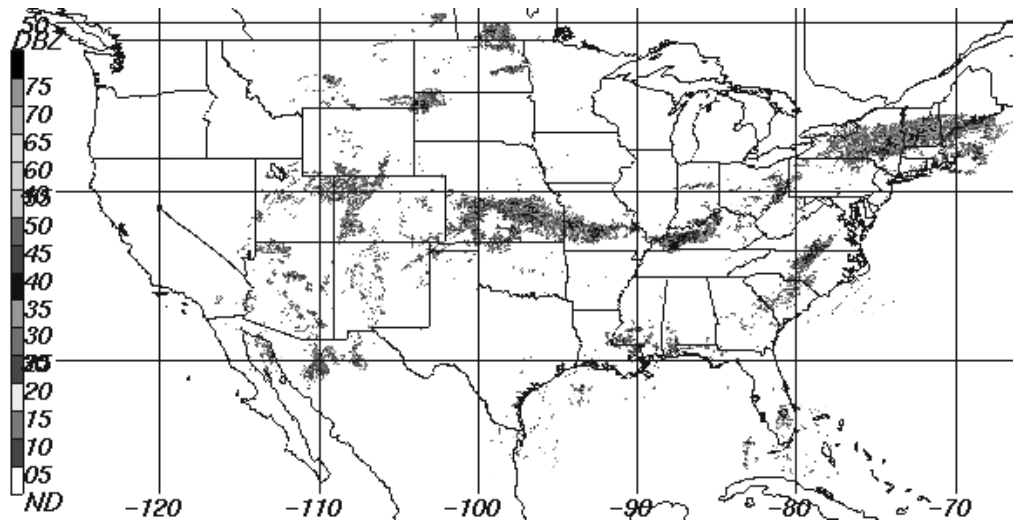


Figure 8. NEXRAD Mosaic Image from 09 UTC 25 July 2001. A stationary front bisected the nation and generated daily squall lines. Image courtesy of NOAA (2001).

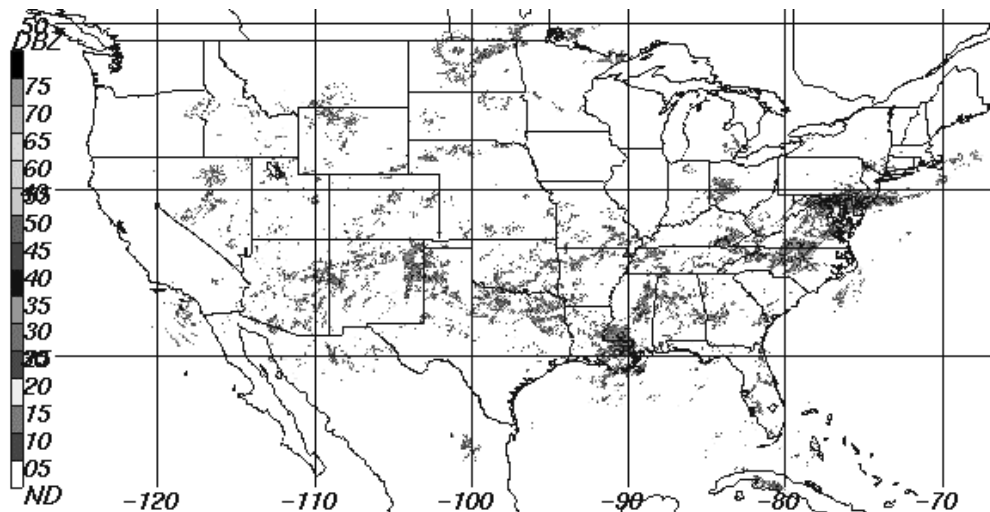


Figure 9. NEXRAD Mosaic Image from 00 UTC 12 August 2001. Image courtesy of NOAA (2001).

**4.1.1.4 10 – 15 September 2001 “Hurricane Gabrielle”.** Figure 10 shows mosaic imagery from just after Tropical Storm Gabrielle’s landfall. Gabrielle formed over the southeastern Gulf of Mexico and cut across the Florida peninsula. At the same time, the southwest monsoon was pumping moisture all the way up into the northern plains, causing showers and thunderstorms throughout.

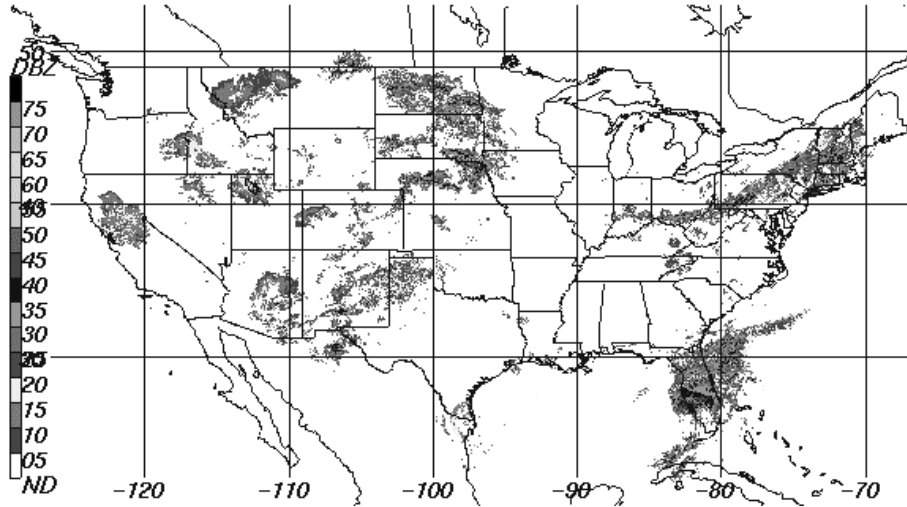


Figure 10. NEXRAD Mosaic Image from 08 UTC 14 September 2001. This image was from just after Tropical Storm Gabrielle's landfall near Venice, FL. Image courtesy of NOAA (2001).

**4.1.2 Domain Summary.** Figure 11 shows summaries of the domain-wide comparisons between GPS-derived and MM5-calculated precipitable water. In order to properly assess the data, it is important to understand the local diurnal patterns. Figure 11a shows the mean GPS and MM5 PW values for each forecast period. Note the significant diurnal variation in the GPS PW. The GPS PW was higher during the daylight hours and this results in higher correlations, lower root mean square errors and lower standard deviations when compared against the 06 UTC initialization products.

The maximum seen in the GPS-derived PW at the 06 UTC initialization occurs at 1500 local Central Standard Time, which is the estimated time of maximum heating. The minimum seen in the GPS 18 UTC Initialization occurs just before local sunrise. Note the 06 UTC and 18 UTC patterns crossing over each other just before 09H and 21H. This signature is hereafter referred to as a “crossover” in the graph. Both GPS-derived PW crossovers occur at their respective local sunrise and sunset. Note the MM5's lack of crossover compared to the GPS values.



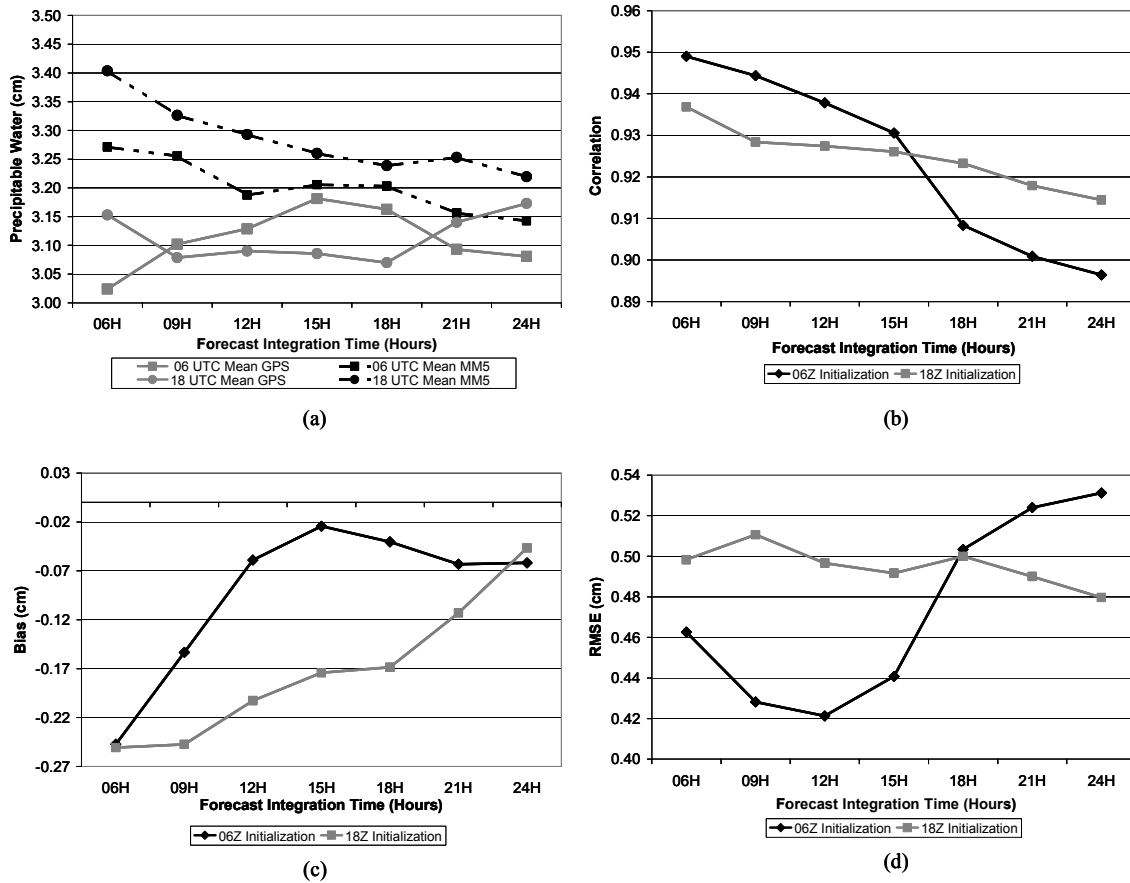


Figure 11. CONUS Domain-Wide Statistical Summaries. (a) Mean GPS-Derived PW and MM5 Calculated PW. (b) Correlation: GPS-Derived PW – MM5-Calculated PW. (c) Bias: GPS-Derived PW – MM5-Calculated PW. (d) RMSE of GPS-Derived PW – MM5-Calculated PW.

The highest correlations (Figure 11b) seemed to occur during the hours of sunlight, which could be attributed to the higher precipitable water content during the day. The crossover occurs just after local maximum heating in the 06 UTC initialization, and just before sunrise in the 18 UTC initialization. In addition, the local minima in bias (Figure 11c) seemed to occur during the day, as the hours approached that of maximum heating. However, in both cases, data noise must be taken into account as the forecast integration time progressed. Decreasing correlation and bias with forecast time is

expected, owing to the nature of numerical weather prediction: the further in the future one attempts to predict, the higher the error of the predictand.

The model's consistent moist bias (Figure 11c) arises from the nature of the moisture variables that are assimilated into the model. For the 06 UTC model run, drier moisture variables are entering the model, and that lack of moisture carries throughout. The converse is true with the 18 UTC model run. Figure 11a shows the model's lack of diurnal variation that the GPS-derived PW can provide.

RMSE in Figure 11d shows the same trends as correlation and bias. The highest values of GPS PW, which occurred during daylight hours, produced the least RMSE. The crossover occurred just after maximum heating in the 06 UTC run and just after minimum heating in the 18 UTC run.

**4.1.3 By-Location Summary Data.** Each forecast period for both initialization times was analyzed for each location in the CONUS GPS network. A thorough discussion of the 6-hour forecasts for both initialization times will be provided here; results for all forecast times are in Appendix C. Sections 4.1.2.1 and 4.1.2.2 discuss all locations' statistics, while Sections 4.1.2.3 and 4.1.2.4 review relationships that surfaced from analysis of these statistics.

**4.1.3.1 Summary statistics for the 06 UTC model initialization.** In this section, trends in comparisons between the GPS site and the MM5 output for each location will be reviewed. Figure 12 shows the mean correlation of each location's 06 hour forecast in the CONUS GPS network. Medicine Bow, Wyoming's (MBWW) low correlation stands out, but its low corresponding number of samples will explain the

anomaly. The mean correlation for all GPS receiver locations was 90.0%, while the mean correlation for locations with more than 10 samples was 91.5%.

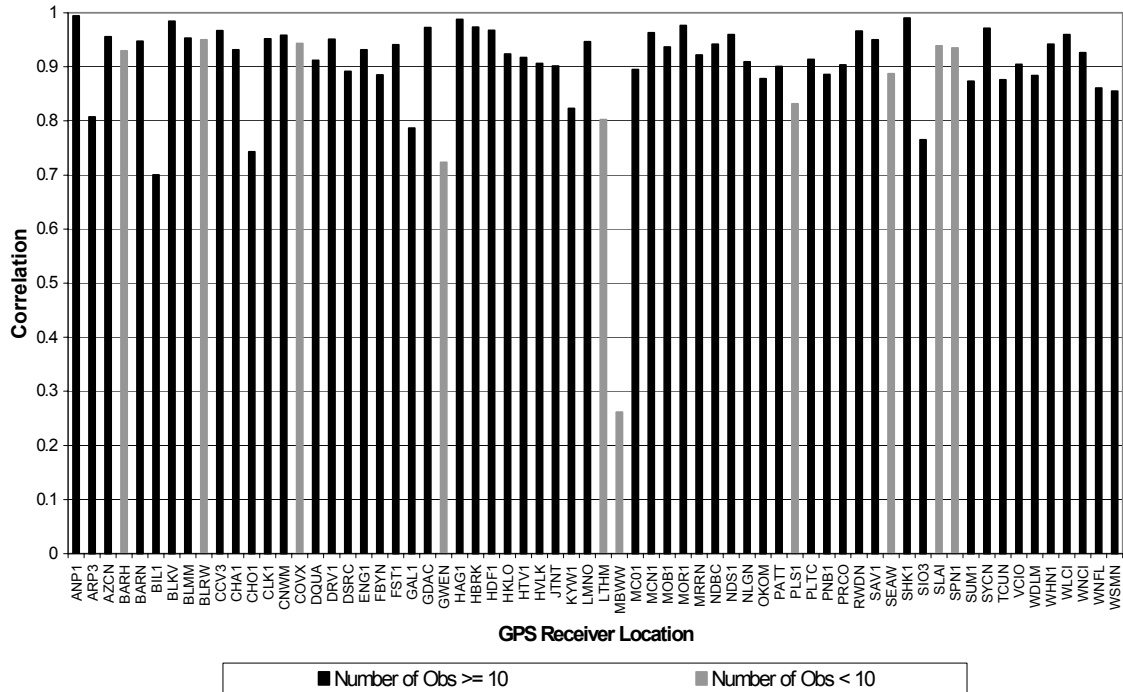


Figure 12. Mean Correlation of Each GPS Receiver Location: CONUS 06 UTC Initialization, 06-Hour Forecast. The locations with gray columns were calculated with less than 10 samples.

Figure 13 shows the mean bias at each location. As is seen in the domain-wide bias summary (Figure 11c), there was an overwhelming moist bias in the majority of the locations. It is interesting to point out that of the eleven sites with positive bias, nine of the sites are west of the Mississippi River. The dependence of the bias on the number of samples in each location calculation seems to be of minimal value in this case: the mean bias of all locations was  $-0.240$  cm, while the mean bias of only locations with more than 10 samples was  $-0.241$  cm. The western sites' drier model outputs most likely were the cause of a positive bias. Sites with a mean GPS PW reading of more than 4 cm had a

bias of  $-0.38$  cm, while those with mean PW readings of less than 2 cm had a bias of  $-0.19$  cm.

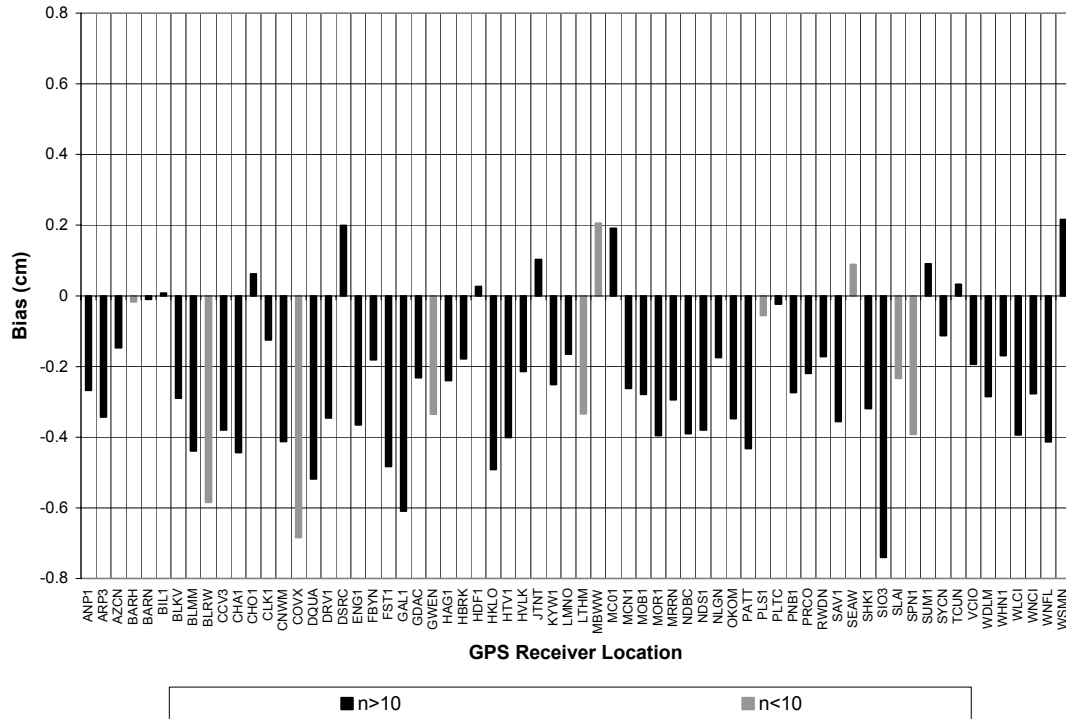


Figure 13. Mean Bias of Each GPS Receiver Location: CONUS 06 UTC Initialization, 06-Hour Forecast. The gray columns are locations that had less than 10 samples in the statistic's calculation. A negative bias signifies the model having more moisture than the GPS receiver site.

Figure 14 shows the RMSE expressed as a percentage of the location's mean GPS precipitable water value. This normalizes the environmental differences between arid (i.e., Arizona) and humid (i.e., Florida) regions throughout the domain. Like correlation and bias, most of the high RMSE locations also happen to have a low sample set. However, if we were to remove all low sample set sites, two sites still stand out as having high RMSEs, Flagstaff, AZ (FST1) and La Jolla, CA (SIO3). The mean normalized RMSE for all sites is 16.49% of the mean GPS PW value, while the mean for sites with more than 10 samples is 15.5%.

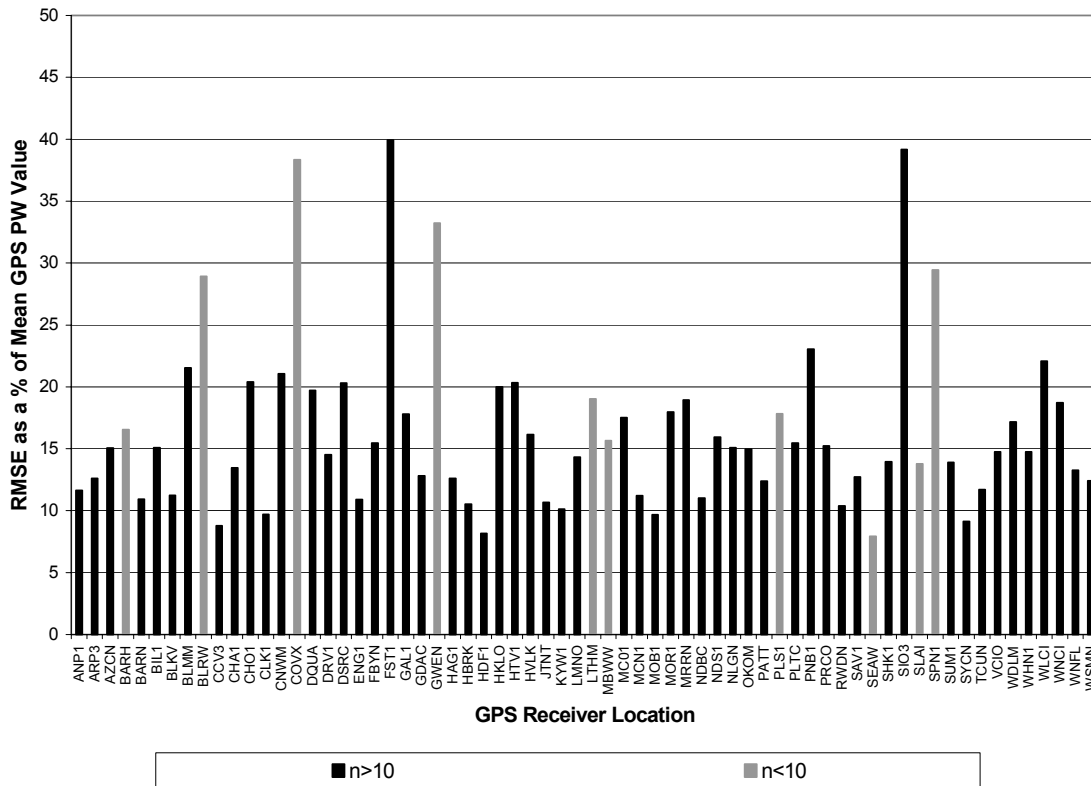


Figure 14. Mean Normalized RMSE of Each GPS Receiver Location: CONUS 06 UTC Initialization, 06 Hour Forecast. The value calculated as  $(RMSE/\text{mean GPS PW}) \times 100$ . The gray columns are locations that had less than 10 samples in the statistic's calculation.

Standard deviation as a percentage of mean GPS precipitable water is shown in Figure 15. Again, by considering those sites with less than 10 samples as questionable, many of the highest standard deviation-sites can be eliminated from the summary. Even if the low-sample sites are eliminated, La Jolla, CA (SIO3) remains as an anomalously high standard deviation. All GPS sites produced a mean normalized standard deviation of 12.37%, while the mean of sites with more than 10 samples was 11.8%.

**4.1.3.2 Summary statistics for the 18 UTC model initialization.** The 18 UTC model output was treated as a separate entity in this study to offset any diurnal differences between the twice-daily runs.

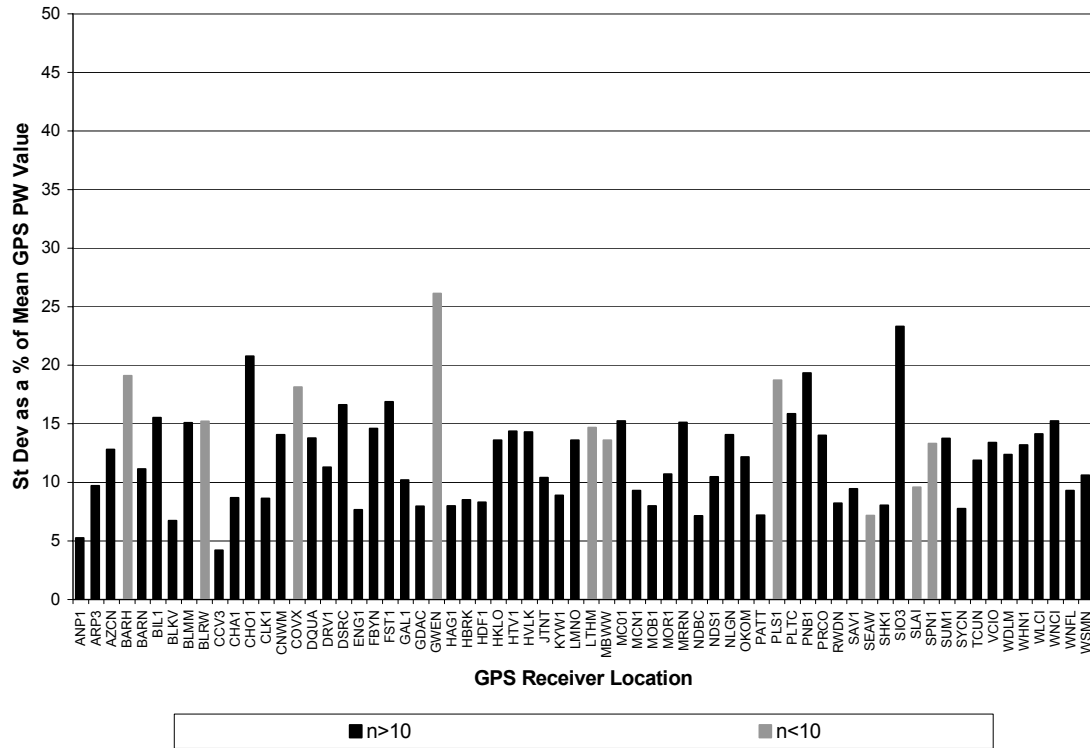


Figure 15. Mean Normalized Standard Deviation of Each GPS Receiver Location: CONUS 06 UTC Initialization, 06 Hour Forecast. The value is calculated as (standard deviation/mean GPS PW)\*100. The gray columns are locations that had less than 10 samples in the statistic's calculation.

Correlation at each of the GPS sites is shown in Figure 16. Again, the lowest correlations have less than 10 samples available for calculation, but Flagstaff, AZ (FST1) still has a low value. The mean correlation of all sites was 84.2%, while the mean correlation of all sites with more than 10 samples was 87.1%.



Figure 17 shows the mean bias for each GPS site. Like the 06 UTC model run, there are very few locations with positive bias. Two of the three positive bias locations had low samples, and the remaining site is Boulder, CO (DSRC), which is in a relatively arid location. The mean bias of all sites was  $-0.237$ , while the mean bias of sites with more than 10 samples was  $-0.255$ , more negative due to removing Bartlett, NH's (BARH) anomalous statistic.

Figure 18 shows the normalized mean RMSE for the 18 UTC model run. The anomalous sites with more than 10 samples were Chico, CA (CHO1), Flagstaff, AZ (FST1), La Jolla, CA (SIO3), and Wolcott, IN (WLCI). The mean normalized RMSE for all sites was 17.9%, while that for sites with more than 10 samples was 16.7%.

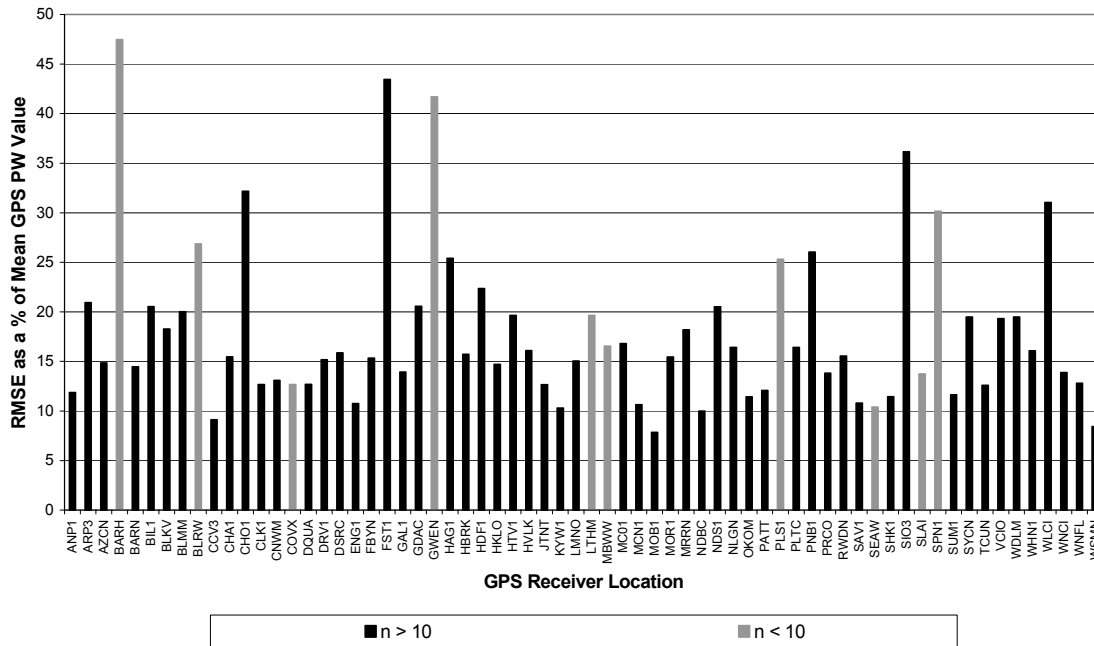


Figure 18. Mean Normalized RMSE of Each GPS Receiver Location: CONUS 18 UTC Initialization, 06-Hour Forecast. The value is calculated as  $(\text{RMSE}/\text{mean GPS PW}) \times 100$ . The locations with gray columns were calculated with less than 10 samples.



The mean normalized standard deviation is shown in Figure 19. The mean normalized standard deviation for all sites was 15.16%, while those sites with more than 10 samples had a mean of 14.15%.

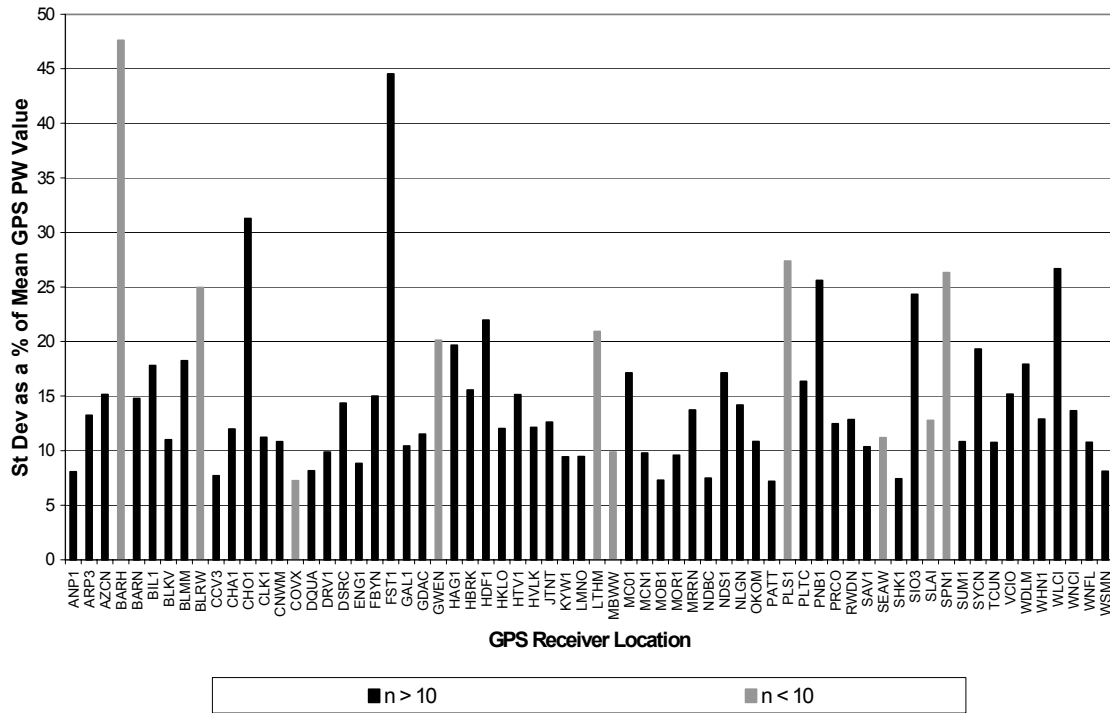


Figure 19. Mean Normalized Standard Deviation of Each GPS Receiver Location: CONUS 18 UTC Initialization, 06-Hour Forecast. The value is calculated as  $(\text{standard deviation}/\text{mean GPS PW}) \times 100$ . The locations with gray columns were calculated with less than 10 samples.

**4.1.3.3 Dependence on number of observations.** As evidenced by the previous two sections, many of the statistics were altered due to some locations having few GPS observations available. Figures 20 and 21 show the number of data points available for generating the statistics in Sections 4.1.2.1 and 4.1.2.2. The mean n for the calculations from the 06 UTC 06 hour forecasts was 18.4, while stripping the sites with less than 10 samples provided a mean n of 20.4. For the 18 UTC model run, the total mean n was 17.3, while the mean n of those sites with 10 or more samples was 19.3.

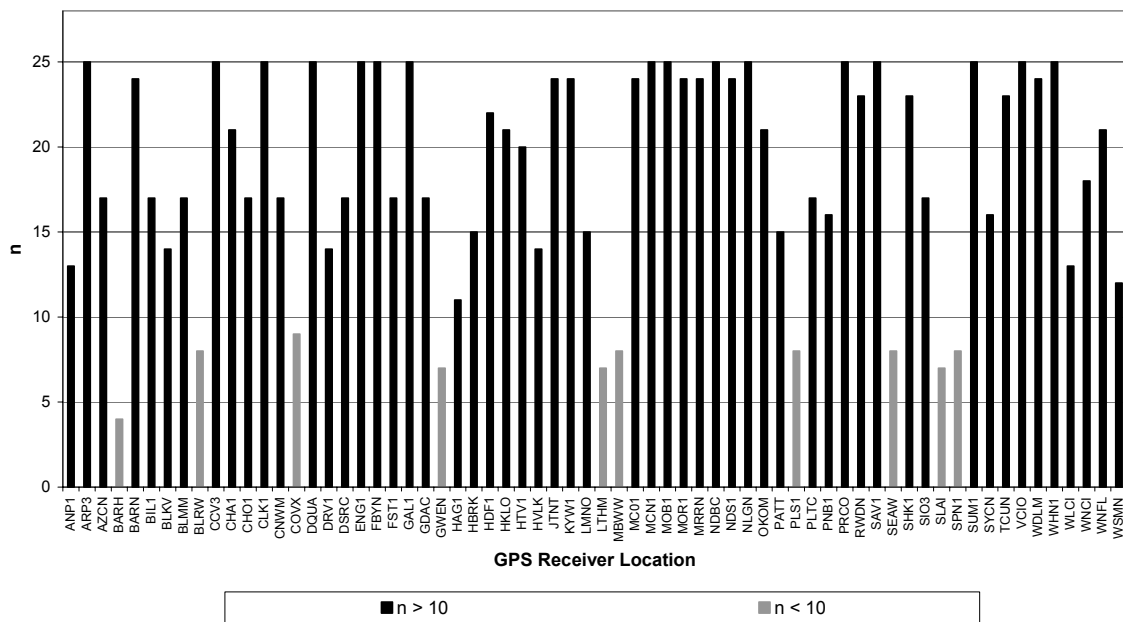


Figure 20. Number of Observations Available for Calculating the 06 UTC Initialization, 06 Hour Forecast Statistics.

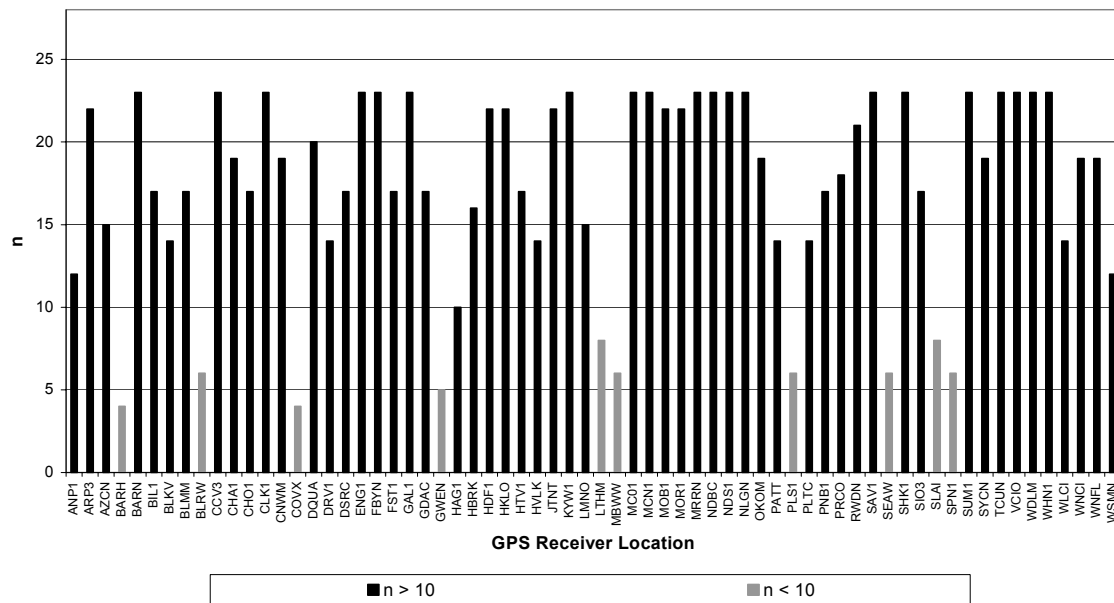


Figure 21. Number of Observations Available for Calculating the 18 UTC Initialization, 06 Hour Forecast Statistics.

#### 4.1.4 Special Studies.

**4.1.4.1 Moist vs. Dry Regimes.** The differences between moist regime and dry regime sites are shown here. The statistics were separated into those sites with mean GPS PW values greater than 4 cm, and those with mean GPS PW values of less than 2 cm. The 18 UTC initialization, 6 hour forecast is the only one reviewed here. Other date/time groups performed comparably. Figure 22 shows the increased error and noise attributed to the less humid GPS receiver sites, and how the MM5 depicts those moisture patterns.

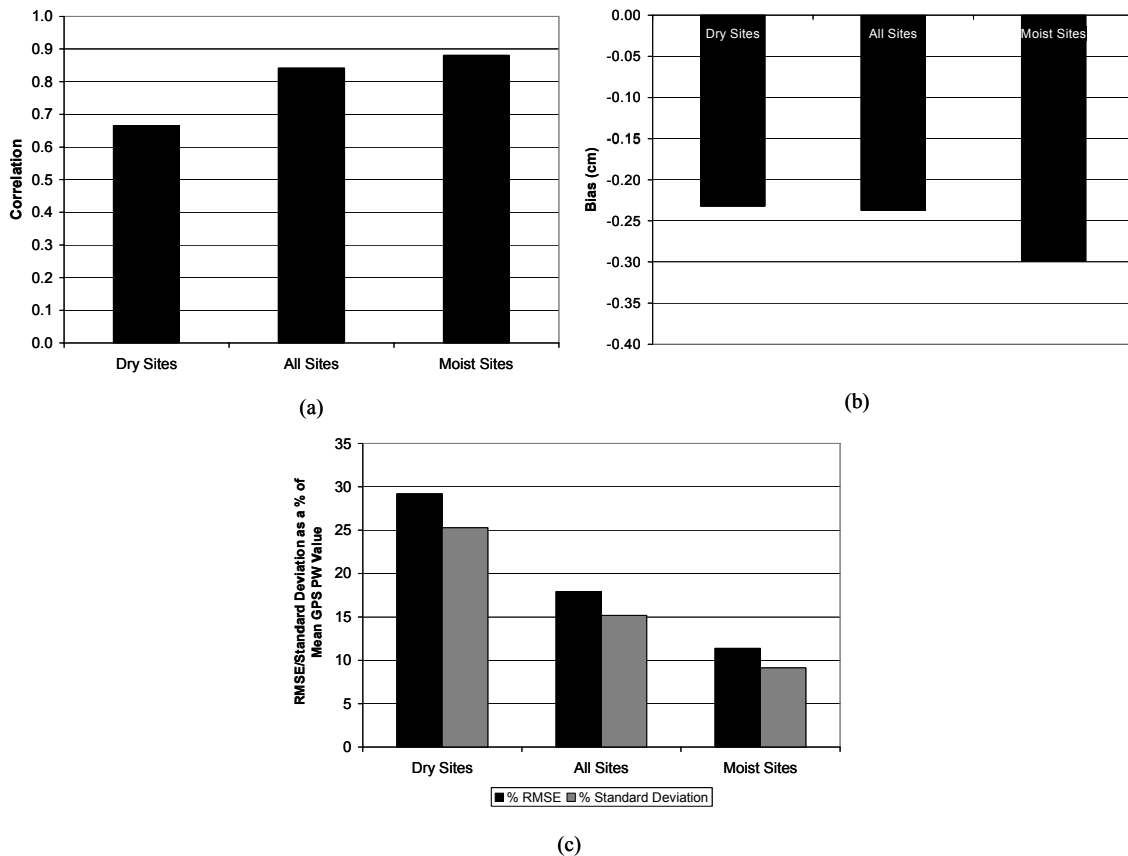


Figure 22. Moist Sites vs. Dry Sites Statistical Summaries: CONUS 18 UTC Initialization, 06 Hour Forecast. (a) Correlation (b) Mean Bias. Bias is defined as (GPS PW – MM5 PW) (c) Mean Normalized RMSE and Standard Deviation. RMSE calculated as (RMSE/mean GPS PW)\*100 and standard deviation calculated as (st dev/mean GPS PW)\*100. Dry sites had a mean GPS PW values of less than 2 cm, while the moist sites had a mean GPS PW values of more than 4 cm.

**4.1.4.2 Error Dependence on Elevation and Elevation Residual.** One of the sources of error in this study was the terrain height difference between each GPS site and its MM5-interpolated site elevation, based on the GRIB file's terrain height parameter. In addition, the inverse proportion between site elevation and mean precipitable water had an impact on the statistics. The elevation values for each GPS receiver site are in Appendix A.

The mean normalized standard deviation for each site was plotted against the GPS site elevations and the difference between the GPS site elevation and the MM5 interpolated elevation. The expected relationship for this comparison was that the lower elevation sites, having more vertical atmosphere through which a GPS signal could refract, would have the highest standard deviation, and that the higher elevation sites would have smaller standard deviations, such that an inverse proportionality would exist.

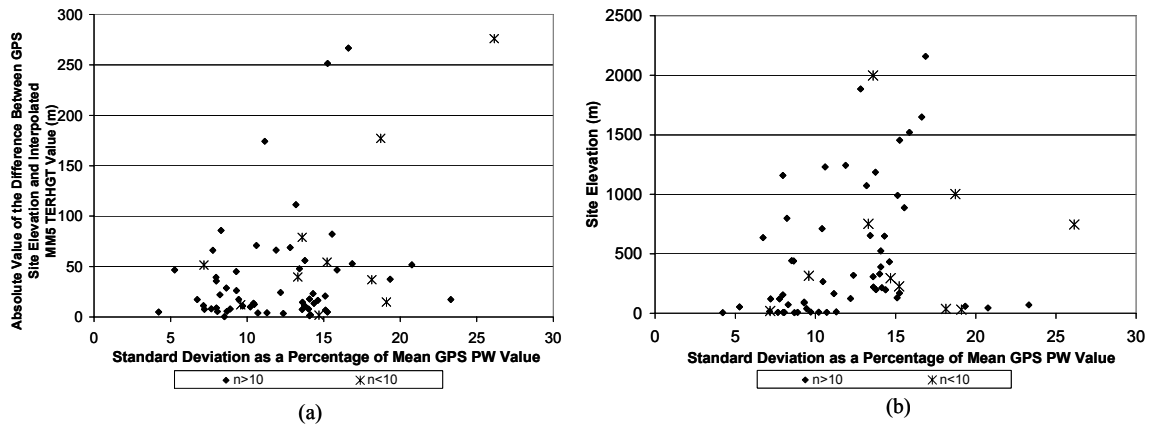


Figure 23. Elevation Comparisons: CONUS 06 UTC Initialization, 06 Hour Forecast. The diamonds are sites with  $n \geq 10$ , while the stars are sites with  $n < 10$ . (a) Mean Normalized Standard Deviation Plotted Against Absolute Value of Elevation Residual. (b) Mean Normalized Standard Deviation Plotted Against GPS Site Elevation.

Figure 23 shows the results of the two comparisons. Sites with less than 10 samples in the calculation were displayed in a different shape to highlight their positions on the chart. The expected relationship did not appear in these cases, but there are numerous other factors that could be clouding the expected relationship, such as model performance at high elevations.

The results seen in Figure 23 seemed to agree better with the comparison made in Section 4.1.3, that drier GPS sites had higher standard deviations than more humid sites. Most of the high-elevation GPS sites were in arid locations, to include Aztec, NM, Grand Junction, CO and Flagstaff, AZ.

**4.1.5 RAOB Comparison.** GPS sites within a prescribed distance of a RAOB site (as explained in Section 3.1.3) underwent additional analysis. The results are shown and discussed below.

Table 13. Summary of GPS-RAOB Comparisons in CONUS. Geodetic information about the RAOB sites is provided in Appendix C.

RAOB Site	GPS ID	Mean GPS		Mean RAOB		Correlation		Bias		%RMSE		%StDev		n
		Coastal	Inland	Coastal	Inland	Coastal	Inland	Coastal	Inland	Coastal	Inland	Coastal	Inland	
CHS	CHA1	4.30		4.66		0.97		-0.37		10.11		5.46		49
CRP	ARP3	4.32		4.42		0.91		-0.09		9.81		9.63		85
DEN	DSRC		1.80		1.88		0.95		-0.08		12.16		11.30	85
FLG	FST1		1.30		1.54		0.98		-0.23		19.93		8.97	64
SGF	CNWM		3.10		3.29		0.96		-0.19		12.53		10.77	61
SIL	NDBC	4.27		4.49		0.98		-0.21		7.49		5.63		88
XMR	CCV3	5.14		5.12		0.85		0.02		6.87		6.94		43
Means		4.30	2.07	4.52	2.24	0.95	0.96	-0.22	-0.17	9.13	14.87	6.91	10.35	72

Table 13 shows the summaries of the GPS-RAOB comparisons. Note the differences between inland and coastal sites. All sites showed the radiosondes producing higher average PW measurements than the GPS receivers. A likely explanation for this

negative bias is the possibility of moisture loading when a radiosonde travels through a cloud or precipitation layer.

This study was conducted during the warmest and most humid of the year (July-September 2001). This impacts how high the PW readings can become, particularly along the coast. Another reason for such high radiosonde readouts is the coastal sites are all on the eastern coasts (either Atlantic or Gulf of Mexico), thus being susceptible to the prevailing westerly winds that would tend to send the radiosonde balloons over the water, perhaps to air with higher PW. In addition, it is appropriate to point out the differences in how GPS-derived PW is calculated compared to radiosonde PW, as detailed in Section 3.2.8. Recall that the GPS measurements infer PW from the refraction of the signal through the total atmosphere, while the RAOB is integrating layers of mean mixing ratio through the troposphere and perhaps part of the stratosphere. Figure 24 shows some statistics comparing inland and coastal sites. The statistics in this figure are calculated only from the sites listed in Table 13.

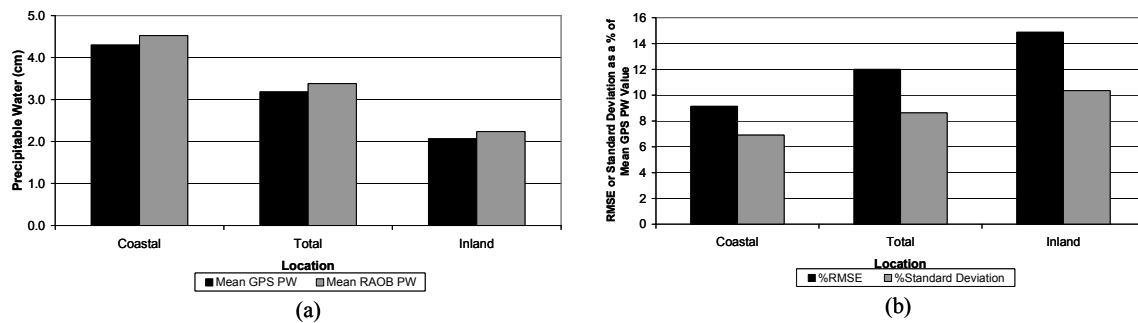


Figure 24. GPS/RAOB Coastal vs. Inland Statistical Summaries. (a) Mean GPS and RAOB PW Grouped by Region. (b) Mean Normalized RMSE and Standard Deviation. The RMSE is calculated as  $(\text{RMSE}/\text{mean GPS PW value}) \times 100$  and standard deviation is calculated as  $(\text{standard deviation}/\text{mean GPS PW value}) \times 100$ .

## 4.2 Alaska

**4.2.1 Case Study.** There was little choice in finding a time period for study in Alaska. The choices for which days to perform comparisons was restricted to the 90-day archive of MM5 GRIB data. During the period of time covered in AFIT's MM5 archive, there was only one 24-day window with GPS-MET observations encompassing all four Alaska GPS sites. At the other times, at least one of the receiver sites did not produce data. Therefore, the Alaska study took place from 6 – 29 July 2001. A number of extratropical cyclones still traversed the study area, bringing the variations in moisture that were desired for a good sample. Figure 25 shows a representative satellite image, with an extratropical cyclone moving across the state. During this period of study, a cyclone such as this one traversed the state approximately once a week. The satellite images available for this time period could only resolve the southern two-thirds of the state, but this didn't impact the quality of the study, for all four of the Alaska GPS receiver sites were in the southern two-thirds of the state.

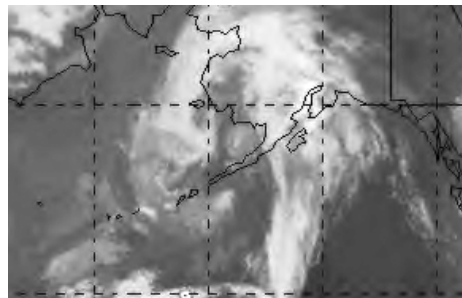


Figure 25. Representative Alaska IR Satellite Image from 12 UTC 19 July 2001. Image courtesy of NOAA (2001).

**4.2.2 Domain Summary.** Figure 26 shows the summaries of the domain-wide comparisons between the Alaska GPS-MET network and the 15 km Alaska MM5

window. The GPS observations were only those that were compared with MM5 data. If no MM5 data was available on a particular model run, then no GPS data was collected for that DTG.

Figure 26a shows the mean GPS PW and mean MM5 PW. The maximum seen in the GPS 12 UTC initialization occurs at 1800 Alaska Time, which is the estimated time of maximum heating. The minimum seen in the GPS 00 UTC initialization occurs just before local sunrise. Both crossovers occur just before their local sunset. Note the lack of diurnal variation in the MM5 lines. The diurnal variations are similar to what is seen in Figure 11 for CONUS.

It is important to point out that diurnal cycles are different in Alaska than in CONUS. In Fairbanks, sunrise in July was between 0213 (1 July) and 0349 (31 July) local time, while its sunsets ranged from 2335 (1 July) through 2203 (31 July). This resulted in a larger maximum in the mean GPS PW plot to accommodate for the longer period of heating. On these charts, sunrise occurred between the 12- and 15-hour forecasts on the 00 UTC initialization only. Sunsets were at the 09-hour forecast time on the 00 UTC line and the 21-hour forecast on the 12 UTC line. Like the CONUS scenario, the MM5 output doesn't seem to reflect the impacts of daily heating on its precipitable water values.

Figure 26b is the mean correlation of the Alaska domain, while Figure 26c shows the mean bias throughout the domain. The crossover between the 06- and 09-hour forecast occurs as the 00 UTC model run is about to experience sunset, while, at the same time, the 12 UTC model has experienced sunrise. The best correlation seemed to occur in the 00 UTC initialization, when maximum heating was *not* taken into account during



this time period. As is expected, the model run with the minimum of bias has the better correlation. The model had a dry bias in this theater, and the model's lack of diurnal variation resulted in a better-looking performance at the 00 UTC model run.

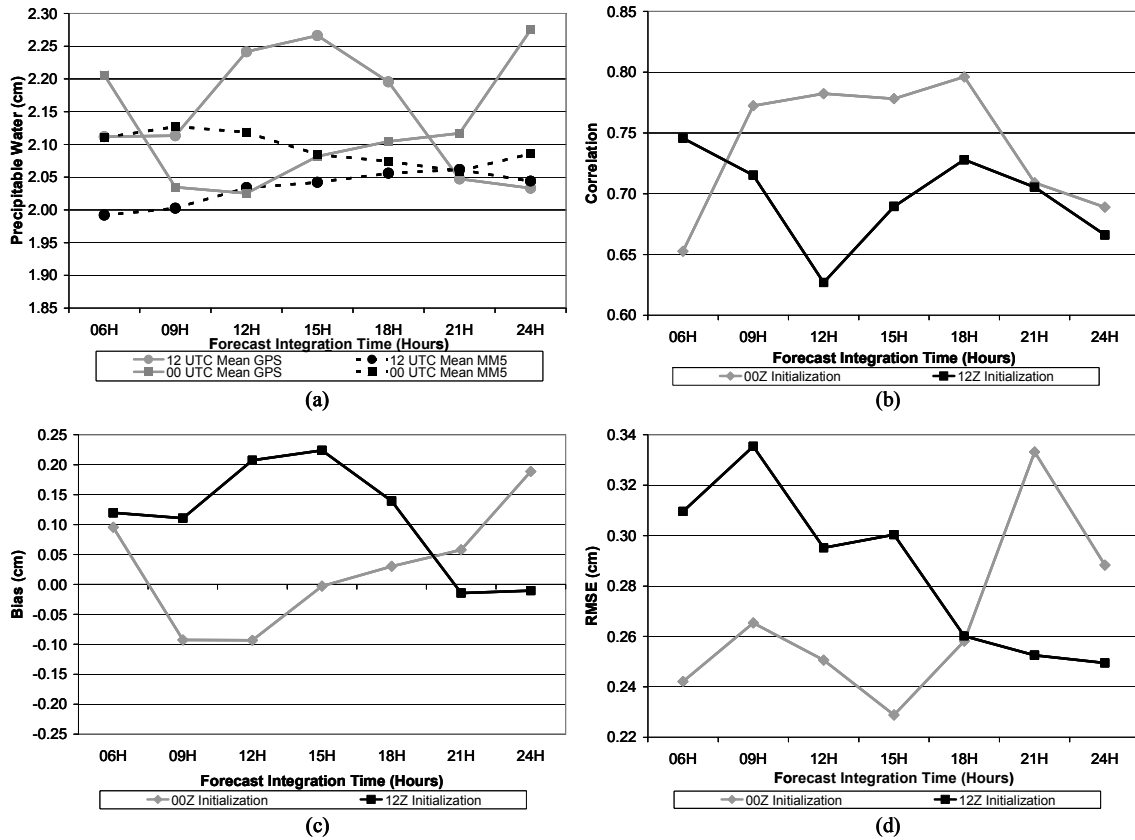


Figure 26. Alaska Domain-Wide Statistical Summaries. (a) Mean GPS-Derived and MM5-Calculated PW. (b) Correlation: GPS-Derived PW – MM5-Calculated PW (c) Bias: GPS-Derived PW – MM5-Calculated PW. (d) RMSE of GPS-Derived PW – MM5-Calculated PW.

Finally, Figure 26d shows the RMSE for the comparisons. Again, the errors seemed to be highest during the parts of the day with solar heating. The lowest errors occur at nighttime, between midnight and 0600L. It is unusual that the 12 UTC initialization's RMSE starts out lower at the 06-hour forecast, and then increases with

forecast integration time. This is again attributed to the onset of maximum heating as the forecast period progresses.

**4.2.3 By-Location Summary Data.** A clearer picture of the comparison can be seen looking at individual location data. The 06-hour forecasts for the 00 and 12 UTC model runs will be discussed here, while the complete data summaries are provided in Appendix C.

**4.2.3.1 Summary statistics for the 00 UTC model initialization.** In this section, trends in comparisons between the GPS site and the MM5 output for each location will be reviewed. In this theater, all locations averaged more than 10 observations, so no separate “low-n” statistics needed to be computed.

Figure 27a shows the mean correlation of the 00 UTC 06 hour forecast. All correlations were at least 80%, which is a desirable value. The mean correlation was 89%.

Figure 27b is the mean bias of each location. As was seen in the domain-wide data, most of this case study showed the model having a dry bias compared to the GPS network. This is corroborated here, showing only a minimal moist bias at the two northernmost sites, Central (CENA) and College (CLGO). The mean bias was 0.8 mm, with the GPS sites more moist than the MM5.

Figures 27c and 27d are the mean normalized RMSE and standard deviation for the Alaska locations. All of the sites performed well, with a mean normalized RMSE of 10.9%, and the mean normalized standard deviation of only 8.81%. College, AK, performed significantly better than the other three sites, bringing to light a concern about

the differences between the GPS sensors. The College GPS site is part of a sub-network independent of NOAA's wind profiler network, which controls the other three GPS-MET sites in Alaska. The College sensor has a different antenna than the other three locations, a TRM33429.00 L1/L2 Micro Centered with Ground Plane, compared to the TRM22020 L1/L2 Compact with Ground Plane at the other three sites.

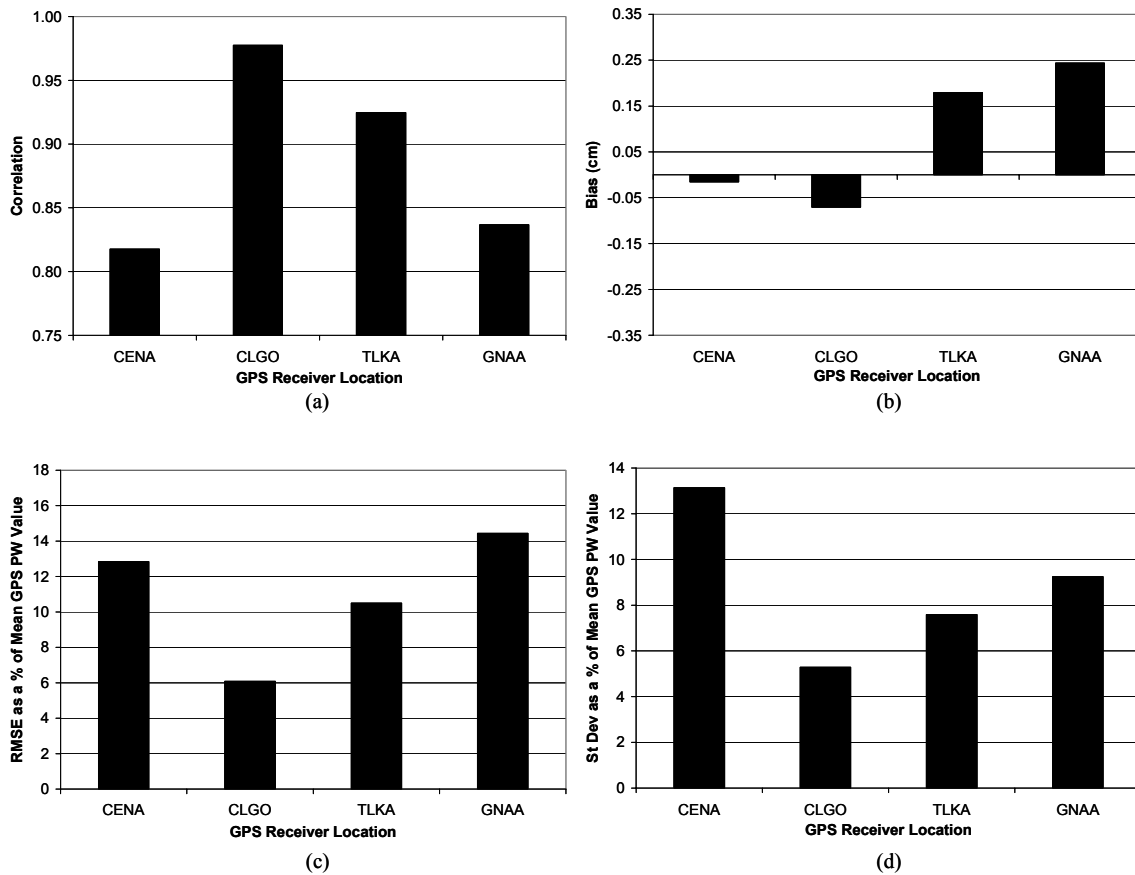


Figure 27. Alaska By-Location Statistical Summaries: 00 UTC Initialization, 06 Hour Forecast. (a) Mean Correlation. (b) Mean Bias. A negative bias signifies the model having more moisture than the GPS receiver site. (c) Mean Normalized RMSE. The value calculated as  $(RMSE/\text{mean GPS PW}) \times 100$ . (d) Mean Normalized Standard Deviation. The value is calculated as  $(\text{standard deviation}/\text{mean GPS PW}) \times 100$ .

**4.2.3.2 Summary statistics for the 12 UTC model initialization.** In this section, trends in comparisons from the 12 UTC model run will be reviewed.

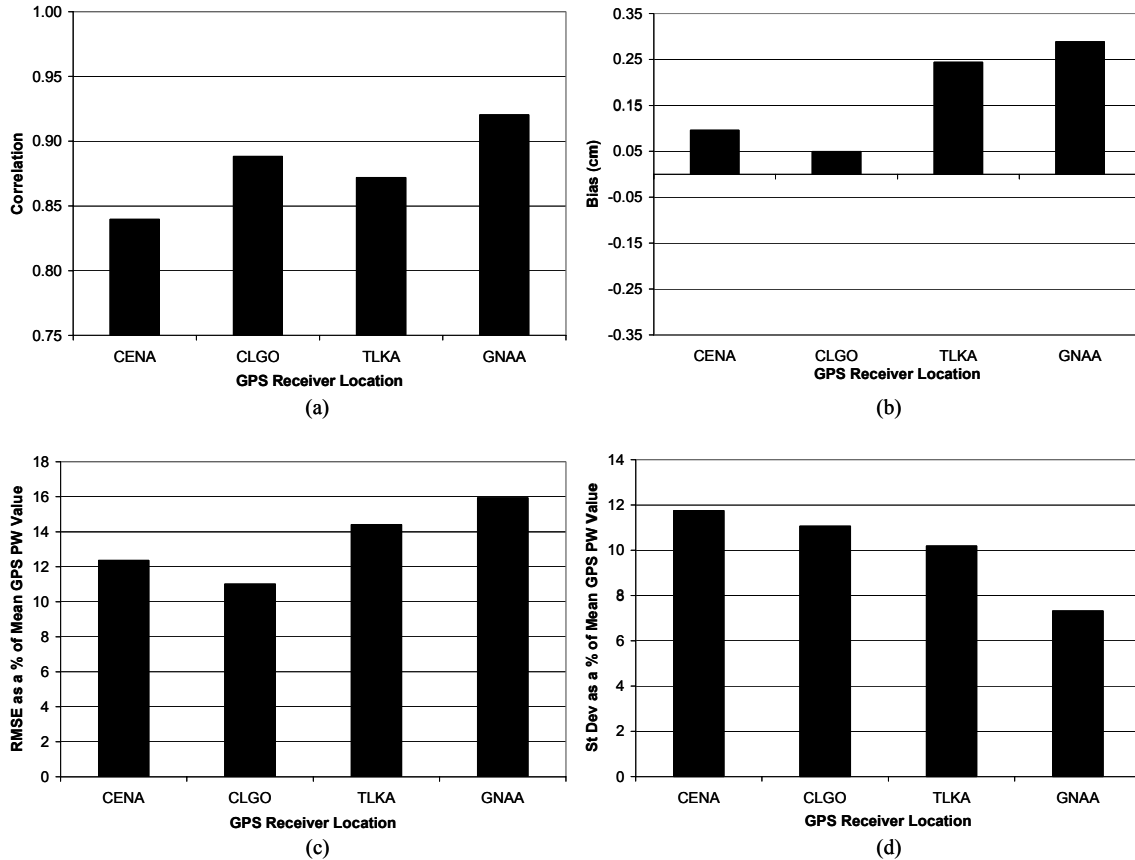


Figure 28. Alaska By-Location Statistical Summaries: 12 UTC Initialization, 06 Hour Forecast. (a) Mean Correlation. (b) Mean Bias. A negative bias signifies the model having more moisture than the GPS receiver site. (c) Mean Normalized RMSE. The value is calculated as  $(\text{RMSE}/\text{mean GPS PW value}) \times 100$ . (d) Mean Normalized Standard Deviation. The value is calculated as  $(\text{standard deviation}/\text{mean GPS PW}) \times 100$ .

Figure 28a shows the correlation between the GPS network observations and the model observations' 6 hour forecasts that were valid at the same time. All four sites showed reasonable correlations, with the mean of all sites being 88.01%. Figure 28b is the bias for the four locations. Note the distinct positive bias at all four locations, which coincided with the stronger positive bias on the 12 UTC forecast line in Figure 26c, the domain-wide mean bias. Talkeetna and Glenallen have the strongest biases, and it is of note that those two stations are the furthest south. The mean bias for all four sites is 1.69 mm.

Figure 28c shows the mean normalized RMSE for all four locations. As is the case with the bias, the southernmost two sites have the highest percentages of RMSE, with the mean through all four sites being 13.43%. The mean normalized standard deviation is shown in Figure 28d. In this case, the stations with the highest standard deviations, College and Central, have the smallest biases and RMSEs.

**4.2.4 RAOB Comparison.** In the Alaska theater, only one of the four GPS sites was near a RAOB site: College (CLGO) is 5.59 km away from the Fairbanks (FAI) radiosonde launch site. The raw radiosonde data was downloaded from the NOAA FSL RAOB site (<http://raob.fsl.noaa.gov>) and PW was computed using a NOAA algorithm. However, the algorithm, when computed on only the mandatory and significant levels that the web site provides, tends to overestimate the radiosonde PW values. This method of computation is different than how NOAA ordinarily computes PW. NOAA has the ability to use the balloon output that's transmitted every second, providing a much more robust database.

Thirty-seven soundings were evaluated with their respective GPS PW measurements and the summary statistics are shown in Table 14 below. Like in CONUS, the RAOB produced a higher average PW value, but in this case the differences are attributed to the errors inherent in computing the radiosonde PWs without using enough levels.

Table 14. Summary Statistics of Fairbanks GPS-PW and RAOB-PW Comparison.

<b>Statistic</b>	<b>Value</b>
Mean GPS PW	2.07
Mean RAOB PW	2.70
Correlation	0.86
Bias	-0.63
RMSE	0.50
Standard Deviation	0.33
n	37

## **V. Conclusions**

This study compared GPS-derived precipitable water with the AFWA MM5, in hopes of recommending future Air Force actions regarding the precipitable water data set. The potential impacts of the GPS PW on moisture forecasts provide much promise for assimilation into Air Force operational models, particularly when the 3DVAR assimilation system comes on line at AFWA. In addition, AFWA could also investigate placement of their own GPS-MET sensors in data sparse locations; the passive remote sensing capability would serve military operations well.

It is important to point out here that the results generated in this study were restricted to the summer season only, so they may not accurately represent other times of year. Also, the errors that did develop cannot be singly attributed to either shortcomings in the GPS observing network nor that of the MM5. These conclusions emphasize the quantitative differences between the two data sets and qualitative observations about the model and the GPS observing system.

The variations that were expected between the two theaters do exist, but it is not known which data set contributed more to the differences. It is likely that the MM5 physics packages, which are the same in both CONUS and Alaska, act differently in the two climate regimes.

The biases that originated from these comparisons were expected to have been the same order of magnitude as other independent comparisons between GPS networks and NWP models. This was found to be true in both CONUS and Alaska.

## **5.1 CONUS Conclusions**

**5.1.1 Domain-Wide Conclusions.** The GPS PW patterns demonstrate the significant diurnal variations that cannot be captured with the existing radiosonde network. The MM5 values performed comparably to the GPS PW at initialization times, but the MM5 does not account for the diurnal changes that occur; the lack of diurnal changes in the MM5 resulted in increased error as the forecast progressed.

The MM5 values were consistently more moist than what was measured with the GPS receivers. This could be attributed to the consistent moist bias the radiosondes seemed to have compared to the GPS network. In addition, the MM5's 18 UTC model run initialized with higher moisture than the 06 UTC run. However, the lack of diurnal variation in the MM5 moisture patterns resulted in consistently higher moisture values throughout the period.

Additionally, the 06 UTC model runs matched the GPS network better than did the 18 UTC runs. A possible reason for this is the higher GPS values in the first 15 hours of the 06 UTC forecast matching the consistently higher MM5 forecast outputs. Finally, in both model runs, the RMSE approached minimum values during the day's local peak heating, when the GPS PW values were the highest.



**5.1.2 By-Location Conclusions.** When assessing individual location trends, it is apparent how important it is to have a sufficient sample size to compute the statistics. Any statistics calculated with less than 10 observation-model pairs were taken out of the calculation and a separate statistic was made available for comparison.

Significant errors persisted in some locations despite removing those sites with less than 10 observations available. The trend in these sites is that most were in the western United States, and one site in particular was on the west coast. Western sites may have inherent model errors due to the lack of upstream initialization information.

A comparison was made with coastal versus non-coastal sites and the differences demonstrated the impact the high number of coastal sites has on the quality of the network when compared to the MM5. It is also of note that most of the coastal sites are Coast Guard/Army Corps of Engineers sites, which often have different models of GPS receivers and antennas than many of the inland sites. The coastal sites had higher errors and biases than the inland sites.

## **5.2 Alaska Conclusions**

**5.2.1 Domain-Wide Conclusions.** Alaska's GPS network consistently observed higher PW values than the MM5 output. In this case, the best correlations occurred during minima in heating. Alaska's summertime sunrise and sunset schedules created an interesting diurnal PW pattern. These caused longer heating periods and probably drove the GPS network's readings to be much higher than the MM5.

**5.2.2 By-Location Conclusions.** Two interesting points came out of the by-location analyses. First, the northern sites, College (CLGO) and Central (CENA) had a negative model bias in the 00 UTC model run, likely due to the model initializing right before local sunset, thus driving the GPS values lower than the MM5.

Secondly, the College (CLGO) GPS site performed markedly better than the other three sites. Two possibilities arise from this observation. One is that the CLGO antenna is a different model than the other three in Alaska. The other option is the terrain surrounding the stations having an impact on the prevailing localized weather patterns.

### **5.3 Recommendations for Future Work**

Three major areas require attention for future work: comparisons of GPS-derived PW from other networks with other AFWA MM5 global domains, assimilation of GPS-derived values into the MM5, and vertical profiling of GPS-derived moisture parameters.

Many other GPS-Meteorology networks exist worldwide for various research endeavors. Matching other AFWA MM5 domain windows with these GPS-MET networks allows many opportunities for additional data and comparisons. Examples of additional research areas include Japan, Taiwan, Southern Europe, and Scandinavia.

Secondly, the next logical step would be to assimilate the GPS-MET data into the operational MM5. Using the 3DVAR assimilation would aptly take advantage of the temporal availability of the GPS data. To do this would require intimate knowledge of the MM5 code and would work best in an advanced degree program with a numerical weather prediction emphasis.

Finally, it would serve well to investigate how to take the one-dimensional precipitable water values and derive a vertical profile, based on other thermodynamic variables. The other variables could be either observed through other sources or else inferred from the 3DVAR initialization. Vertical profiling of GPS-MET data with GOES sounder data is currently being researched and the results have been promising.

## Bibliography

- Applequist, Scott, AFWA/DNXM, Scientist, Mesoscale Modeling Branch, Offutt AFB, NE, Personal Correspondence, August 2001.
- Bevis, Michael, Steven Businger, Steven Chiswell, Thomas A. Herring, Richard A. Anthes, Christian Rocken, and Randolph H. Ware, 1994: GPS Meteorology: Mapping zenith wet delays onto precipitable water. *Journal of Applied Meteorology*, **33**, 379-386.
- Bevis, Michael, Steven Businger, Thomas A. Herring, Christian Rocken, Richard A. Anthes, and Randolph H. Ware, 1992: GPS Meteorology: Remote sensing of atmospheric water vapor using the Global Positioning System. *Journal of Geophysical Research*, **97**, No D14, 15,787-15,801.
- Borbas, E., 1998: Derivation of precipitable water from GPS data: an application to meteorology. *Physics and Chemistry of the Earth*, **23**, 87-90.
- Businger, Steven, Steven R. Chiswell, Michael Bevis, Jingping Duan, Richard A. Anthes, Christian Rocken, Randolph H. Ware, Michael Exner, T. VanHove, Fredrick S. Solheim, 1996: The promise of GPS in atmospheric monitoring. *Bulletin of the American Meteorological Society*, **77**, 5-18.
- Craig, Robert, AFWA/DNXM, *MM5 Model Physics*, 20 June 2000 [online article: <ftp://ws1-ftp.afwa.af.mil/pubs/aboutmm5/toc/physics/index.htm>].
- Cucurull, Lidia, Jordi Vila, Pepa Sedo and Antonia Rius, October 2001: MASS/MM5 meteorological model validation and data assimilation. *Meteorological Applications of GPS Integration Column Water Vapor Measurements in the Western Mediterranean Final Report*, Report to the European Commission, Document No. D01233, 72-84.
- Cucurull, L., B. Navascues, G. Ruffini, P. Elosegui, A. Rius and J. Vila, 2000: The use of GPS to validate NWP systems: The HIRLAM model. *Journal of Atmospheric and Oceanic Technology*, **17**, 773-787.
- Dana, Peter H., 1999: *The Geographer's Craft Project*, Department of Geography, The University of Colorado at Boulder [online web tutorial <http://www.colorado.edu/geography/gcraft/contents.html>.]
- De Pondeca, Manuel S.F.V., Xiaolei Zou, 2001: A case study of the variational assimilation of GPS zenith delay observations into a mesoscale model. *Journal of Applied Meteorology*, **40**, 1559-1576.

- Department of Commerce, National Oceanic and Atmospheric Administration.  
*Precipitable Water Vapor Comparisons Using Various GPS Processing Technique*. Document No. 1203-GP-36, 28 August 1995.
- Emardson, T. Ragne and Henrico J.P. Derks, 2000: On the relation between the wet delay and the integrated precipitable water vapour in the European atmosphere. *Meteorological Applications*, **7**, 61-68.
- Glickman, Todd S., et al., 2000: *Glossary of Meteorology*. American Meteorological Society, 855 pp.
- Grell, G.A., J. Dudhia, and D. Stauffer, 1995: *A Description of the Fifth Generation Penn State/NCAR Mesoscale Model (MM5)*. NCAR Tech. Note TN-398+STR, 122 pp.
- Gutman, Seth I., Benjamin, Stanley G., 2001: The role of ground-based GPS meteorological observation in numerical weather prediction. *GPS Solutions*, **4**, 16-24.
- Hoffman-Wellenhof, B. and Herbert Lichtenegger, 1993: *GPS: Theory and Practice*. Springer-Verlag, 326 pp.
- Kopken, Christina, 2001: Validation of integrated water vapor from numerical models using ground-based GPS, SSM/I, and water vapor radiometer measurements. *Journal of Applied Meteorology*, **40**, 1105-1117.
- Kuo, Ying-Hwa, Yong-Run Guo, and Ed R. Westwater, 1993: Assimilation of precipitable water measurements into a mesoscale numerical model. *Monthly Weather Review*, **121**, 1215-1238.
- Leick, Alfred, 1990: *GPS Satellite Surveying*. John Wiley, 352 pp.
- Liou, Yuei-An, Yu-Tun Teng, T. Van Hove, J. Liljegren, 2001: Comparison of precipitable water observations in the near tropics by GPS, microwave radiometer, and radiosondes. *Journal of Applied Meteorology*, **40**, 5-15.
- National Aeronautics and Space Administration, Jet Propulsion Laboratory, *International GPS Service Data and Products*, May 2001, [online article: <http://igscb.jpl.nasa.gov/components/prods.html>].
- National Oceanic and Atmospheric Administration, National Climatic Data Center, *NEXRAD National Mosaic Reflectivity Image Database*, 2002, [online: <http://lwf.ncdc.noaa.gov/oa/ncdc.html>].

- Niell, A.E., A.J. Coster, F.S. Solheim, V.B. Mendes, P.C. Toor, R.B. Langley, and C.A. Upham, 2001: Comparison of measurements of atmospheric wet delay by radiosonde, water vapor radiometer, GPS and VLBI. *Journal of Atmospheric and Oceanic Technology*, **18**, 830-850.
- Ritz, Richard L., Michael D. McAtee, Robert T. Swanson, Jr., July 2001: Data assimilation at the Air Force Weather Agency. Preprint Volume, *14<sup>th</sup> Conference on Numerical Weather Prediction*.
- Saastamoinen, J., 1972: Atmospheric correction for the troposphere and stratosphere in radio ranging of satellites. *The Use of Artificial Satellites for Geodesy, Geophysical Monograph Series*, **15**, 247-251.
- Smith, Bruce A., 30 July 2001: Boeing Satellite Systems to Build GPS Block 2F. *Aviation Week and Space Technology*, **155**, 30.
- Smith, Tracy, Stanley G. Benjamin, Barry E. Schwartz, and Seth I. Gutman, 2000: Using GPS-IPW in a 4-D data assimilation system. *Earth Planets Space*, **52**, 921-926.
- Swanson, Robert T., AFWA/DNXT, Chief, Technology Transition Branch, Offutt AFB, NE, Personal Correspondence, October 2001.
- Trimble Navigation Inc., *How GPS Works*, [online tutorial, <http://www.trimble.com/gps>], 1996.
- Ware, Randolph H., David W. Fulker, Seth A. Stein, David N. Anderson, Susan K. Avery, Richard D. Clark, Kelvin K. Droegemeier, Joachim P. Kuettnner, J. Bernard Minster, and Soroosh Sorooshian, 2000: SuomiNet: A real-time national GPS network for atmospheric research and education. *Bulletin of the American Meteorological Society*, **81**, 677-693.
- Wilks, Daniel S., 1995: *Statistical Methods in the Atmospheric Sciences*. Academic Press, 467 pp.
- Wolfe, Daniel E., Seth I. Gutman, 2000: Developing an operational, surface-based, GPS, water vapor observing system for NOAA: Network design and results. *Journal of Atmospheric and Oceanic Technology*, **17**, 426-440.
- Yang, Xiaohua, Bent H. Sass, Gunnar Elgered, Jan M. Johansson, T. Ragne Emardson, 1999: A comparison of precipitable water vapor estimates by an NWP simulation and GPS observations. *Journal of Applied Meteorology*, **38**, 941-956.

## Appendix A: Geodetic Information

This data is provided to give the reader detailed information about the locations, elevations and model positioning for each of the GPS-MET sites and their nearby RAOB sites (if a RAOB site is within range). The MM5 IX and MM5 JX columns are the grid positions on the AFWA 15 km MM5 grid and are used to assist in grid-to-station interpolation. Table A-1 is the CONUS geodetic information, while Table A-2 is Alaska's information.

Table A-1. CONUS Geodetic Information

ID	Location	Latitude	Longitude	MM5 IX	MM5 JX	GPS Receiver Elevation (m)	MM5 Interpolated Elevation (m)	MM5-GPS dz (m)	RAOB	RAOB dx (m)	RAOB-GPS dz (m)
ANP1	Annapolis, MD	39.01	-76.61	297	120.2	53	6.24	46.7569			
ARP3	Aransas Pass, TX	27.84	-97.06	182.5	25.32	11	0	11	CRP	44.01	3
AZCN	Aztec, NM	36.84	-107.91	120.8	96.54	1885	1816.17	68.8204			
BARH	Bar Harbor, ME	44.40	-68.22	328.8	170.2	31	16.12	14.8733			
BARN	Bartlett, NH	44.10	-71.16	315.2	163.3	165	339.19	-174.198			
BIL1	Billings, MT	45.97	-108.00	130.1	161.5	887	969.19	-82.1951			
BLKV	Blacksburg, VA	37.20	-80.41	278.8	102.7	636	653.26	-17.267			
BLMM	Bloomfield, MO	36.88	-89.97	224.4	93.02	130	109.08	20.9145			
BLRW	Blue River, WI	43.22	-90.53	218.1	138.3	226	280.42	-54.4268			
CCV3	Cape Canaveral, FL	28.46	-80.55	290.3	39.66	5	0	5	XMR	2.23	0
CHA1	Charleston, SC	32.76	-79.84	288.5	71.72	6	0.26	5.7305	CHS	23.63	9
CHO1	Chico, CA	39.43	-121.66	49.28	132.8	45	96.61	-51.6135			
CLK1	Clark, SD	44.93	-97.96	179.6	149.7	440	468.63	-28.6326			
CNWM	Conway, MO	37.52	-92.70	208.4	96.72	390	388.60	1.3908	SGF	69.82	4
COVX	Chesapeake Light, VA	36.90	-75.71	305.7	106.7	37	0	37			
DQUA	Dequeen, AR	34.11	-94.29	199.9	71.69	199	143.04	55.9553			
DRV1	Driver, VA	36.96	-76.56	300.9	105.9	13	8.88	4.1195			
DSRC	Boulder, CO	39.99	-105.26	138.6	117.1	1649	1915.70	-266.702	DEN	40.66	-38
ENG1	English Turn, LA	29.88	-89.94	228.5	41.95	9	0.78	8.2178			
FBYN	Fairbury, NE	40.08	-97.31	182.3	114.8	433	449.53	-16.5334			
FST1	Flagstaff, AZ	35.22	-111.82	96.16	88.92	2159	2211.78	-52.7822	FLG	1.11	20
GAL1	Galveston, TX	29.33	-94.74	197.7	36.45	10	0	10			
GDAC	Granada, CO	37.78	-102.18	154.3	99.57	1159	1119.58	39.4105			
GWEN	Appleton, WA	45.78	-121.33	65.19	175.5	746	470.05	275.9499			
HAG1	Hagerstown, MD	39.55	-77.71	290.2	122.5	155	190.75	-35.7526			
HBRK	Hillsboro, KS	38.30	-97.29	182.2	102	443	442.67	0.3285			
HDF1	Hudson Falls, NY	43.27	-73.54	305.2	154	72	157.94	-85.9444			
HKLO	Haskell, OK	35.68	-95.86	190.4	83.01	221	206.32	14.681			
HTV1	Hartsville, TN	36.36	-86.09	247.2	91.51	198	211.47	-13.4706			
HVLK	Haviland, KS	38.30	-99.11	171.9	102.3	648	624.85	23.1503			
JTNT	Jayton, TX	33.02	-100.98	159	64.56	711	724.64	-13.6392			
KYW1	Key West, FL	24.58	-81.65	288.4	9.54	8	0	8			
LMNO	Lamont, OK	36.69	-97.48	180.9	90.41	308	315.52	-7.5227			
LTHM	Lathrop, MO	39.58	-94.17	199.7	111.3	295	293.18	1.8147			
MBWW	Medicine Bow, WY	41.90	-106.19	135.3	131.3	1999	2078.07	-79.0701			
MC01	Grand Junction, CO	39.09	-108.53	119.8	113.1	1454	1705.46	-251.458			
MCN1	Macon, GA	32.70	-83.56	266	67.21	88	114.17	-26.1736			
MOB1	Mobile Point, AL	30.23	-88.02	240.5	45.61	9	0	9			
MOR1	Moriches, NY	40.79	-72.75	314.2	138.1	8	3.99	4.0127			

## Appendix A: Geodetic Information

Table A-1 (continued): CONUS Geodetic Information

ID	Location	Latitude	Longitude	MM5 IX	MM5 JX	GPS Receiver Elevation (m)	MM5 Interpolated Elevation (m)	MM5-GPS dz (m)	RAOB	RAOB dx (m)	RAOB-GPS dz (m)
MRRN	Merriman, NE	42.90	-101.70	159.6	136.1	991	997.79	-6.7922			
NDBC	Stennis, MS	30.36	-89.61	230.3	45.66	16	4.71	11.2897	SIL	20.45	-8
NDS1	Neodesha, KS	37.30	-95.60	191.8	94.75	266	253.50	12.4971			
NLGN	Neligh, NE	42.21	-97.80	180	130.2	525	542.78	-17.7815			
OKOM	Okolona, MS	34.08	-88.86	232.6	73.28	125	100.58	24.4151			
PATT	Palestine, TX	31.78	-95.72	191.3	54.51	121	113.27	7.7337			
PLS1	Polson, MT	47.66	-114.11	102.9	178.9	1002	1179.05	-177.053			
PLTC	Platteville, CO	40.18	-104.73	141.7	118.1	1521	1474.26	46.7418			
PNB1	Penobscot, ME	44.45	-68.77	326	169.6	59	21.40	37.5984			
PRCO	Purcell, OK	34.98	-97.52	180.5	78	331	339.06	-8.0615			
RWDN	Mccook, NE	40.09	-100.65	164	115.6	799	820.98	-21.9778			
SAV1	Savannah, GA	32.14	-81.70	278	65.08	40	22.42	17.5801			
SEAW	Seattle WFO, WA	47.69	-122.26	65.19	189.9	20	71.47	-51.4691			
SHK1	Sandy Hook, NJ	40.47	-74.01	308.2	134	9	3.44	5.559			
SIO3	Scripps/La Jolla, CA	32.86	-117.25	60.25	79.69	71	53.60	17.4031			
SLAI	Slater, IA	41.90	-93.69	201.9	128	315	302.78	12.2155			
SPN1	Spokane, WA	47.52	-117.52	86.71	182	752	712.35	39.646			
SUM1	Summerfield, TX	34.83	-102.51	150.7	78.4	1186	1197.10	-11.1024			
SYCN	Syracuse, NY	43.12	-76.09	292.6	149.5	122	188.15	-66.1533			
TCUN	Tucumcari, NM	35.09	-103.61	144.3	80.87	1243	1309.37	-66.3683			
VCIO	Vici, OK	36.07	-99.22	170.7	86.21	653	605.20	47.7974			
WDLN	Wood Lake, MN	44.67	-95.44	192.4	147.7	319	315.47	3.5298			
WHN1	Whitney, NE	42.74	-103.33	151	135.6	1072	1183.34	-111.336			
WLCI	Wolcott, IN	40.81	-87.05	238.1	122.8	215	212.79	2.2077			
WNCI	Winchester, IL	39.65	-90.48	220.1	112.8	170	174.93	-4.9254			
WNFL	Winfield, LA	31.90	-92.78	209.6	55.79	95	49.94	45.0612			
WSMN	White Sands, NM	32.41	-106.35	125.6	63.28	1229	1299.96	-70.955			

Table A-2. Alaska Geodetic Information

ID	Location	Latitude	Longitude	MM5 IX	MM5 JX	Elevation (m)	MM5 Interpolated Elevation (m)	MM5-GPS dz (m)	RAOB	RAOB dx (m)	RAOB-GPS dz (m)
CENA	Central, AK	65.5	-144.68	75.52	81.41	273	528.34	-255.34			
GNAA	Glenallen, AK	62.11	-145.97	79.29	56.64	586	619.99	-33.99			
TLKA	Talkeetna, AK	62.31	-150.42	64.22	54.04	154	155.8	-1.8			
CLGO	College, AK	64.87	-147.86	67.63	74.19	196	227.2	-31.2	FAI	5.59	-61



## Appendix B: RAOB Geodetic Information

This information is provided to give the location and elevation information for each of the RAOB sites used in this study.

Table B-1. RAOB Geodetic Information for CONUS and Alaska

Site ID	Site Name	Latitude (degrees)	Longitude (degrees)	Elevation (m)	Nearest GPS Site	Distance from Nearest GPS Site (km)
<b>CONUS</b>						
CHS	Charleston, SC	32.90	-80.03	15	Charleston, SC (CHA1)	23.63
CRP	Corpus Christi, TX	27.77	-97.50	14	Aransas Pass, TX (ARP3)	44.01
DEN	Denver, CO	39.77	-104.88	1611	Boulder, CO (DSRC)	40.66
FLG	Flagstaff, AZ	35.23	-111.82	2179	Flagstaff, AZ (FST1)	1.11
OTX	Spokane, WA	47.68	-117.63	728	Spokane, WA (SPN1)	19.63
SGF	Springfield, MO	37.23	-93.40	394	Conway, MO (CNWM)	69.82
SIL	Slidell, LA	30.33	-89.82	8	Stennis Space Center, MS (NDBC)	20.45
XMR	Cape Canaveral, FL	28.48	-80.55	5	Cape Canaveral, FL (CCV3)	2.23
<b>Alaska</b>						
FAI	Fairbanks, AK	64.82	-147.87	135	College, AK (CLGO)	5.59

## **Appendix C: Location-Specific Statistics**

The following tables provide the full statistics that complement the summary values discussed in Chapter 4 of the thesis text. Bias is defined as the observed GPS-MET PW value minus the MM5 PW value. %RMSE is defined as the RMSE value divided by the Mean GPS PW value times 100, while the %StDev is defined as the Standard Deviation value divided by the Mean GPS PW times 100. The tables in the C-1 series are for CONUS, while the tables in the C-2 series are for Alaska.

## Appendix C: Location-Specific Statistics

Table C-1-1. CONUS Statistics: 06 UTC Initialization, 06H Forecast

ID	Correlation	Bias	RMSE	RMSE%	StDev	%Stdev	Mean GPS	Mean MM5	n
ANP1	0.9938	-0.2673	0.2968	11.6236	0.1345	5.2659	2.5538	2.8211	13
ARP3	0.8072	-0.3427	0.5228	12.5932	0.4029	9.706	4.1512	4.4939	25
AZCN	0.9554	-0.1466	0.2595	15.0628	0.2208	12.8136	1.7229	1.8695	17
BARH	0.9295	-0.0166	0.4668	16.549	0.5387	19.0971	2.821	2.8376	4
BARN	0.9474	-0.0101	0.2459	10.926	0.2509	11.1516	2.2502	2.2603	24
BIL1	0.7005	0.0075	0.2624	15.0918	0.2704	15.5499	1.7388	1.7313	17
BLKV	0.9844	-0.2897	0.3549	11.2416	0.2128	6.7391	3.1574	3.4472	14
BLMM	0.9528	-0.4392	0.5988	21.5478	0.4196	15.0979	2.7789	3.2181	17
BLRW	0.95	-0.5849	0.6719	28.9181	0.3535	15.2167	2.3234	2.9082	8
CCV3	0.9664	-0.3803	0.431	8.7934	0.2069	4.222	4.9012	5.2815	25
CHA1	0.9313	-0.4432	0.5701	13.4673	0.3675	8.6806	4.2333	4.6765	21
CHO1	0.7429	0.0623	0.397	20.3961	0.4041	20.763	1.9465	1.8841	17
CLK1	0.952	-0.1244	0.2539	9.7102	0.2259	8.6393	2.6145	2.7389	25
CNWM	0.9584	-0.4121	0.5415	21.0561	0.3621	14.0798	2.5715	2.9836	17
COVX	0.9435	-0.6836	0.7638	38.3409	0.3614	18.1411	1.9922	2.6758	9
DQUA	0.9121	-0.5181	0.7112	19.7001	0.4973	13.7747	3.61	4.1281	25
DRV1	0.9508	-0.3458	0.5224	14.5276	0.4064	11.3011	3.5958	3.9415	14
DSRC	0.8919	0.1996	0.3286	20.2971	0.2691	16.6207	1.6188	1.4193	17
ENG1	0.9313	-0.3655	0.5038	10.8976	0.3539	7.655	4.6229	4.9884	25
FBNY	0.885	-0.1806	0.4809	15.448	0.4549	14.6129	3.1133	3.2939	25
FST1	0.9406	-0.4827	0.5292	39.9312	0.2235	16.869	1.3252	1.8079	17
GAL1	0.7866	-0.6096	0.7371	17.7861	0.4229	10.2044	4.1441	4.7537	25
GDAC	0.9725	-0.2316	0.2906	12.8006	0.1809	7.9692	2.27	2.5016	17
GWEN	0.7232	-0.3349	0.489	33.2146	0.3848	26.138	1.4721	1.8071	7
HAG1	0.9878	-0.2398	0.3006	12.6031	0.1902	7.9753	2.3855	2.6252	11
HBRK	0.9732	-0.1779	0.2855	10.5157	0.2312	8.5146	2.7153	2.8932	15
HDF1	0.9675	0.0262	0.2166	8.1659	0.2201	8.2966	2.6528	2.6265	22
HKLO	0.9236	-0.4914	0.6575	20.001	0.4476	13.6149	3.2872	3.7787	21
HTV1	0.9169	-0.4016	0.5539	20.3297	0.3915	14.3668	2.7248	3.1264	20
HVLK	0.9063	-0.2141	0.4123	16.1384	0.3657	14.3123	2.555	2.7691	14
JTNT	0.9017	0.1029	0.3452	10.6816	0.3366	10.4153	3.2315	3.1286	24
KYWI	0.8231	-0.2513	0.4924	10.1183	0.4325	8.8882	4.866	5.1173	24
LMNO	0.9466	-0.1658	0.4158	14.3238	0.3947	13.5965	2.9027	3.0685	15
LTHM	0.8025	-0.3338	0.4775	19.015	0.3689	14.6873	2.5114	2.8452	7
MBWW	0.2617	0.2061	0.3533	15.6566	0.3067	13.5945	2.2564	2.0503	8
MC01	0.8949	0.1913	0.3661	17.5081	0.3189	15.2499	2.0912	1.8999	24
MCN1	0.9625	-0.2617	0.4495	11.2018	0.3731	9.2961	4.013	4.2747	25
MOB1	0.9367	-0.2791	0.4756	9.6658	0.3931	7.9881	4.9206	5.1997	25
MOR1	0.9766	-0.3957	0.4869	17.9803	0.2899	10.7035	2.7082	3.1039	24
MRRN	0.9218	-0.2942	0.4718	18.938	0.3767	15.1227	2.4912	2.7854	24
NDBC	0.942	-0.3904	0.5059	11.0003	0.3284	7.1408	4.5987	4.989	25
NDS1	0.9593	-0.3796	0.4955	15.945	0.3253	10.4675	3.1075	3.4871	24
NLGN	0.9091	-0.1741	0.4316	15.0765	0.4031	14.0796	2.863	3.0372	25
OKOM	0.8777	-0.3475	0.5726	14.9628	0.4663	12.1853	3.8269	4.1744	21
PATT	0.9006	-0.4324	0.5227	12.3924	0.3039	7.2059	4.2177	4.6501	15
PLS1	0.8317	-0.0558	0.2976	17.832	0.3125	18.7248	1.6691	1.725	8
PLTC	0.9137	-0.0239	0.2635	15.4535	0.2705	15.8633	1.7053	1.7292	17
PNB1	0.8856	-0.2739	0.4698	23.045	0.3942	19.3376	2.0385	2.3124	16
PRCO	0.9036	-0.2195	0.5058	15.2317	0.4651	14.0059	3.3209	3.5404	25
RWDN	0.9663	-0.1716	0.2718	10.3739	0.2155	8.2251	2.6203	2.792	23
SAV1	0.9496	-0.3556	0.5192	12.7087	0.386	9.4493	4.0851	4.4407	25
SEAW	0.8869	0.089	0.1669	7.9361	0.151	7.1779	2.103	2.014	8
SHK1	0.9899	-0.3189	0.3865	13.9472	0.2233	8.0571	2.771	3.0899	23
SIO3	0.765	-0.7397	0.9062	39.151	0.5396	23.3127	2.3147	3.0544	17
SLAI	0.9387	-0.2334	0.3052	13.7735	0.2124	9.5858	2.2157	2.4491	7
SPN1	0.9348	-0.3917	0.4321	29.4426	0.1953	13.3028	1.4677	1.8594	8
SUM1	0.8731	0.091	0.3769	13.8794	0.3733	13.7464	2.7158	2.6248	25
SYCN	0.9714	-0.1132	0.1993	9.1287	0.1694	7.7595	2.1828	2.296	16
TCUN	0.8757	0.0326	0.3017	11.6945	0.3067	11.8875	2.58	2.5474	23
VCIO	0.9045	-0.1938	0.4281	14.7395	0.3895	13.4132	2.9042	3.098	25
WDLM	0.8835	-0.2854	0.4025	17.1685	0.2899	12.3653	2.3444	2.6298	24
WHN1	0.9421	-0.1687	0.3492	14.7591	0.3121	13.1903	2.3661	2.5347	25
WLCI	0.9595	-0.3937	0.4997	22.0671	0.3203	14.1443	2.2645	2.6582	13
WNCI	0.9261	-0.2766	0.4527	18.7061	0.3687	15.2377	2.4198	2.6964	18
WNFL	0.8607	-0.4127	0.5653	13.2649	0.3959	9.2897	4.2616	4.6743	21
WSMN	0.8554	0.216	0.3762	12.4052	0.3216	10.6066	3.0323	2.8162	12
Means	0.9003	-0.2401	0.4393	16.4977	0.3303	12.3741	2.8460	3.0861	18.4
Means of n > 10	0.9146	-0.2411		15.5030		11.8041			20.4

## Appendix C: Location-Specific Statistics

Table C-1-2. CONUS Statistics: 06 UTC Initialization, 09H Forecast

ID	Correlation	Bias	RMSE	RMSE%	StDev	%Stdev	Mean GPS	Mean MM5	n
ANP1	0.9662	-0.2061	0.2996	13.392	0.2281	10.1955	2.2373	2.4434	11
ARP3	0.7696	-0.1978	0.4653	11.0849	0.4306	10.2587	4.1975	4.3953	23
AZCN	0.9677	-0.152	0.2215	11.7897	0.1672	8.9005	1.8786	2.0305	14
BARH	0.8814	-0.0719	0.4163	15.8226	0.4735	17.9963	2.6312	2.7031	4
BARN	0.9637	0.0542	0.2347	10.0751	0.2334	10.0232	2.3291	2.2749	23
BIL1	0.8433	0.0031	0.2062	11.1914	0.214	11.6126	1.8429	1.8398	14
BLKV	0.9687	-0.1482	0.3125	10.1154	0.2854	9.2406	3.0889	3.2371	14
BLMM	0.9644	-0.3172	0.4568	15.9668	0.3411	11.9231	2.8611	3.1783	14
BLRW	0.9416	-0.3009	0.4729	18.9949	0.3899	15.6644	2.4894	2.7903	8
CCV3	0.9228	-0.189	0.4065	8.2278	0.368	7.4479	4.9407	5.1297	23
CHA1	0.9109	-0.2158	0.4895	11.3671	0.4514	10.4821	4.3061	4.5219	19
CHO1	0.672	-0.006	0.4935	25.1216	0.512	26.068	1.9643	1.9703	14
CLK1	0.8914	-0.1466	0.3287	12.0181	0.3009	10.9988	2.7353	2.8819	23
CNWM	0.9506	-0.2544	0.4603	16.1201	0.3954	13.8469	2.8552	3.1096	17
COVX	0.7363	-0.7674	0.8402	49.3239	0.3746	21.9909	1.7033	2.4707	6
DQUA	0.9121	-0.4096	0.6093	16.4071	0.4612	12.4195	3.7134	4.123	23
DRV1	0.9536	-0.317	0.4991	14.047	0.4	11.2582	3.5529	3.8699	14
DSRC	0.84	0.2528	0.3778	21.5792	0.2905	16.5964	1.7507	1.4978	15
ENG1	0.9272	-0.0984	0.4183	8.9069	0.4156	8.8514	4.6958	4.7942	23
FBYN	0.8755	-0.1145	0.433	13.5235	0.427	13.3356	3.2021	3.3166	23
FST1	0.9231	-0.4587	0.518	37.7366	0.2491	18.1439	1.3727	1.8315	15
GAL1	0.6988	-0.3315	0.6166	14.4575	0.5315	12.4638	4.2647	4.5963	23
GDAC	0.9267	-0.1068	0.2926	11.6518	0.282	11.228	2.5113	2.6182	15
GWEN	0.9235	-0.2644	0.3321	23.0152	0.2172	15.0472	1.4431	1.7075	7
HAG1	0.8543	-0.2549	0.3905	20.9685	0.3137	16.848	1.8622	2.1171	9
HBRK	0.9415	-0.0743	0.3172	11.2044	0.3209	11.3371	2.8308	2.9051	13
HDF1	0.9449	0.0528	0.2935	11.0329	0.2958	11.1208	2.6601	2.6073	21
HKLO	0.8826	-0.3213	0.5718	16.6982	0.4846	14.1535	3.4242	3.7455	21
HTV1	0.9639	-0.2224	0.3563	11.946	0.2865	9.6047	2.9826	3.205	18
HVLK	0.8037	-0.1894	0.4184	14.9268	0.3883	13.8539	2.8031	2.9925	13
JTNT	0.9276	0.082	0.2736	8.2202	0.2669	8.0186	3.3279	3.2459	23
KYW1	0.6845	-0.3385	0.6684	14.0113	0.5893	12.3528	4.7703	5.1088	23
LMNO	0.9429	-0.082	0.4029	13.3636	0.4094	13.578	3.015	3.097	14
LTHM	0.6285	-0.2002	0.6339	23.8474	0.6589	24.7862	2.6583	2.8586	6
MBWW	0.4179	0.1652	0.2776	12.8449	0.2385	11.0367	2.1612	1.9961	8
MC01	0.8878	0.3091	0.4289	19.2372	0.3044	13.65	2.2298	1.9206	22
MCN1	0.9711	-0.1493	0.3662	9.1416	0.3419	8.5343	4.0057	4.155	23
MOB1	0.9353	-0.2096	0.4635	9.5291	0.4227	8.6902	4.8643	5.0739	23
MOR1	0.9761	-0.2264	0.3755	13.4532	0.3063	10.9745	2.7912	3.0176	23
MRRN	0.9406	-0.2083	0.3596	13.5277	0.2998	11.2755	2.6585	2.8668	23
NDBC	0.9497	-0.158	0.3558	7.6583	0.3259	7.0152	4.6453	4.8034	23
NDS1	0.9109	-0.2488	0.4816	14.8608	0.4216	13.0096	3.2407	3.4896	23
NLGN	0.933	-0.1142	0.3428	11.4778	0.3305	11.066	2.9868	3.1009	23
OKOM	0.8586	-0.1505	0.4871	12.3612	0.476	12.0787	3.9408	4.0913	19
PATT	0.864	-0.2352	0.4379	10.2401	0.3833	8.9633	4.2763	4.5115	14
PLS1	0.876	0.025	0.286	17.3021	0.3077	18.6167	1.6527	1.6277	7
PLTC	0.791	-0.0423	0.3426	18.4802	0.3519	18.9828	1.854	1.8963	15
PNB1	0.9128	-0.0825	0.3858	17.7833	0.3901	17.9814	2.1694	2.2519	15
PRCO	0.8836	-0.0305	0.4313	12.5302	0.4399	12.7797	3.4419	3.4724	23
RWDN	0.9151	-0.0924	0.2942	10.3849	0.2855	10.0803	2.8325	2.925	23
SAV1	0.9428	-0.3098	0.4967	12.4594	0.397	9.9577	3.9867	4.2965	23
SEAW	0.7223	0.0988	0.2012	8.8402	0.1874	8.2332	2.2764	2.1776	8
SHK1	0.9803	-0.2394	0.3714	13.3742	0.2904	10.457	2.7773	3.0166	23
SIO3	0.7239	-0.8963	1.0694	46.43	0.6038	26.2152	2.3033	3.1997	15
SLAI	0.9164	-0.3162	0.374	18.9378	0.2189	11.0821	1.975	2.2912	6
SPN1	0.785	-0.1697	0.3578	22.1991	0.3402	21.1075	1.6117	1.7815	7
SUM1	0.8329	0.1295	0.3797	13.7901	0.3654	13.268	2.7538	2.6242	22
SYCN	0.9217	-0.0811	0.2347	10.6373	0.2271	10.2897	2.2066	2.2877	17
TCUN	0.9156	0.0723	0.2506	9.6456	0.2456	9.4528	2.5983	2.526	22
VCIO	0.8714	-0.1481	0.4078	13.5016	0.3889	12.8762	3.0201	3.1682	22
WDLN	0.8755	-0.2322	0.4133	16.2017	0.3495	13.703	2.5507	2.7829	23
WHN1	0.93	-0.0592	0.3142	12.3518	0.3155	12.4029	2.5438	2.603	23
WLCI	0.9464	-0.3195	0.4193	19.2158	0.2817	12.9126	2.1819	2.5013	14
WNCI	0.8982	-0.133	0.4325	17.3851	0.4242	17.0519	2.4879	2.6209	17
WNFL	0.9276	-0.2993	0.4228	10.0077	0.3067	7.2616	4.2243	4.5236	19
WSMN	0.6947	0.3864	0.4821	14.8125	0.3039	9.337	3.255	2.8686	10
Means	0.8760	-0.1557	0.4132	15.4357	0.3534	12.9089	2.9001	3.0558	17.0303
Means of n > 10	0.8933	-0.1495		14.3029		12.1742			19.0545

## Appendix C: Location-Specific Statistics

Table C-1-3. CONUS Statistics: 06 UTC Initialization, 12H Forecast

ID	Correlation	Bias	RMSE	RMSE%	StDev	%Stdev	Mean GPS	Mean MM5	n
ANP1	0.9318	0.008	0.479	18.7213	0.5002	19.551	2.5583	2.5503	12
ARP3	0.7457	-0.0885	0.5055	12.1451	0.5089	12.2264	4.1625	4.251	23
AZCN	0.9264	-0.1235	0.289	16.34	0.2705	15.2927	1.7687	1.8921	15
BARH	0.9338	0.0999	0.3356	12.0706	0.37	13.3059	2.7805	2.6806	4
BARN	0.9511	0.1163	0.3052	12.4717	0.2882	11.7777	2.4467	2.3304	24
BIL1	0.8432	-0.0729	0.2337	12.57	0.2305	12.3946	1.8593	1.9321	14
BLKV	0.9561	-0.0405	0.3068	10.5692	0.3156	10.872	2.9025	2.943	14
BLMM	0.9603	-0.0226	0.4183	14.5586	0.4313	15.014	2.8729	2.8955	16
BLRW	0.9654	-0.1333	0.3544	13.0842	0.3511	12.9613	2.709	2.8423	8
CCV3	0.8982	-0.1008	0.4102	8.3117	0.4065	8.2381	4.935	5.0358	23
CHA1	0.8075	-0.023	0.5443	12.0874	0.5587	12.4075	4.5027	4.5257	19
CHO1	0.8312	0.0268	0.3356	16.2542	0.3472	16.8138	2.065	2.0382	14
CLK1	0.8505	-0.1611	0.4176	15.1638	0.3939	14.3048	2.7538	2.9149	23
CNWM	0.9481	-0.1227	0.4066	13.8767	0.3983	13.5922	2.9304	3.0531	19
COVX	0.9223	-0.7379	0.819	42.6817	0.3797	19.7906	1.9188	2.6567	8
DQUA	0.9092	-0.1745	0.4698	11.8163	0.4475	11.2564	3.9757	4.1501	20
DRV1	0.9784	-0.1697	0.3467	9.4823	0.3147	8.6066	3.6562	3.8258	13
DSRC	0.9036	0.2187	0.3275	18.7493	0.2518	14.4138	1.7469	1.5282	16
ENG1	0.8989	-0.0387	0.4616	9.661	0.4703	9.8434	4.7783	4.8169	23
FBYN	0.942	-0.1046	0.3117	10.108	0.2999	9.7268	3.0835	3.1881	24
FST1	0.9233	-0.3609	0.4368	29.5735	0.2547	17.2473	1.4769	1.8378	15
GAL1	0.806	-0.1512	0.3757	8.7511	0.3517	8.1909	4.2932	4.4444	23
GDAC	0.9365	-0.0558	0.2618	10.7814	0.2641	10.8787	2.4281	2.484	16
GWEN	0.8213	-0.1681	0.3292	22.4562	0.3058	20.8564	1.4661	1.6342	7
HAG1	0.9782	-0.1619	0.2683	12.0739	0.2255	10.1501	2.222	2.3839	10
HBRK	0.9532	-0.0736	0.3327	11.8752	0.3358	11.987	2.8013	2.875	15
HDF1	0.9336	0.1594	0.4085	15.1836	0.385	14.3084	2.6906	2.5312	22
HKLO	0.8965	-0.089	0.459	13.322	0.4604	13.3632	3.4454	3.5344	23
HTV1	0.9574	0.0999	0.4159	12.9132	0.4169	12.9462	3.2206	3.1207	16
HVLK	0.908	-0.1488	0.3295	11.8808	0.3051	11.0007	2.7736	2.9224	14
JTNT	0.95	0.0777	0.2356	7.1782	0.2272	6.922	3.2828	3.2051	24
KYW1	0.6529	-0.2981	0.7199	14.9295	0.67	13.8951	4.8219	5.12	23
LMNO	0.9615	-0.1512	0.3315	11.1526	0.3054	10.2736	2.9727	3.1239	15
LTHM	0.9316	-0.0882	0.4434	16.2816	0.476	17.4794	2.7233	2.8115	6
MBWW	0.8873	0.048	0.1389	6.4572	0.1394	6.4786	2.1514	2.1034	8
MC01	0.865	0.2535	0.4069	19.2064	0.3255	15.3608	2.1188	1.8652	23
MCN1	0.9342	0.1823	0.5432	13.4403	0.5232	12.9454	4.0418	3.8595	23
MOB1	0.9435	-0.1455	0.3961	8.231	0.3767	7.8281	4.8127	4.9582	23
MOR1	0.9494	-0.0881	0.3964	14.05	0.3952	14.0061	2.8213	2.9095	23
MRRN	0.9449	-0.1479	0.3215	12.2894	0.2916	11.1456	2.6158	2.7638	24
NDBC	0.9276	-0.0816	0.3983	8.3372	0.3982	8.3358	4.7775	4.8591	24
NDS1	0.9164	-0.1178	0.4505	13.9677	0.4441	13.772	3.225	3.3427	24
NLGN	0.9365	-0.0416	0.3349	10.9213	0.3394	11.0698	3.0664	3.108	24
OKOM	0.8431	0.1161	0.5349	13.8298	0.535	13.8333	3.8677	3.7516	21
PATT	0.9412	-0.2158	0.3404	7.958	0.2732	6.3869	4.2769	4.4927	14
PLS1	0.7711	0.0191	0.2849	16.9416	0.307	18.258	1.6816	1.6625	7
PLTC	0.865	-0.1259	0.286	17.2709	0.2664	16.0914	1.6557	1.7816	14
PNB1	0.8987	-0.2538	0.3875	19.6668	0.303	15.38	1.9701	2.224	15
PRCO	0.9158	0.0577	0.4079	11.9608	0.4124	12.0952	3.41	3.3523	24
RWDN	0.8631	-0.1169	0.3923	13.8222	0.3825	13.4779	2.8383	2.9553	24
SAV1	0.898	0.0975	0.5037	11.7771	0.5052	11.8139	4.2766	4.1791	23
SEAW	0.5637	0.099	0.2487	10.6748	0.2439	10.4687	2.3295	2.2305	8
SHK1	0.9438	-0.1034	0.4649	16.6171	0.464	16.5824	2.798	2.9013	22
SIO3	0.6996	-0.8538	1.0533	46.5808	0.637	28.1718	2.2613	3.1151	16
SLAI	0.5886	-0.0811	0.3383	15.6845	0.3548	16.4469	2.1571	2.2383	7
SPN1	0.6819	0.0059	0.4183	22.7785	0.4518	24.6011	1.8366	1.8307	7
SUM1	0.8874	0.2224	0.392	14.1018	0.3304	11.8851	2.7798	2.5573	22
SYCN	0.7176	-0.0106	0.5686	24.5454	0.5872	25.346	2.3167	2.3273	16
TCUN	0.9175	0.0982	0.2832	11.091	0.2717	10.6373	2.5538	2.4556	23
VCIO	0.881	-0.0929	0.4171	13.7654	0.4153	13.7082	3.0298	3.1227	24
WDLM	0.805	-0.1152	0.4324	16.2754	0.4261	16.0401	2.6566	2.7718	23
WHN1	0.9269	-0.0495	0.3198	12.7396	0.323	12.8687	2.51	2.5595	23
WLCI	0.9593	-0.1877	0.2769	11.5909	0.2119	8.8684	2.389	2.5767	13
WNCI	0.9067	-0.0476	0.3928	15.4473	0.4012	15.7782	2.5428	2.5903	18
WNFL	0.7993	-0.0167	0.4309	10.1716	0.4412	10.4149	4.2366	4.2533	21
WSMN	0.829	0.3241	0.449	14.6322	0.3259	10.6207	3.0686	2.7445	11
Means	0.8806	-0.0670	0.4006	14.6348	0.3731	13.3728	2.9409	3.0079	17.4697
Means of n > 10	0.8938	-0.0623		14.0498		12.8921			19.3393

## Appendix C: Location-Specific Statistics

Table C-1-4. CONUS Statistics: 06 UTC Initialization, 15H Forecast

ID	Correlation	Bias	RMSE	RMSE%	StDev	%Stdev	Mean GPS	Mean MM5	n
ANP1	0.9511	0.1277	0.3608	12.9209	0.3502	12.5412	2.7921	2.6645	14
ARP3	0.6655	-0.2521	0.5719	14.5042	0.5244	13.2987	3.943	4.1952	24
AZCN	0.8985	-0.1468	0.3372	20.2073	0.3135	18.7875	1.6687	1.8156	16
BARN	0.8575	0.1845	0.4894	19.9449	0.463	18.8705	2.4537	2.2692	24
BIL1	0.6893	-0.068	0.3369	17.8686	0.3415	18.1151	1.8853	1.9533	15
BLKV	0.9289	0.2089	0.4313	14.5058	0.3915	13.1689	2.9731	2.7641	14
BLMM	0.9546	0.1058	0.4595	15.5916	0.4618	15.6703	2.947	2.8412	16
BLRW	0.9526	-0.0753	0.3127	10.8612	0.3245	11.2694	2.8794	2.9547	8
CCV3	0.9155	-0.2202	0.4429	9.0844	0.3925	8.0517	4.8749	5.0951	24
CHA1	0.7386	-0.198	0.7569	17.6896	0.7495	17.5171	4.2789	4.4769	20
CHO1	0.7635	-0.1208	0.4224	21.6155	0.4189	21.44	1.954	2.0748	15
CLK1	0.8922	-0.0593	0.3456	12.2807	0.3478	12.3588	2.8145	2.8738	24
CNWM	0.9347	0.0113	0.4042	13.6517	0.4151	14.0203	2.961	2.9497	19
COVX	0.9896	-0.3419	0.4535	20.0309	0.3331	14.7142	2.264	2.6059	5
DQUA	0.9224	0.0591	0.5125	13.3646	0.5248	13.6841	3.8351	3.776	17
DRV1	0.9424	-0.1355	0.4528	12.2588	0.4484	12.1389	3.6939	3.8293	14
DSRC	0.8995	0.2357	0.3552	18.8126	0.2745	14.5372	1.8881	1.6525	16
ENG1	0.9169	0.0579	0.3894	7.9536	0.3933	8.0342	4.8955	4.8375	24
FBYN	0.8981	-0.1021	0.417	13.252	0.413	13.1248	3.1465	3.2486	24
FST1	0.8866	-0.2924	0.4108	24.9947	0.298	18.1326	1.6436	1.936	16
GAL1	0.7753	-0.1282	0.4298	9.8343	0.4191	9.5885	4.3703	4.4985	24
GDAC	0.9086	-0.1667	0.3474	14.9279	0.3148	13.5263	2.3275	2.4942	16
GWEN	0.8628	-0.209	0.3073	20.9492	0.2433	16.5869	1.4667	1.6757	7
HAG1	0.9445	-0.1647	0.366	16.1136	0.3415	15.0312	2.2717	2.4363	12
HBRK	0.9399	-0.0515	0.333	11.6824	0.3398	11.9202	2.8506	2.9022	16
HDF1	0.9069	0.266	0.4632	16.7759	0.3877	14.0435	2.761	2.4951	23
HKLO	0.8766	0.0098	0.5165	14.6641	0.528	14.991	3.5219	3.5121	23
HTV1	0.9049	0.0785	0.5517	17.463	0.5602	17.7344	3.1591	3.0806	20
HVLK	0.8765	-0.1522	0.3698	13.0412	0.3497	12.3335	2.8357	2.988	14
JTNT	0.9285	0.072	0.2697	8.2419	0.2655	8.1133	3.2725	3.2005	24
KYWI	0.7329	-0.2526	0.6049	12.4697	0.5614	11.5737	4.851	5.1036	24
LMNO	0.9335	-0.0987	0.3855	12.0205	0.3858	12.028	3.2073	3.306	15
LTHM	0.8606	-0.0469	0.3299	12.2245	0.3527	13.0696	2.6986	2.7455	7
MBWW	0.7983	-0.0184	0.1713	8.046	0.182	8.5516	2.1285	2.1469	8
MC01	0.8943	0.217	0.3843	18.4645	0.3242	15.5796	2.0812	1.8641	23
MCN1	0.915	0.2014	0.567	13.779	0.5414	13.1576	4.1147	3.9134	24
MOB1	0.8782	-0.046	0.4826	9.9458	0.4912	10.1231	4.8525	4.8985	23
MOR1	0.8708	-0.0083	0.5975	20.2979	0.6102	20.7324	2.9435	2.9518	24
MRRN	0.9253	-0.1502	0.3854	14.7182	0.3626	13.8458	2.6185	2.7688	24
NDBC	0.9402	-0.0249	0.3573	7.3973	0.3641	7.538	4.8298	4.8548	24
NDS1	0.8967	-0.0302	0.492	15.2463	0.5021	15.5595	3.2267	3.2569	23
NLGN	0.9502	-0.0317	0.2932	9.4295	0.2977	9.5758	3.1093	3.1411	24
OKOM	0.8857	0.2574	0.5575	14.1499	0.5067	12.8612	3.9399	3.6825	21
PATF	0.8237	-0.1895	0.4674	10.8259	0.4434	10.27	4.3176	4.5071	14
PLS1	0.6086	-0.0046	0.3841	22.1239	0.4149	23.8949	1.7363	1.7408	7
PLTC	0.8401	-0.0867	0.2748	13.2559	0.2714	13.0932	2.0731	2.1597	13
PNB1	0.8668	-0.0906	0.4079	18.7553	0.4116	18.9283	2.1746	2.2652	15
PRCO	0.8994	0.2487	0.5551	15.3396	0.5092	14.0699	3.6191	3.3703	20
RWDN	0.9307	-0.0382	0.3026	9.9971	0.3069	10.1401	3.0264	3.0646	23
SAV1	0.8942	0.116	0.5148	11.8656	0.5124	11.809	4.3387	4.2226	24
SEAW	0.5878	0.0088	0.2503	11.0643	0.2675	11.8209	2.2626	2.2538	8
SHK1	0.9257	-0.1218	0.4853	17.3736	0.4799	17.1793	2.7932	2.915	24
SIO3	0.6352	-0.842	1.0761	47.9618	0.6921	30.8453	2.2437	3.0858	16
SLAI	0.7337	-0.0195	0.3162	13.6225	0.3409	14.686	2.3214	2.3409	7
SPN1	0.9121	-0.1433	0.2844	16.6488	0.2654	15.5337	1.7084	1.8517	7
SUM1	0.8734	0.2532	0.4054	14.4755	0.3237	11.5586	2.8008	2.5476	23
SYCN	0.9207	0.0965	0.2924	12.4326	0.284	12.076	2.3517	2.2552	18
TCUN	0.9289	0.1199	0.2878	11.174	0.2675	10.3858	2.5756	2.4556	23
VCIO	0.8771	-0.0859	0.4132	13.496	0.4129	13.4852	3.0619	3.1478	24
WDLN	0.8222	-0.1429	0.4631	17.0593	0.45	16.5758	2.7149	2.8578	24
WHN1	0.9253	-0.1462	0.3596	14.7539	0.3356	13.7701	2.4373	2.5834	24
WLCI	0.9288	-0.0994	0.2604	10.4746	0.2505	10.0767	2.4861	2.5855	13
WNCI	0.894	0.0512	0.4363	15.9647	0.4458	16.314	2.7327	2.6815	18
WNFL	0.8076	0.112	0.505	11.7632	0.5046	11.7537	4.2933	4.1814	21
WSMN	0.8344	0.2378	0.361	12.3251	0.2864	9.776	2.9293	2.6915	10
Means	0.8688	-0.0349	0.4204	14.8620	0.3983	13.9320	2.9881	3.0230	17.9692
Means of n > 10	0.8780	-0.0253		14.8296		13.8474			19.7143

## Appendix C: Location-Specific Statistics

Table C-1-5. CONUS Statistics: 06 UTC Initialization, 18H Forecast

ID	Correlation	Bias	RMSE	RMSE%	StDev	%Stdev	Mean GPS	Mean MM5	n
ANP1	0.9667	-0.0317	0.3011	11.6734	0.314	12.1752	2.5791	2.6108	11
ARP3	0.4795	-0.3258	0.6396	16.6419	0.5633	14.6573	3.8432	4.169	22
AZCN	0.8142	-0.0144	0.4571	24.2496	0.4741	25.1526	1.885	1.8994	14
BARH	0.6498	1.0947	1.6049	47.4956	1.3551	40.1042	3.379	2.2843	4
BARN	0.9358	0.2447	0.4406	17.8605	0.3746	15.1851	2.4667	2.222	23
BIL1	0.7147	-0.1466	0.3504	18.782	0.3287	17.6185	1.8656	2.0122	16
BLKV	0.9553	0.0639	0.3207	10.5313	0.3261	10.7097	3.0449	2.981	14
BLMM	0.8436	0.03	0.8229	27.0951	0.8494	27.965	3.0372	3.0071	16
BLRW	0.9055	-0.3092	0.5166	17.415	0.447	15.0698	2.9664	3.2756	7
CCV3	0.8381	-0.0913	0.4546	9.2289	0.4553	9.244	4.9259	5.0172	23
CHA1	0.6602	-0.1498	0.7401	17.1312	0.7446	17.2364	4.3202	4.47	19
CHO1	0.7909	-0.3431	0.5484	31.5158	0.4418	25.3936	1.74	2.0831	16
CLK1	0.8485	-0.115	0.3933	14.511	0.3846	14.1886	2.7105	2.8255	23
CNWM	0.9348	-0.0121	0.4303	14.0937	0.4426	14.4966	3.0531	3.0652	18
COVX	0.9965	-0.1009	0.3763	14.0024	0.4186	15.5759	2.6875	2.7885	4
DQUA	0.7768	-0.0281	0.6029	14.809	0.6188	15.1982	4.0713	4.0994	19
DRV1	0.9454	-0.2861	0.5306	14.0992	0.4637	12.3225	3.7631	4.0492	14
DSRC	0.8334	0.2825	0.4266	21.2324	0.3302	16.4341	2.0094	1.7269	16
ENG1	0.9232	-0.0754	0.4065	8.6713	0.4084	8.7123	4.6875	4.7629	23
FBYN	0.8991	0.0018	0.4236	12.7894	0.4331	13.0767	3.3123	3.3106	23
FST1	0.3323	-0.1582	0.8042	46.5481	0.8143	47.1352	1.7276	1.8858	16
GAL1	0.7579	-0.2872	0.5226	12.2892	0.4464	10.4984	4.2524	4.5395	23
GDAC	0.9294	-0.2104	0.3525	14.6877	0.2921	12.1712	2.4	2.6104	16
GWEN	0.9358	-0.2604	0.3022	19.9054	0.1679	11.0612	1.518	1.7784	6
HAG1	0.9725	-0.1276	0.2043	10.472	0.1682	8.6217	1.951	2.0786	10
HBRK	0.8806	-0.0192	0.4627	15.4348	0.4786	15.9627	2.998	3.0172	15
HDF1	0.7086	0.0661	0.5536	21.8738	0.5625	22.2282	2.5308	2.4646	22
HKLO	0.8961	-0.0234	0.5102	14.2331	0.5217	14.5527	3.5849	3.6083	22
HTV1	0.9606	-0.0419	0.3822	12.5773	0.3916	12.8864	3.0391	3.0809	17
HVLK	0.8381	-0.1679	0.4267	14.9414	0.4084	14.2979	2.8562	3.024	13
JTNT	0.8284	0.1307	0.4282	12.6854	0.4174	12.3648	3.3756	3.245	22
KYW1	0.6794	-0.0985	0.5336	10.7649	0.5362	10.8176	4.9564	5.055	23
LMNO	0.9664	-0.1307	0.2913	8.7451	0.2702	8.1113	3.3314	3.4621	14
LTHM	0.5256	0.1473	0.6398	22.3936	0.6725	23.5384	2.8571	2.7099	7
MBWW	0.5584	0.0613	0.39	16.9715	0.416	18.1034	2.2979	2.2366	7
MC01	0.8525	0.1718	0.4246	20.5357	0.3974	19.2224	2.0675	1.8958	22
MCN1	0.9086	0.2283	0.5961	14.5571	0.563	13.7492	4.0948	3.8665	23
MOB1	0.899	-0.022	0.4444	9.0788	0.4543	9.281	4.895	4.9171	22
MOR1	0.9014	-0.0781	0.565	19.7949	0.5727	20.0662	2.8541	2.9323	22
MRRN	0.9282	-0.2188	0.4131	16.164	0.3582	14.0173	2.5556	2.7745	23
NDBC	0.9074	-0.088	0.4132	8.8585	0.4128	8.85	4.6647	4.7527	23
NDS1	0.8522	-0.0689	0.5721	17.3439	0.5807	17.6048	3.2987	3.3676	23
NLGN	0.9026	-0.0734	0.3942	12.5946	0.396	12.6525	3.1297	3.2031	23
OKOM	0.9317	0.147	0.412	10.7424	0.3954	10.3101	3.8349	3.6879	19
PATT	0.7365	-0.1906	0.5436	12.707	0.5283	12.3498	4.278	4.4686	14
PLS1	0.1974	0.0067	0.5624	30.8408	0.6074	33.3095	1.8236	1.8168	7
PLTC	0.862	-0.002	0.3386	15.9971	0.3525	16.65	2.1169	2.119	13
PNB1	0.7701	-0.0082	0.663	27.3686	0.6846	28.264	2.4223	2.4305	16
PRCO	0.8794	0.1563	0.5392	15.1837	0.5311	14.9529	3.5515	3.3952	18
RWDN	0.8814	-0.0646	0.39	12.7381	0.3941	12.8725	3.0615	3.126	21
SAV1	0.8499	0.2856	0.6637	15.2689	0.6126	14.0933	4.3468	4.0613	23
SEAW	0.7213	-0.0505	0.2185	9.7347	0.2296	10.23	2.2449	2.2954	7
SHK1	0.8896	0.129	0.6904	22.7216	0.6935	22.823	3.0387	2.9096	23
SIO3	0.6573	-0.8678	1.0828	47.2726	0.6688	29.1985	2.2906	3.1585	16
SLAI	0.6081	-0.0942	0.5755	23.1239	0.6132	24.64	2.4886	2.5827	7
SPN1	0.8226	-0.1303	0.319	18.9037	0.3145	18.638	1.6874	1.8177	7
SUM1	0.8769	0.1634	0.358	12.9362	0.3257	11.7695	2.7673	2.604	23
SYCN	0.9008	-0.0961	0.3717	16.8777	0.3695	16.7772	2.2022	2.2983	18
TCUN	0.8947	0.0247	0.314	12.2037	0.3201	12.4393	2.5733	2.5486	23
VCIO	0.8339	0.002	0.469	15.1261	0.4795	15.466	3.1004	3.0984	23
WDLM	0.7246	-0.224	0.6087	23.0275	0.5787	21.8934	2.6434	2.8674	23
WHN1	0.9569	-0.1323	0.283	11.2968	0.2558	10.2108	2.5053	2.6377	23
WLCI	0.7176	-0.1936	0.592	25.1243	0.5823	24.7129	2.3564	2.55	13
WNCI	0.8533	0.2546	0.625	21.0634	0.5873	19.7939	2.9671	2.7125	18
WNFL	0.846	0.1445	0.4784	11.3258	0.4686	11.0928	4.2242	4.0797	19
WSMN	0.7381	0.236	0.4096	13.6523	0.3512	11.7033	3.0005	2.7644	11
Means	0.8149	-0.0316	0.4988	17.6139	0.4760	16.7046	3.0168	3.0484	17.0303
Means of n > 10	0.8368	-0.0437		16.8166		15.9327			18.9464

## Appendix C: Location-Specific Statistics

Table C-1-6. CONUS Statistics: 06 UTC Initialization, 21H Forecast

ID	Correlation	Bias	RMSE	RMSE%	StDev	%Stdev	Mean GPS	Mean MM5	n
ANP1	0.9487	-0.2232	0.3742	16.0228	0.3126	13.3862	2.3354	2.5586	13
ARP3	0.4591	-0.3424	0.6468	17.0123	0.5611	14.7571	3.8021	4.1445	23
AZCN	0.7873	-0.1299	0.4523	25.4572	0.4475	25.1845	1.7769	1.9068	16
BARH	0.86	0.2868	0.952	32.2194	1.0149	34.3492	2.9546	2.6678	5
BARN	0.8119	0.2241	0.5612	23.1629	0.5261	21.713	2.423	2.1989	23
BIL1	0.8185	-0.2129	0.3635	19.6366	0.3043	16.4391	1.8513	2.0641	16
BLKV	0.9561	-0.0772	0.3246	10.8786	0.3272	10.9656	2.9842	3.0614	14
BLMM	0.8779	0.1862	0.7359	24.168	0.7353	24.1481	3.0451	2.8588	16
BLRW	0.8856	-0.367	0.6077	20.9624	0.5231	18.0455	2.899	3.266	7
CCV3	0.7	-0.0217	0.6172	12.6527	0.6307	12.929	4.8781	4.8998	23
CHA1	0.8348	-0.0407	0.7067	17.5548	0.7221	17.9381	4.0257	4.0664	22
CHO1	0.8128	-0.5086	0.6411	39.1941	0.4031	24.6444	1.6356	2.1442	16
CLK1	0.7295	-0.2488	0.5185	20.1932	0.4651	18.1142	2.5676	2.8164	23
CNWM	0.8867	-0.0625	0.5668	19.4981	0.5807	19.9756	2.9068	2.9693	17
COVX	0.9018	-0.4469	0.7546	33.7637	0.666	29.8008	2.235	2.682	6
DQUA	0.8457	-0.0343	0.6251	16.7812	0.6395	17.1697	3.7247	3.759	21
DRV1	0.9475	-0.0498	0.464	12.2417	0.4787	12.6303	3.7901	3.8399	14
DSRC	0.9101	0.2101	0.3082	16.0871	0.2329	12.1563	1.9156	1.7056	16
ENG1	0.8921	-0.0238	0.4218	9.1867	0.4306	9.3782	4.5914	4.6153	23
FBYN	0.9232	-0.0714	0.3828	11.5577	0.3846	11.6099	3.3123	3.3837	23
FST1	0.5075	-0.2511	0.7298	45.4884	0.7077	44.1119	1.6044	1.8555	16
GAL1	0.6742	-0.2967	0.6085	14.4542	0.5432	12.9028	4.2097	4.5064	23
GDAC	0.8392	-0.2257	0.5212	20.9489	0.4852	19.502	2.4881	2.7138	16
GWEN	0.8967	-0.3287	0.3807	26.915	0.2075	14.6666	1.4146	1.7433	7
HAG1	0.9893	-0.1233	0.1641	8.8557	0.1141	6.1577	1.853	1.9763	10
HBRK	0.9071	-0.0511	0.3982	13.6413	0.4078	13.9723	2.9188	2.9698	16
HDF1	0.8717	0.1867	0.448	17.4484	0.4169	16.2352	2.5678	2.3812	22
HKLO	0.8573	-0.2212	0.6161	18.0565	0.5885	17.2494	3.4119	3.6331	22
HTV1	0.9637	-0.1875	0.4353	15.483	0.4042	14.3784	2.8115	2.999	18
HVLK	0.8664	-0.0933	0.4403	14.9982	0.4478	15.2561	2.9354	3.0287	13
JTNT	0.8019	0.0933	0.4673	14.2691	0.4682	14.2961	3.2747	3.1814	23
KYW1	0.6774	-0.0747	0.5194	10.6541	0.5256	10.7805	4.8753	4.9499	23
LMNO	0.9675	-0.0721	0.2706	8.1947	0.27	8.1755	3.3027	3.3748	15
LTHM	0.6319	0.0203	0.5109	19.481	0.5457	20.8096	2.6225	2.6022	8
MBWW	0.0924	0.2227	0.4548	18.8097	0.4283	17.714	2.4179	2.1951	7
MC01	0.8464	0.1215	0.4392	21.2047	0.432	20.8567	2.0714	1.9499	22
MCN1	0.9031	0.2248	0.5818	14.593	0.5486	13.7615	3.9866	3.7617	23
MOB1	0.847	0.0759	0.5305	11.0382	0.5368	11.1701	4.806	4.7301	23
MOR1	0.8685	0.1375	0.7835	25.8429	0.7886	26.0138	3.0317	2.8942	23
MRRN	0.9444	-0.1765	0.3458	13.349	0.304	11.7372	2.5901	2.7666	23
NDBC	0.8774	-0.0378	0.4386	9.5606	0.4468	9.7391	4.5879	4.6257	23
NDS1	0.8663	-0.0949	0.5522	16.9636	0.5562	17.087	3.2551	3.35	23
NLGN	0.8606	-0.1385	0.4861	15.9103	0.4764	15.5932	3.0554	3.194	23
OKOM	0.9138	0.1486	0.4701	12.4706	0.4583	12.1556	3.7699	3.6214	19
PATT	0.7735	-0.1092	0.4685	11.3997	0.4728	11.504	4.11	4.2192	14
PLS1	0.6322	-0.0956	0.4477	25.6466	0.4724	27.0623	1.7456	1.8412	7
PLTC	0.9262	-0.1075	0.2743	13.6273	0.2606	12.9481	2.0125	2.12	16
PNB1	0.9469	-0.2384	0.4044	17.9327	0.3374	14.9608	2.2551	2.4935	16
PRCO	0.8372	0.0681	0.5706	16.7032	0.5829	17.0645	3.4161	3.348	18
RWDN	0.9245	-0.041	0.3094	10.2188	0.3143	10.3789	3.0279	3.0689	21
SAV1	0.8319	0.218	0.7138	17.3286	0.695	16.8717	4.1193	3.9014	23
SEAW	0.4226	-0.1038	0.3512	16.2336	0.3625	16.7514	2.1637	2.2675	7
SHK1	0.8896	-0.01	0.5915	20.3565	0.6047	20.8111	2.9057	2.9156	23
SIO3	0.5987	-0.9514	1.1674	53.9522	0.6987	32.2913	2.1637	3.1151	16
SLAI	0.4376	-0.2154	0.8069	32.6661	0.8399	34.0032	2.47	2.6854	7
SPN1	0.5706	-0.1145	0.3427	20.9878	0.3488	21.3654	1.6327	1.7473	7
SUM1	0.9132	0.157	0.3162	11.5515	0.2806	10.2511	2.737	2.58	23
SYCN	0.8394	-0.0778	0.4771	21.4801	0.4843	21.8067	2.2209	2.2988	18
TCUN	0.8902	0.0829	0.3385	12.8406	0.3359	12.7423	2.6364	2.5534	22
VCIO	0.8812	0.0055	0.417	13.4435	0.4263	13.7445	3.1017	3.0963	23
WDLM	0.746	-0.2196	0.5602	21.8283	0.527	20.533	2.5664	2.786	23
WHN1	0.8808	-0.0218	0.4202	16.0802	0.4291	16.4194	2.6132	2.635	23
WLCI	0.7736	-0.2769	0.6397	28.2083	0.6002	26.4665	2.2678	2.5447	13
WNCI	0.8456	0.1026	0.5633	19.6502	0.5709	19.9161	2.8666	2.764	17
WNFL	0.7853	0.1133	0.6214	15.1181	0.6277	15.272	4.1102	3.9969	19
WSMN	0.6562	0.1778	0.4245	14.363	0.4063	13.7474	2.9553	2.7775	10
Means	0.8070	-0.0720	0.5128	18.7648	0.4875	17.5238	2.9336	3.0056	17.3333
Means of n > 10	0.8381	-0.0645		17.6927		16.4643			19.2143



## Appendix C: Location-Specific Statistics

Table C-1-7. CONUS Statistics: 06 UTC Initialization, 24H Forecast

ID	Correlation	Bias	RMSE	RMSE%	StDev	%Stdev	Mean GPS	Mean MM5	n
ANP1	0.9418	-0.073	0.2945	12.7945	0.2969	12.9014	2.3015	2.3745	13
ARP3	0.4452	-0.3053	0.6083	15.5779	0.5379	13.7766	3.9047	4.21	23
AZCN	0.7543	-0.1162	0.4981	27.3457	0.5013	27.5243	1.8213	1.9375	15
BARH	0.8535	0.0204	0.9595	34.2791	1.0725	38.3166	2.799	2.7786	5
BARN	0.9172	0.2154	0.3928	16.9757	0.3359	14.5144	2.314	2.0985	23
BIL1	0.7753	-0.2055	0.363	19.3157	0.3091	16.4444	1.8794	2.0849	16
BLKV	0.9576	0.0541	0.3017	9.7844	0.3081	9.989	3.084	3.0299	14
BLMM	0.8948	0.2319	0.7288	23.3451	0.7136	22.8573	3.1218	2.8899	16
BLRW	0.9552	-0.3965	0.5176	17.6597	0.3594	12.2607	2.931	3.3275	7
CCV3	0.7577	0.008	0.5426	11.1426	0.5547	11.3918	4.8695	4.8616	23
CHA1	0.8381	-0.0365	0.6565	16.5721	0.6709	16.9359	3.9615	3.9979	22
CHO1	0.8224	-0.4755	0.6112	35.2421	0.3967	22.8725	1.7344	2.2098	16
CLK1	0.6936	-0.2431	0.5287	20.7382	0.4801	18.8298	2.5494	2.7925	23
CNWM	0.904	-0.012	0.51	17.3895	0.5239	17.8611	2.9329	2.9449	19
COVX	0.9869	-0.4806	0.5856	25.6858	0.3741	16.409	2.28	2.7606	5
DQUA	0.8353	-0.0165	0.5979	16.2173	0.6111	16.5754	3.6867	3.7032	23
DRV1	0.9252	0.027	0.5078	13.3218	0.5263	13.805	3.8121	3.785	14
DSRC	0.8641	0.1479	0.3167	17.8108	0.2892	16.2663	1.7781	1.6302	16
ENG1	0.915	-0.0963	0.3834	8.4369	0.3794	8.3499	4.544	4.6403	23
FBNY	0.8821	-0.2231	0.5147	15.9575	0.4742	14.703	3.2253	3.4485	23
FST1	0.5795	-0.2966	0.688	46.3942	0.6411	43.2331	1.483	1.7796	16
GAL1	0.5813	-0.2984	0.6534	15.7297	0.5944	14.3078	4.154	4.4525	23
GDAC	0.8171	-0.2633	0.5377	22.0258	0.4842	19.8332	2.4413	2.7046	16
GWEN	0.706	-0.3296	0.5025	32.9191	0.4156	27.2235	1.5265	1.8561	6
HAG1	0.9765	-0.0345	0.2404	10.9632	0.2495	11.3793	2.1927	2.2272	11
HBRK	0.8337	-0.0693	0.4719	16.0642	0.4831	16.4478	2.9373	3.0066	15
HDF1	0.8546	0.2228	0.4976	19.0325	0.4559	17.4384	2.6143	2.3916	21
HKLO	0.8284	-0.3083	0.7221	21.6961	0.6683	20.0805	3.3283	3.6366	22
HTV1	0.923	-0.1116	0.5466	19.4557	0.5506	19.5983	2.8094	2.921	18
HVLK	0.8874	-0.1596	0.4435	15.1563	0.4307	14.719	2.9262	3.0857	13
JTNT	0.7376	0.1826	0.5221	15.8737	0.5001	15.2056	3.2892	3.1066	23
KYW1	0.5931	-0.0116	0.5884	12.1213	0.6015	12.3913	4.8543	4.8659	23
LMNO	0.9659	-0.026	0.269	8.2438	0.2778	8.5149	3.2629	3.2889	14
LTHM	0.4474	-0.0728	0.6259	25.0104	0.6646	26.5556	2.5025	2.5753	8
MBWW	0.8751	0.2244	0.3	12.3337	0.215	8.8386	2.4321	2.2077	7
MC01	0.8645	0.1245	0.395	19.0399	0.3845	18.5378	2.0743	1.9498	20
MCN1	0.9109	0.2678	0.5966	15.0377	0.545	13.7389	3.9671	3.6993	23
MOB1	0.8876	0.2363	0.5072	10.5076	0.4589	9.5064	4.8272	4.5909	23
MOR1	0.8632	0.0916	0.7171	24.541	0.7272	24.8868	2.922	2.8304	23
MRRN	0.9029	-0.29	0.5004	19.7677	0.417	16.4731	2.5316	2.8216	23
NDBC	0.8643	-0.0271	0.4656	10.216	0.4753	10.4279	4.558	4.5851	23
NDS1	0.8505	-0.1213	0.5741	17.6239	0.5738	17.6135	3.2578	3.3791	23
NLGN	0.8146	-0.1201	0.5302	17.3554	0.528	17.2843	3.0548	3.1749	23
OKOM	0.8419	0.252	0.6681	17.5575	0.6357	16.7062	3.8051	3.5531	19
PATT	0.6088	-0.0291	0.6786	16.6427	0.7036	17.2552	4.0777	4.1068	14
PLS1	0.7205	-0.1502	0.4714	29.2868	0.4826	29.9843	1.6094	1.7596	7
PLTC	0.8372	-0.1735	0.3663	19.5234	0.3332	17.7592	1.8763	2.0497	16
PNB1	0.9443	-0.3524	0.5097	22.9217	0.3803	17.1031	2.2237	2.5761	16
PRCO	0.7331	0.0876	0.657	19.3187	0.6657	19.5764	3.4007	3.3131	23
RWDN	0.8574	-0.1418	0.4633	15.6303	0.4514	15.2308	2.964	3.1058	22
SAV1	0.8979	0.2796	0.5787	13.9197	0.518	12.4605	4.1574	3.8778	23
SEAW	0.5466	0.0152	0.2291	10.3029	0.2469	11.104	2.2234	2.2083	7
SHK1	0.9338	0.0701	0.5665	19.8775	0.5753	20.1888	2.8498	2.7797	22
SIO3	0.5626	-0.824	1.0684	47.5779	0.7024	31.2793	2.2456	3.0696	16
SLA1	0.598	-0.2458	0.5545	22.8729	0.5369	22.1457	2.4243	2.6701	7
SPN1	0.5464	-0.1848	0.4	25.8988	0.3831	24.8102	1.5443	1.729	7
SUM1	0.9155	0.1577	0.3146	11.3747	0.2784	10.0651	2.7661	2.6085	23
SYCN	0.811	-0.0217	0.4985	22.0568	0.5133	22.7141	2.2599	2.2816	17
TCUN	0.881	0.0258	0.3223	11.9123	0.3288	12.1535	2.7056	2.6798	22
VCIO	0.8542	0.0502	0.4583	14.9663	0.4668	15.2435	3.062	3.0118	21
WDLN	0.6584	-0.2377	0.5912	24.1153	0.5535	22.5766	2.4517	2.6894	23
WHN1	0.9149	-0.0921	0.3714	14.554	0.3678	14.4158	2.5517	2.6438	23
WLCI	0.8371	-0.3241	0.669	29.934	0.6092	27.2576	2.2351	2.5591	13
WNCI	0.7983	-0.013	0.5574	20.8785	0.5734	21.4779	2.6698	2.6828	18
WNFL	0.9023	0.0194	0.4392	10.881	0.4508	11.1683	4.0366	4.0173	19
WSMN	0.6927	0.1523	0.3918	12.8893	0.3805	12.5174	3.0394	2.8871	10
Means	0.8088	-0.0734	0.5173	19.0545	0.4878	17.7578	2.9190	2.9925	17.3333
Means of n > 10	0.8240	-0.0580		18.2383		17.0422			19.2500

## Appendix C: Location-Specific Statistics

Table C-1-8. CONUS Statistics: 18 UTC Initialization, 06H Forecast

ID	Correlation	Bias	RMSE	RMSE%	StDev	%Stdev	Mean GPS	Mean MM5	n
ANP1	0.9851	-0.2339	0.3087	11.8692	0.2104	8.0883	2.6008	2.8348	12
ARP3	0.5991	-0.6407	0.8151	20.9456	0.5157	13.2521	3.8914	4.5321	22
AZCN	0.9359	-0.0457	0.2771	14.853	0.2828	15.1635	1.8653	1.9111	15
BARH	0.6453	0.7944	1.6043	47.4772	1.6093	47.6277	3.379	2.5845	4
BARN	0.927	-0.0094	0.3486	14.4648	0.3563	14.7846	2.41	2.4194	23
BIL1	0.7193	-0.2086	0.3854	20.5491	0.334	17.8092	1.8753	2.0839	17
BLKV	0.9513	-0.4537	0.557	18.2777	0.3353	11.0024	3.0474	3.5011	14
BLMM	0.9324	-0.2873	0.6141	20.0238	0.5595	18.2417	3.0669	3.3542	17
BLRW	0.8336	-0.4084	0.771	26.8577	0.7164	24.9549	2.8707	3.2791	6
CCV3	0.8916	-0.2556	0.4526	9.1249	0.382	7.7003	4.9605	5.2161	23
CHA1	0.8535	-0.4267	0.6505	15.4606	0.5044	11.9896	4.2072	4.6338	19
CHO1	0.6998	-0.1788	0.5413	32.1547	0.5267	31.2851	1.6835	1.8623	17
CLK1	0.8909	-0.1718	0.3427	12.675	0.3032	11.2141	2.704	2.8758	23
CNWM	0.963	-0.2433	0.4098	13.1005	0.3389	10.8319	3.1284	3.3716	19
COVX	0.9929	-0.2955	0.3405	12.6705	0.1953	7.2684	2.6875	2.983	4
DQUA	0.9354	-0.4026	0.517	12.6832	0.3328	8.1638	4.0766	4.4792	20
DRV1	0.9622	-0.4324	0.5553	15.1765	0.3616	9.8818	3.6591	4.0915	14
DSRC	0.8639	0.1528	0.3198	15.8729	0.2896	14.3728	2.0147	1.8619	17
ENG1	0.9111	-0.3063	0.5147	10.766	0.4229	8.8463	4.7804	5.0867	23
FBYN	0.8787	-0.1457	0.4997	15.335	0.4887	14.9988	3.2585	3.4042	23
FST1	0.3986	-0.0787	0.7434	43.4463	0.762	44.5317	1.7111	1.7898	17
GAL1	0.7709	-0.4067	0.5979	13.9345	0.4481	10.4442	4.2907	4.6973	23
GDAC	0.927	-0.4159	0.4956	20.553	0.2777	11.5176	2.4112	2.8271	17
GWEN	0.6633	-0.6225	0.6902	41.6838	0.3332	20.1236	1.6558	2.2783	5
HAG1	0.916	-0.3361	0.4954	25.3941	0.3837	19.6658	1.951	2.2871	10
HBRK	0.8694	-0.1327	0.4728	15.7133	0.4686	15.5759	3.0088	3.1415	16
HDF1	0.7467	-0.1531	0.5467	22.3559	0.5371	21.9661	2.4453	2.5984	22
HKLO	0.9327	-0.3246	0.5408	14.7022	0.4427	12.0356	3.6785	4.0031	22
HTV1	0.939	-0.3854	0.5806	19.6329	0.4477	15.1369	2.9574	3.3428	17
HVLK	0.9168	-0.3182	0.463	16.1003	0.349	12.1377	2.8757	3.1939	14
JTNT	0.8228	-0.0977	0.4368	12.6493	0.4358	12.619	3.4534	3.5511	22
KYW1	0.7837	-0.2225	0.5055	10.2905	0.4642	9.4483	4.9128	5.1352	23
LMNO	0.9491	-0.401	0.5053	15.045	0.3182	9.474	3.3587	3.7597	15
LTHM	0.7562	0.0419	0.6098	19.6327	0.6504	20.9387	3.1063	3.0644	8
MBWW	0.3581	-0.3075	0.3669	16.5394	0.2192	9.8806	2.2182	2.5257	6
MC01	0.8701	-0.025	0.3474	16.7996	0.3543	17.1328	2.0679	2.0929	23
MCN1	0.9553	-0.1879	0.43	10.6462	0.3955	9.7917	4.039	4.2269	23
MOB1	0.9318	-0.1607	0.3849	7.8524	0.358	7.3031	4.9021	5.0628	22
MOR1	0.9819	-0.3402	0.428	15.4421	0.2658	9.5913	2.7714	3.1116	22
MRRN	0.9301	-0.3062	0.4549	18.1758	0.344	13.743	2.503	2.8092	23
NDBC	0.9333	-0.322	0.4732	9.9921	0.3546	7.487	4.7356	5.0575	23
NDS1	0.8757	-0.3967	0.6867	20.525	0.5731	17.1306	3.3455	3.7422	23
NLGN	0.8998	-0.2677	0.5003	16.4173	0.4321	14.1809	3.0473	3.315	23
OKOM	0.9262	-0.1635	0.4265	11.4279	0.4047	10.8441	3.7323	3.8958	19
PATT	0.8892	-0.4225	0.5162	12.0817	0.3078	7.2033	4.2725	4.695	14
PLS1	0.2974	-0.0738	0.4702	25.3113	0.5087	27.383	1.8577	1.9315	6
PLTC	0.8454	-0.0968	0.3478	16.4167	0.3467	16.3639	2.1186	2.2153	14
PNB1	0.8402	-0.1857	0.6208	26.0278	0.6106	25.6002	2.3852	2.571	17
PRCO	0.9347	-0.2447	0.5092	13.8133	0.4595	12.4653	3.686	3.9307	18
RWDN	0.8961	-0.2737	0.4644	15.5444	0.3845	12.869	2.9879	3.2615	21
SAV1	0.9265	-0.1613	0.4676	10.7912	0.4488	10.3568	4.3336	4.4949	23
SEAW	0.6095	-0.0407	0.2309	10.3933	0.249	11.2067	2.2217	2.2624	6
SHK1	0.9882	-0.2634	0.3411	11.4436	0.2217	7.4359	2.9809	3.2443	23
SIO3	0.7017	-0.6364	0.8402	36.1682	0.5654	24.3393	2.3229	2.9594	17
SLAI	0.93	-0.179	0.3633	13.735	0.3379	12.7767	2.645	2.824	8
SPN1	0.6929	-0.3136	0.5197	30.1421	0.4539	26.3276	1.7242	2.0378	6
SUM1	0.9014	-0.1354	0.3274	11.6341	0.3048	10.831	2.8145	2.9499	23
SYCN	0.8682	-0.1103	0.4262	19.4783	0.4229	19.3297	2.188	2.2983	19
TCUN	0.9253	-0.1806	0.328	12.5899	0.28	10.7462	2.6057	2.7863	23
VCIO	0.8655	-0.3872	0.6052	19.3206	0.4756	15.1832	3.1322	3.5194	23
WDLM	0.8046	-0.2246	0.5153	19.4945	0.4742	17.9398	2.6433	2.8679	23
WHN1	0.9425	-0.2461	0.3971	16.0733	0.3187	12.8988	2.4708	2.7169	23
WLCI	0.7076	-0.422	0.7531	31.0331	0.6474	26.6756	2.4269	2.8488	14
WNCI	0.9307	-0.122	0.423	13.8825	0.4161	13.6564	3.0467	3.1687	19
WNFL	0.7852	-0.3084	0.5373	12.7973	0.4521	10.7668	4.1986	4.507	19
WSMN	0.8504	-0.0982	0.2546	8.4173	0.2453	8.1108	3.0248	3.1231	12
Mean	0.8418	-0.2372	0.5040	17.9073	0.4245	15.1613	3.0217	3.2589	17.2879
Mean n>10	0.8711	-0.2545		16.7399		14.1456			19.3214

## Appendix C: Location-Specific Statistics

Table C-1-9. CONUS Statistics: 18 UTC Initialization, 09H Forecast

ID	Correlation	Bias	RMSE	RMSE%	StDev	%Stdev	Mean GPS	Mean MM5	n
ANP1	0.9427	-0.3875	0.5279	22.4854	0.372	15.846	2.3479	2.7354	14
ARP3	0.5654	-0.5785	0.7694	20.014	0.5187	13.4915	3.8445	4.423	23
AZCN	0.8988	-0.1652	0.3432	19.5218	0.3101	17.6376	1.7582	1.9235	17
BARH	0.8751	0.3432	0.8771	31.7192	0.8842	31.9762	2.7653	2.4221	6
BARN	0.8359	0.0741	0.4809	20.2633	0.4858	20.4715	2.3732	2.2991	23
BIL1	0.8461	-0.2011	0.3132	16.7624	0.2474	13.2447	1.8682	2.0693	17
BLKV	0.9156	-0.3872	0.5774	19.1156	0.4446	14.7175	3.0208	3.408	14
BLMM	0.9541	-0.3043	0.5222	16.8844	0.4374	14.1427	3.0925	3.3968	17
BLRW	0.9748	-0.6395	0.8295	30.1298	0.5788	21.0245	2.7532	3.3926	6
CCV3	0.7874	-0.2576	0.5869	11.9313	0.5392	10.9613	4.9192	5.1769	23
CHA1	0.9254	-0.3435	0.6007	15.3524	0.5044	12.8904	3.9129	4.2565	22
CHO1	0.76	-0.4138	0.6067	38.3125	0.4573	28.8775	1.5835	1.9974	17
CLK1	0.8431	-0.2701	0.4153	16.151	0.3226	12.5435	2.5715	2.8417	23
CNWM	0.942	-0.2701	0.5066	16.7765	0.4411	14.6055	3.0199	3.29	18
COVX	0.911	-0.4817	0.707	31.6347	0.567	25.3671	2.235	2.7167	6
DQUA	0.9626	-0.3407	0.4656	12.4008	0.3256	8.6726	3.7543	4.095	20
DRV1	0.9847	-0.3101	0.43	11.6505	0.3092	8.3769	3.6912	4.0013	14
DSRC	0.8829	0.1419	0.2856	14.7504	0.2555	13.1946	1.9365	1.7945	17
ENG1	0.9162	-0.272	0.4616	9.9324	0.3813	8.2047	4.6477	4.9197	23
FBYN	0.9065	-0.1971	0.4736	14.7049	0.4403	13.6717	3.2208	3.4179	23
FST1	0.5515	-0.1234	0.6374	39.7999	0.6446	40.2489	1.6015	1.7249	17
GAL1	0.8207	-0.356	0.5272	12.4189	0.3976	9.3665	4.245	4.601	23
GDAC	0.7867	-0.2133	0.5637	22.4358	0.5378	21.4061	2.5124	2.7257	17
GWEN	0.7289	-0.5756	0.6238	41.3183	0.2636	17.4607	1.5098	2.0854	6
HAG1	0.9904	-0.2985	0.3384	18.2614	0.1681	9.0696	1.853	2.1515	10
HBRK	0.8611	-0.0947	0.4583	15.6151	0.4622	15.7483	2.9347	3.0294	17
HDF1	0.8901	-0.0406	0.3833	15.303	0.3901	15.575	2.5045	2.5451	22
HKLO	0.8886	-0.4677	0.7095	20.5652	0.5467	15.8463	3.45	3.9176	21
HTV1	0.9225	-0.4386	0.6304	23.1409	0.466	17.1049	2.7241	3.1627	18
HVLK	0.9178	-0.2245	0.4025	13.6178	0.3467	11.7293	2.9557	3.1802	14
JTNT	0.8104	-0.1676	0.4715	14.1319	0.4506	13.5055	3.3361	3.5037	23
KYW1	0.704	-0.1915	0.5523	11.4574	0.5297	10.9881	4.8207	5.0122	23
LMNO	0.9189	-0.2495	0.4637	14.0663	0.4036	12.2451	3.2963	3.5457	16
LTHM	0.6165	-0.1365	0.5198	19.6323	0.532	20.0921	2.6478	2.7843	9
MBWW	0.126	0.1558	0.3633	15.0645	0.3595	14.9073	2.4115	2.2557	6
MC01	0.8147	0.031	0.4328	20.9577	0.4413	21.3739	2.0649	2.0339	23
MCN1	0.9281	-0.1919	0.5075	12.8277	0.4804	12.1425	3.9566	4.1484	23
MOB1	0.8609	-0.1322	0.5186	10.8035	0.5127	10.6813	4.8002	4.9324	23
MOR1	0.9827	-0.2087	0.3506	11.9053	0.2881	9.7814	2.945	3.1537	23
MRRN	0.9182	-0.2602	0.4383	17.5225	0.3606	14.4158	2.5012	2.7615	23
NDBC	0.9041	-0.1953	0.4319	9.3122	0.3938	8.4918	4.6377	4.833	23
NDS1	0.8789	-0.3394	0.6278	19.0649	0.54	16.3991	3.2928	3.6322	23
NLGN	0.9318	-0.316	0.4939	16.4955	0.3881	12.9625	2.9939	3.3099	23
OKOM	0.8744	-0.2149	0.6092	16.5029	0.5857	15.8653	3.6915	3.9064	19
PATT	0.7589	-0.4235	0.6397	15.5095	0.4975	12.0614	4.1244	4.5479	14
PLS1	0.601	-0.1452	0.2879	16.2728	0.2724	15.3937	1.7695	1.9147	6
PLTC	0.8794	-0.1947	0.3579	17.7346	0.3096	15.3383	2.0182	2.213	17
PNB1	0.9357	-0.3091	0.4741	21.3169	0.3705	16.6585	2.2239	2.5331	17
PRCO	0.9319	-0.3095	0.5189	14.7516	0.4285	12.1827	3.5173	3.8268	18
RWDN	0.9321	-0.2256	0.3767	12.7453	0.3092	10.4594	2.9558	3.1814	21
SAV1	0.9553	-0.2269	0.4279	10.467	0.3709	9.0742	4.0879	4.3147	23
SEAW	0.4883	-0.1799	0.35	16.4485	0.3288	15.454	2.1277	2.3076	6
SHK1	0.9807	-0.2739	0.3831	13.4998	0.2739	9.6509	2.8378	3.1117	23
SIO3	0.5763	-0.7686	0.9756	44.549	0.6194	28.2813	2.19	2.9586	17
SLAI	0.942	-0.0947	0.2762	10.8332	0.2774	10.8802	2.55	2.6447	8
SPN1	0.5928	-0.3522	0.5396	32.6858	0.4479	27.1283	1.651	2.0032	6
SUM1	0.9137	-0.1099	0.2981	10.7251	0.2833	10.1939	2.7791	2.889	23
SYCN	0.8239	-0.117	0.4945	22.242	0.4936	22.2029	2.2231	2.34	19
TCUN	0.9338	0.0057	0.249	9.3014	0.2548	9.5178	2.6772	2.6716	22
VCIO	0.8566	-0.2357	0.513	16.3943	0.4658	14.8879	3.1289	3.3646	23
WDLM	0.8165	-0.2078	0.4745	18.4913	0.4362	16.9971	2.5663	2.7741	23
WHN1	0.8189	-0.2264	0.5929	23.4111	0.5603	22.1233	2.5325	2.7589	23
WLCI	0.8265	-0.5261	0.7751	32.369	0.5907	24.6686	2.3945	2.9206	14
WNCI	0.9405	-0.245	0.4543	15.2071	0.3937	13.1772	2.9874	3.2324	18
WNFL	0.6339	-0.3288	0.6345	15.5332	0.5575	13.6484	4.0848	4.4136	19
WSMN	0.583	-0.1192	0.3776	12.7108	0.3758	12.6491	2.9706	3.0899	11
Means	0.8330	-0.2443	0.5047	18.5744	0.4277	15.6054	2.9303	3.1746	17.5606
Mean n>10	0.8593	-0.2503		17.5031		14.8263			19.5357

## Appendix C: Location-Specific Statistics

Table C-1-10. CONUS Statistics: 18 UTC Initialization, 12H Forecast

ID	Correlation	Bias	RMSE	RMSE%	StDev	%Stdev	Mean GPS	Mean MM5	n
ANP1	0.934	-0.263	0.4045	17.1687	0.3199	13.5781	2.3562	2.6191	13
ARP3	0.5306	-0.3823	0.6345	15.9499	0.5183	13.0298	3.978	4.3603	22
AZCN	0.9039	-0.1567	0.3551	19.8531	0.3298	18.4405	1.7887	1.9454	15
BARH	0.8782	0.2981	0.8111	30.9774	0.8264	31.5591	2.6185	2.3204	6
BARN	0.9587	0.1032	0.2544	11.1238	0.238	10.4068	2.2873	2.1841	22
BIL1	0.744	-0.2611	0.3849	20.9413	0.2921	15.8895	1.8381	2.0993	16
BLKV	0.8788	-0.3309	0.6107	19.8165	0.5326	17.2835	3.0816	3.4126	14
BLMM	0.9758	-0.1427	0.3552	10.8815	0.3359	10.2914	3.2643	3.407	16
BLRW	0.9369	-0.1823	0.4314	14.9046	0.4284	14.7981	2.8947	3.077	6
CCV3	0.8706	-0.1953	0.4393	9.0063	0.4028	8.2574	4.8779	5.0732	22
CHA1	0.9337	-0.2469	0.4954	12.6445	0.44	11.2328	3.9175	4.1644	21
CHO1	0.7309	-0.4419	0.6403	39.1596	0.4785	29.2645	1.635	2.0769	16
CLK1	0.8322	-0.2991	0.4581	17.9221	0.3551	13.8934	2.5561	2.8552	22
CNWM	0.9367	-0.2146	0.4696	15.1802	0.4291	13.872	3.0935	3.3082	19
COVX	0.9992	-0.4733	0.4766	18.9876	0.0648	2.5812	2.51	2.9833	4
DQUA	0.9424	-0.4047	0.5427	14.0612	0.37	9.5876	3.8593	4.264	22
DRV1	0.9642	-0.2146	0.4597	12.5402	0.4218	11.5084	3.6654	3.88	14
DSRC	0.8978	0.1713	0.2992	16.2736	0.2534	13.7796	1.8387	1.6674	16
ENG1	0.9116	-0.1644	0.4146	8.9766	0.3896	8.4348	4.6187	4.7831	22
FBYN	0.9247	-0.2484	0.4497	14.0795	0.3837	12.0129	3.1937	3.4421	22
FST1	0.5914	-0.1965	0.6509	44.2279	0.6409	43.5472	1.4716	1.6681	16
GAL1	0.7702	-0.342	0.5612	13.3591	0.4554	10.8408	4.201	4.5431	22
GDAC	0.6637	-0.1773	0.5923	23.5493	0.5836	23.2058	2.515	2.6923	16
GWEN	0.7796	-0.4059	0.4675	28.3071	0.2592	15.6987	1.6514	2.0573	5
HAG1	0.9723	-0.1487	0.3063	13.8651	0.2822	12.777	2.209	2.3577	10
HBRK	0.8259	0.0198	0.4522	15.0538	0.4676	15.5671	3.004	2.9842	15
HDF1	0.9146	0.0844	0.3634	13.9299	0.3626	13.9013	2.6087	2.5243	20
HKLO	0.9297	-0.5469	0.6838	19.8371	0.4211	12.2157	3.4471	3.994	20
HTV1	0.942	-0.3811	0.5297	19.826	0.3793	14.194	2.672	3.0531	17
HVLK	0.883	-0.1779	0.4551	15.531	0.4359	14.878	2.93	3.1079	13
JTNT	0.7366	-0.1424	0.559	16.6935	0.5533	16.5229	3.3487	3.491	22
KYW1	0.5101	-0.1694	0.7279	15.1283	0.7246	15.0592	4.8115	4.9808	22
LMNO	0.8586	-0.0958	0.502	14.8709	0.5114	15.1488	3.3757	3.4715	14
LTHM	0.4212	-0.315	0.7552	30.4517	0.728	29.3555	2.48	2.795	9
MBWW	0.4764	0.001	0.2373	9.8129	0.26	10.7494	2.4187	2.4176	6
MC01	0.8689	0.0809	0.3722	17.9583	0.3728	17.9848	2.0727	1.9918	20
MCN1	0.9356	-0.0295	0.459	11.5784	0.4688	11.8263	3.9641	3.9936	22
MOB1	0.8228	-0.0699	0.6017	12.3981	0.6117	12.604	4.8534	4.9232	22
MOR1	0.9802	-0.2137	0.3488	12.1374	0.2822	9.8187	2.8737	3.0874	22
MRRN	0.8634	-0.3099	0.5727	23.1721	0.4929	19.9444	2.4715	2.7814	22
NDBC	0.8578	-0.0976	0.4914	10.6742	0.4929	10.7077	4.6035	4.7011	22
NDS1	0.8368	-0.2013	0.5917	17.7487	0.5695	17.0828	3.334	3.5354	22
NLGN	0.8911	-0.2532	0.5544	18.4762	0.5048	16.8242	3.0005	3.2537	22
OKOM	0.8663	-0.1821	0.6377	17.1527	0.6288	16.9146	3.7176	3.8998	18
PATT	0.8937	-0.4486	0.5848	14.158	0.3894	9.4267	4.1306	4.5792	14
PLS1	0.5191	-0.142	0.3914	23.764	0.3995	24.259	1.6468	1.7888	6
PLTC	0.8917	-0.1873	0.3231	16.7153	0.272	14.0689	1.9331	2.1204	16
PNB1	0.8867	-0.2819	0.5967	27.019	0.5432	24.5956	2.2086	2.4904	16
PRCO	0.8862	-0.2692	0.51	14.5798	0.4434	12.6752	3.4983	3.7675	22
RWDN	0.9555	-0.2116	0.3409	11.6164	0.2739	9.333	2.9345	3.1461	21
SAV1	0.9567	0.1145	0.3496	8.4417	0.3381	8.1641	4.1419	4.0274	22
SEAW	0.7608	-0.0661	0.1675	7.5688	0.1686	7.6187	2.2132	2.2792	6
SHK1	0.959	-0.2291	0.465	16.5938	0.4147	14.7966	2.8024	3.0315	21
SIO3	0.46	-0.622	0.8454	36.1288	0.5914	25.2732	2.34	2.962	16
SLAI	0.8344	-0.0784	0.3658	14.9679	0.382	15.63	2.4437	2.5221	8
SPN1	0.5268	-0.4307	0.6057	38.5949	0.4666	29.729	1.5695	2.0002	6
SUM1	0.9041	0.0031	0.2902	10.2834	0.2971	10.5248	2.8224	2.8193	22
SYCN	0.8267	-0.129	0.5372	23.6977	0.5375	23.7119	2.2669	2.396	17
TCUN	0.8606	-0.0756	0.3814	14.0222	0.3827	14.0678	2.7202	2.7957	22
VCIO	0.8576	-0.0781	0.4685	14.9295	0.474	15.1034	3.1384	3.2165	20
WDLM	0.8302	-0.3167	0.4876	19.785	0.3795	15.3985	2.4645	2.7811	22
WHN1	0.8981	-0.1756	0.4193	17.0343	0.3897	15.8334	2.4615	2.637	22
WLCI	0.8686	-0.5276	0.8016	33.4359	0.628	26.1977	2.3973	2.925	13
WNCI	0.8712	-0.267	0.5962	20.9033	0.5486	19.2327	2.8523	3.1192	18
WNFL	0.8593	-0.2789	0.4824	11.9799	0.405	10.0581	4.0266	4.3055	18
WSMN	0.6118	-0.1444	0.37	12.5819	0.3591	12.2113	2.941	3.0854	10
Means	0.8303	-0.1994	0.4885	17.9544	0.4301	15.6815	2.9373	3.1367	16.7727
Mean n>10	0.8512	-0.2030		17.2617		15.2322			18.6607

## Appendix C: Location-Specific Statistics

Table C-1-11. CONUS Statistics: 18 UTC Initialization, 15H Forecast

ID	Correlation	Bias	RMSE	RMSE%	StDev	%Stdev	Mean GPS	Mean MM5	n
ANP1	0.8929	-0.1973	0.4499	19.1206	0.4208	17.885	2.3531	2.5504	13
ARP3	0.5726	-0.3087	0.607	14.7319	0.5349	12.9828	4.12	4.4287	22
AZCN	0.87	-0.1429	0.3512	18.9156	0.3321	17.8846	1.8567	1.9996	15
BARH	0.8173	0.3267	0.924	35.5226	0.9664	37.1505	2.6012	2.2745	5
BARN	0.9299	0.102	0.3043	13.8076	0.2934	13.3146	2.2039	2.1018	22
BIL1	0.7803	-0.2333	0.3561	19.5303	0.2778	15.2365	1.8231	2.0564	16
BLKV	0.8773	-0.3414	0.6461	20.859	0.5692	18.3774	3.0974	3.4388	14
BLMM	0.9412	-0.1343	0.4899	15.5485	0.4866	15.4431	3.1508	3.2851	16
BLRW	0.9449	-0.0049	0.4444	15.4546	0.4868	16.9286	2.8758	2.8807	6
CCV3	0.8053	-0.1615	0.5288	11.0039	0.5154	10.7248	4.8057	4.9672	22
CHA1	0.8325	-0.3245	0.723	17.6477	0.6639	16.2031	4.0971	4.4216	19
CHO1	0.7476	-0.3832	0.5686	32.2174	0.4339	24.5825	1.765	2.1482	16
CLK1	0.8611	-0.2494	0.404	15.6889	0.3253	12.6326	2.5753	2.8247	22
CNWM	0.9195	-0.1071	0.4931	16.316	0.4953	16.3885	3.0221	3.1291	18
COVX	0.9711	-0.52	0.6063	28.4846	0.3369	15.8256	2.1286	2.6485	7
DQUA	0.8896	-0.3626	0.6357	16.5898	0.5344	13.9467	3.8318	4.1944	22
DRV1	0.9046	-0.0089	0.6524	17.2364	0.677	17.8854	3.7853	3.7942	14
DSRC	0.9022	0.1704	0.2973	16.4268	0.2517	13.9037	1.81	1.6396	16
ENG1	0.9175	-0.1022	0.427	9.0503	0.4243	8.9939	4.7177	4.8199	22
FBYN	0.9307	-0.1594	0.3911	12.1272	0.3656	11.3352	3.225	3.3844	22
FST1	0.6055	-0.1979	0.6111	43.5519	0.5972	42.5569	1.4032	1.6011	16
GAL1	0.7485	-0.3717	0.606	14.4059	0.4899	11.6463	4.2068	4.5785	22
GDAC	0.6502	-0.1077	0.5873	23.616	0.5963	23.9771	2.4869	2.5945	16
GWEN	0.6154	-0.2429	0.418	24.0963	0.3803	21.9234	1.7346	1.9775	5
HAG1	0.9725	-0.1252	0.2675	12.0749	0.2492	11.2484	2.215	2.3402	10
HBRK	0.761	-0.1923	0.6657	22.9299	0.6597	22.7225	2.9033	3.0957	15
HDF1	0.8829	0.0673	0.4288	16.8564	0.4339	17.0583	2.5439	2.4765	21
HKLO	0.919	-0.4051	0.5825	16.4893	0.4294	12.1568	3.5325	3.9375	20
HTV1	0.9002	-0.3561	0.5782	21.9497	0.4696	17.8263	2.6344	2.9904	17
HVLK	0.9231	-0.284	0.4206	14.8657	0.3229	11.412	2.8292	3.1132	13
JTNT	0.7228	-0.0854	0.595	17.4913	0.6027	17.7177	3.402	3.4873	22
KYW1	0.5142	-0.1839	0.7199	15.022	0.7124	14.8655	4.7922	4.9761	22
LMNO	0.8781	-0.2141	0.4803	14.8258	0.4461	13.7727	3.2393	3.4533	14
LTHM	0.4786	0.0396	0.5993	23.5539	0.6343	24.928	2.5444	2.5048	9
MBWW	0.6808	0.0827	0.1937	8.3899	0.1918	8.3108	2.3082	2.2255	6
MC01	0.858	0.1541	0.3536	17.1618	0.3265	15.8468	2.0602	1.906	20
MCN1	0.9524	-0.0776	0.3993	10.2533	0.4009	10.2943	3.8945	3.9721	22
MOB1	0.8777	-0.0589	0.4855	9.9814	0.4933	10.1408	4.8644	4.9233	22
MOR1	0.9626	-0.2215	0.452	16.5851	0.4033	14.7969	2.7256	2.9471	22
MRRN	0.9372	-0.1821	0.4096	15.9846	0.376	14.6719	2.5625	2.7446	21
NDBC	0.9166	-0.0391	0.4173	9.0039	0.4253	9.1752	4.6351	4.6742	22
NDS1	0.8456	-0.1851	0.5726	17.1143	0.5546	16.576	3.3456	3.5308	22
NLGN	0.9256	-0.2811	0.54	18.396	0.4719	16.077	2.9353	3.2164	22
OKOM	0.9283	-0.0391	0.4293	11.2196	0.4399	11.4968	3.8261	3.8653	18
PATT	0.901	-0.445	0.5644	13.4612	0.3602	8.591	4.1926	4.6376	14
PLS1	0.561	-0.1207	0.4659	28.0359	0.4929	29.6636	1.6617	1.7823	6
PLTC	0.9283	-0.1727	0.2787	14.1702	0.2264	11.5096	1.9667	2.1394	15
PNB1	0.9251	-0.1871	0.4036	18.8676	0.3693	17.2666	2.1389	2.326	16
PRCO	0.8233	-0.1652	0.5469	15.2707	0.5336	14.9001	3.5811	3.7463	22
RWDN	0.8755	-0.2637	0.4503	16.4184	0.3744	13.6527	2.7424	3.0062	20
SAV1	0.8893	-0.032	0.5628	14.2381	0.5751	14.5496	3.9529	3.9849	22
SEAW	0.6077	-0.0468	0.2167	9.7338	0.2318	10.4107	2.2267	2.2735	6
SHK1	0.9793	-0.2267	0.38	13.8829	0.3125	11.4163	2.7372	2.9639	21
SIO3	0.4279	-0.5297	0.827	34.2689	0.6559	27.1797	2.4131	2.9428	16
SLAI	0.8752	0.1197	0.3277	12.7709	0.3262	12.7099	2.5663	2.4466	8
SPN1	0.532	-0.4846	0.6237	39.0739	0.4301	26.9464	1.5962	2.0808	6
SUM1	0.9326	0.0169	0.2455	8.5712	0.2506	8.7521	2.8638	2.8469	22
SYCN	0.8489	-0.1987	0.5296	24.3177	0.5052	23.1942	2.1779	2.3767	18
TCUN	0.9244	-0.0368	0.2536	9.4971	0.2571	9.6285	2.6698	2.7066	21
VCIO	0.8858	-0.1256	0.4248	13.3321	0.4158	13.0501	3.1861	3.3118	21
WDLM	0.7965	-0.328	0.5091	20.6208	0.3985	16.1414	2.4689	2.7969	22
WHN1	0.883	-0.2376	0.4506	18.6296	0.3918	16.201	2.4186	2.6562	22
WLC1	0.9697	-0.3485	0.4463	17.8603	0.2901	11.611	2.4988	2.8474	13
WNC1	0.8136	-0.2062	0.6077	22.6075	0.5904	21.9637	2.6883	2.8945	16
WNFL	0.7977	-0.1384	0.5229	12.5491	0.5189	12.4522	4.167	4.3054	18
WSMN	0.8821	-0.0739	0.1814	5.9164	0.1746	5.6955	3.0655	3.1394	10
Means	0.8307	-0.1649	0.4838	17.6696	0.4421	16.0047	2.9311	3.0959	16.7121
Mean n>10	0.8525	-0.1791		16.8049		15.2056			18.5536

## Appendix C: Location-Specific Statistics

Table C-1-12. CONUS Statistics: 18 UTC Initialization, 18H Forecast

ID	Correlation	Bias	RMSE	RMSE%	StDev	%Stdev	Mean GPS	Mean MM5	n
ANP1	0.9225	-0.1573	0.4672	19.8917	0.4666	19.8666	2.3489	2.5062	9
ARP3	0.4334	-0.4161	0.7368	18.2031	0.6257	15.4584	4.0475	4.4636	18
AZCN	0.9217	-0.1583	0.3038	17.1882	0.2708	15.3233	1.7675	1.9258	12
BARH	0.8	0.0697	0.5802	17.8104	0.7055	21.6554	3.2577	3.188	3
BARN	0.9227	0.1418	0.369	15.3468	0.3512	14.605	2.4045	2.2627	17
BIL1	0.647	-0.2484	0.3923	22.2813	0.3172	18.012	1.7608	2.0093	12
BLKV	0.9051	-0.2683	0.5317	15.9722	0.4815	14.4625	3.329	3.5973	11
BLMM	0.9812	-0.3813	0.4665	17.4081	0.2807	10.4746	2.68	3.0613	12
BLRW	0.9624	-0.427	0.6207	25.48	0.4934	20.2555	2.436	2.863	6
CCV3	0.8551	-0.1602	0.4065	8.1774	0.3844	7.7333	4.9712	5.1314	18
CHA1	0.809	0.0831	0.5975	13.932	0.6111	14.2491	4.2886	4.2055	16
CHO1	0.7399	-0.321	0.5281	28.0533	0.438	23.2659	1.8825	2.2035	12
CLK1	0.8761	-0.2562	0.3813	15.3061	0.2906	11.6652	2.4913	2.7475	18
CNWM	0.9731	-0.4857	0.5585	22.7279	0.2879	11.7171	2.4574	2.9432	12
COVX	0.9386	-0.765	0.8343	44.9784	0.3647	19.6625	1.855	2.62	6
DQUA	0.9431	-0.4056	0.579	15.8154	0.4252	11.6147	3.6611	4.0666	18
DRV1	0.844	-0.1975	0.65	17.8596	0.6495	17.8457	3.6396	3.8371	11
DSRC	0.8435	0.1345	0.3366	20.118	0.3223	19.2614	1.6733	1.5388	12
ENG1	0.8794	0.0552	0.4379	9.4306	0.447	9.6267	4.6431	4.5879	18
FBYN	0.8238	-0.1384	0.5276	16.8775	0.5239	16.7586	3.1259	3.2643	18
FST1	0.8206	-0.252	0.51	35.6346	0.4631	32.3582	1.4312	1.6833	12
GAL1	0.5455	-0.5696	0.8377	20.5561	0.632	15.5103	4.075	4.6446	18
GDAC	0.874	-0.2033	0.4012	18.1733	0.3612	16.3643	2.2075	2.4108	12
GWEN	0.8189	-0.3964	0.4445	32.4568	0.2249	16.4194	1.3696	1.766	5
HAG1	0.9954	-0.1291	0.1871	8.7444	0.1463	6.8387	2.14	2.2691	7
HBRK	0.9674	-0.2561	0.3493	12.6301	0.2504	9.0545	2.766	3.0221	10
HDF1	0.8664	0.1558	0.4691	16.8315	0.457	16.3967	2.7871	2.6313	16
HKLO	0.9049	-0.4115	0.6362	19.1202	0.5022	15.0932	3.3274	3.7389	15
HTV1	0.8592	-0.1939	0.5909	20.8296	0.5765	20.3215	2.8369	3.0308	16
HVLK	0.8775	-0.1119	0.3934	14.5063	0.3976	14.66	2.712	2.8238	10
JTNT	0.7188	-0.1664	0.5894	17.7343	0.5818	17.5061	3.3234	3.4898	18
KYW1	0.6898	-0.0873	0.5621	11.5341	0.5724	11.7447	4.8734	4.9607	17
LMNO	0.8846	-0.1792	0.5079	16.8038	0.4963	16.4217	3.0225	3.2017	12
LTHM	0.7827	0.0893	0.2408	10.3122	0.245	10.4909	2.335	2.2457	6
MBWW	0.684	0.1754	0.2777	11.9932	0.2359	10.1854	2.3157	2.1402	6
MC01	0.9449	0.1502	0.2893	13.3196	0.2548	11.7348	2.1716	2.0215	17
MCN1	0.9243	0.0072	0.5221	12.5219	0.5372	12.8837	4.1692	4.162	18
MOB1	0.8673	0.1905	0.5227	10.4953	0.5009	10.0565	4.9804	4.7898	18
MOR1	0.9475	-0.2209	0.5035	18.3439	0.4664	16.9917	2.745	2.9659	17
MRRN	0.9157	-0.3423	0.5057	20.1496	0.3836	15.2867	2.5096	2.852	17
NDBC	0.8877	0.0603	0.426	9.1165	0.434	9.2863	4.6731	4.6127	18
NDS1	0.9371	-0.2416	0.436	14.1032	0.3735	12.0809	3.0917	3.3333	18
NLGN	0.8208	-0.2296	0.6553	23.1763	0.6316	22.3372	2.8276	3.0571	18
OKOM	0.8676	-0.1209	0.5559	14.3783	0.5617	14.527	3.8665	3.9873	15
PATT	0.9261	-0.2956	0.4064	9.4066	0.2914	6.7437	4.3205	4.6161	12
PLS1	0.3829	-0.0874	0.4795	28.9058	0.5165	31.1349	1.659	1.7463	6
PLTC	0.9324	-0.184	0.2997	16.7923	0.2471	13.8436	1.785	1.969	12
PNB1	0.9414	-0.0498	0.3285	15.058	0.3406	15.6102	2.1818	2.2317	11
PRCO	0.8673	-0.1665	0.5261	15.1936	0.5136	14.8309	3.4629	3.6294	18
RWDN	0.8061	-0.2614	0.5405	20.1927	0.4886	18.2537	2.6767	2.9382	16
SAV1	0.8067	0.1098	0.6948	16.5666	0.7059	16.8327	4.1939	4.0841	18
SEAW	0.7429	-0.1969	0.235	10.611	0.1404	6.3414	2.2143	2.4112	6
SHK1	0.9747	-0.0585	0.3437	12.2973	0.3491	12.4906	2.7951	2.8536	17
SIO3	0.5406	-0.4493	0.8595	35.9486	0.7653	32.009	2.3908	2.8401	12
SLA1	0.8299	0.0695	0.3352	15.2842	0.3592	16.3787	2.1933	2.1238	6
SPN1	0.9391	-0.4608	0.4751	32.2276	0.1268	8.6034	1.4743	1.9352	6
SUM1	0.8693	0.0254	0.3366	12.3977	0.3453	12.7209	2.7147	2.6893	18
SYCN	0.9387	0.078	0.2332	9.8055	0.2305	9.6921	2.3786	2.3006	11
TCUN	0.8449	-0.013	0.2774	10.7525	0.2862	11.093	2.5797	2.5926	16
VCIO	0.8763	-0.2406	0.4793	16.124	0.4266	14.3504	2.9727	3.2132	18
WDLN	0.775	-0.4346	0.5501	23.2776	0.3477	14.7124	2.3634	2.798	17
WHN1	0.8874	-0.1891	0.4167	17.1552	0.3821	15.7315	2.4291	2.6182	18
WLC1	0.9584	-0.3231	0.5159	22.0953	0.4265	18.2699	2.3347	2.6577	9
WNCI	0.9445	-0.3201	0.4447	18.7887	0.3224	13.6204	2.3668	2.6869	12
WNFL	0.8411	-0.2097	0.519	12.4336	0.4914	11.7728	4.1741	4.3837	15
WSMN	0.9301	0.0859	0.1739	5.5493	0.1604	5.1178	3.1346	3.0486	9
Means	0.8482	-0.1690	0.4726	17.6240	0.4134	14.9730	2.8799	3.0490	13.3030
Mean n>10	0.8518	-0.1674		16.8624		14.9423			15.1538

## Appendix C: Location-Specific Statistics

Table C-1-13. CONUS Statistics: 18 UTC Initialization, 21H Forecast

ID	Correlation	Bias	RMSE	RMSE%	StDev	%Stdev	Mean GPS	Mean MM5	n
ANP1	0.8198	-0.1178	0.5103	23.916	0.5308	24.8769	2.1337	2.2515	8
ARP3	0.6877	-0.3751	0.6614	16.0933	0.5605	13.6387	4.1097	4.4848	18
AZCN	0.9313	-0.0226	0.2347	12.4399	0.245	12.9863	1.8864	1.909	11
BARH	0.606	-0.4046	0.7169	23.9877	0.7248	24.252	2.9887	3.3933	3
BARN	0.9029	0.0854	0.3965	15.5482	0.3984	15.6237	2.5502	2.4648	18
BIL1	0.7993	-0.2576	0.3634	19.6868	0.2702	14.6379	1.846	2.1036	10
BLKV	0.9085	-0.1875	0.4262	13.3629	0.3998	12.5338	3.1897	3.3773	12
BLMM	0.9691	-0.1842	0.3426	13.1785	0.303	11.6552	2.5997	2.7839	11
BLRW	0.9397	-0.2035	0.5602	21.7031	0.5638	21.8411	2.5814	2.7849	7
CCV3	0.8592	0.0585	0.4367	8.6575	0.4453	8.8281	5.0443	4.9857	18
CHA1	0.7673	0.0796	0.6911	15.8259	0.7091	16.2361	4.3672	4.2876	16
CHO1	0.7143	-0.324	0.6123	32.2622	0.5477	28.8554	1.898	2.222	10
CLK1	0.7893	-0.1945	0.3814	14.6991	0.3376	13.0106	2.5947	2.7892	18
CNWM	0.9213	-0.1176	0.53	18.532	0.5364	18.7526	2.8601	2.9777	14
COVX	0.5019	-0.8423	0.9396	55.0738	0.4655	27.2874	1.706	2.5483	5
DQUA	0.9588	-0.2876	0.4389	11.7972	0.3412	9.1703	3.7206	4.0082	18
DRV1	0.8465	-0.3421	0.7127	19.8413	0.6531	18.1799	3.5922	3.9343	12
DSRC	0.8699	0.2008	0.3435	19.627	0.2923	16.7016	1.75	1.5492	11
ENG1	0.8913	0.2321	0.4885	10.2612	0.4423	9.2911	4.7608	4.5287	18
FBYN	0.8982	-0.1012	0.4118	12.7432	0.4107	12.7104	3.2315	3.3327	18
FST1	0.881	-0.3573	0.4654	32.2764	0.3128	21.6936	1.4419	1.7992	11
GAL1	0.357	-0.5005	0.9208	21.9648	0.7953	18.9717	4.1921	4.6925	18
GDAC	0.8439	-0.1181	0.4158	17.8161	0.4181	17.9164	2.3336	2.4517	11
GWEN	0.8752	-0.3313	0.3757	25.0631	0.1941	12.9497	1.4992	1.8305	6
HAG1	0.973	-0.0443	0.1191	6.4366	0.1211	6.5453	1.85	1.8943	6
HBRK	0.976	-0.1982	0.2861	10.1483	0.2175	7.7143	2.819	3.0172	10
HDF1	0.8855	0.2396	0.4533	15.8097	0.3966	13.833	2.8669	2.6273	17
HKLO	0.8819	-0.2727	0.5467	16.0145	0.4894	14.3356	3.4139	3.6866	16
HTV1	0.9225	0.0344	0.4554	14.5438	0.4712	15.0496	3.1312	3.0968	14
HVLK	0.7749	-0.1885	0.4539	16.1772	0.4353	15.5125	2.806	2.9945	10
JTNT	0.6499	-0.0936	0.605	18.4204	0.6151	18.7264	3.2844	3.378	18
KYW1	0.7373	-0.2109	0.5663	11.7167	0.5408	11.1888	4.8331	5.044	18
LMNO	0.9246	-0.2215	0.4587	14.8852	0.4213	13.6716	3.0818	3.3033	11
LTHM	0.8821	0.4435	0.7011	27.845	0.6072	24.113	2.518	2.0745	5
MBWW	0.3605	0.1372	0.3315	14.6015	0.326	14.357	2.2706	2.1333	7
MC01	0.9415	0.277	0.376	16.468	0.262	11.4764	2.2832	2.0062	17
MCN1	0.9303	0.184	0.5434	12.8263	0.5262	12.4185	4.237	4.053	18
MOB1	0.8786	0.2675	0.5324	10.7426	0.4736	9.5574	4.9557	4.6882	18
MOR1	0.9491	-0.0392	0.4321	15.2218	0.4428	15.5986	2.8387	2.8779	18
MRRN	0.9258	-0.1279	0.3526	12.8702	0.3381	12.341	2.7398	2.8678	18
NDBC	0.9136	0.0195	0.3606	7.6732	0.3706	7.8841	4.7001	4.6806	18
NDS1	0.9206	-0.2739	0.4943	15.6049	0.4234	13.3666	3.1673	3.4412	18
NLGN	0.7499	-0.355	0.8093	27.2513	0.7484	25.2001	2.9698	3.3247	18
OKOM	0.8652	0.0444	0.5141	12.7746	0.5302	13.1735	4.0247	3.9803	15
PATT	0.9269	-0.2743	0.3971	9.3198	0.2999	7.0384	4.2612	4.5355	12
PLS1	0.7042	-0.2258	0.3957	24.8991	0.356	22.3996	1.5893	1.8151	6
PLTC	0.9247	-0.1187	0.249	13.4857	0.2295	12.4325	1.8464	1.9651	11
PNB1	0.8948	-0.0148	0.465	19.8746	0.4875	20.834	2.3399	2.3547	11
PRCO	0.9179	-0.1603	0.4022	11.7843	0.3796	11.1209	3.4131	3.5734	18
RWDN	0.707	-0.2463	0.5876	20.5096	0.5489	19.161	2.8649	3.1112	18
SAV1	0.9202	0.0103	0.4206	10.0191	0.4327	10.3065	4.1982	4.1879	18
SEAW	0.7582	-0.1657	0.231	10.1767	0.1739	7.658	2.2703	2.436	7
SHK1	0.9598	-0.0244	0.3885	13.6867	0.399	14.0556	2.8384	2.8628	18
SIO3	0.3897	-0.4803	1.0456	45.0882	0.9741	42.0051	2.3191	2.7994	11
SLAI	0.8869	-0.0811	0.2411	12.2268	0.2539	12.8743	1.972	2.0531	5
SPN1	0.9114	-0.5025	0.523	37.2485	0.1586	11.2996	1.404	1.9065	6
SUM1	0.8504	0.0544	0.3322	12.4147	0.3378	12.624	2.6759	2.6215	17
SYCN	0.9106	0.0142	0.2587	11.0594	0.2698	11.5338	2.3393	2.3251	12
TCUN	0.8596	0.0573	0.2869	11.3797	0.2898	11.4933	2.5211	2.4638	17
VCIO	0.8029	-0.2367	0.5229	17.7553	0.4807	16.3205	2.9453	3.1819	17
WDLN	0.7782	-0.3826	0.5549	22.6202	0.4137	16.8612	2.4533	2.8358	18
WHN1	0.8769	-0.0842	0.4014	15.2163	0.4039	15.3087	2.6381	2.7223	18
WLCI	0.8713	-0.2193	0.4425	19.7902	0.4052	18.1199	2.236	2.4553	10
WNCI	0.9361	-0.1658	0.3744	15.4822	0.3506	14.4986	2.4182	2.5841	12
WNFL	0.8605	-0.1093	0.4507	10.825	0.4525	10.8705	4.1631	4.2723	15
WSMN	0.8617	0.2111	0.302	9.4101	0.2309	7.1947	3.2095	2.9984	8
Means	0.8347	-0.1233	0.4703	17.4040	0.4240	15.2223	2.9180	3.0412	13.2879
Mean n>10	0.8493	-0.1134	0.4703	16.1523	0.4240	14.8495	2.9180	3.0412	15.0566

## Appendix C: Location-Specific Statistics

Table C-1-14. CONUS Statistics: 18 UTC Initialization, 24H Forecast

ID	Correlation	Bias	RMSE	RMSE%	StDev	%Stdev	Mean GPS	Mean MM5	n
ANP1	0.8132	0.0323	0.5534	23.1325	0.5907	24.6876	2.3925	2.3602	8
ARP3	0.7256	-0.3206	0.6	14.6748	0.5238	12.8112	4.0886	4.4092	16
AZCN	0.9427	0.0217	0.2317	12.4715	0.2432	13.0885	1.858	1.8363	10
BARH	0.3096	-0.398	0.6024	18.7015	0.5539	17.1943	3.2213	3.6193	3
BARN	0.9084	0.1719	0.4136	15.6765	0.3877	14.6965	2.6383	2.4664	17
BIL1	0.8426	-0.2218	0.326	16.5183	0.2533	12.8366	1.9733	2.1952	9
BLKV	0.9009	-0.2004	0.4198	13.67	0.3869	12.5983	3.0708	3.2712	11
BLMM	0.9351	-0.1321	0.5209	19.7203	0.5285	20.0068	2.6414	2.7734	11
BLRW	0.9599	0.1026	0.6252	21.4327	0.6755	23.1603	2.9168	2.8143	6
CCV3	0.8477	0.0287	0.4882	9.744	0.5033	10.0462	5.0102	4.9815	16
CHA1	0.8373	0.0316	0.5324	11.9957	0.5515	12.4265	4.4384	4.4068	14
CHO1	0.7957	-0.2343	0.479	23.4796	0.4431	21.7207	2.04	2.2743	9
CLK1	0.8378	-0.073	0.3371	12.4771	0.3399	12.5805	2.7017	2.7748	16
CNWM	0.9293	0.0791	0.4384	14.7855	0.4475	15.0917	2.9651	2.8859	14
COVX	0.6564	-0.8522	0.9065	61.5827	0.3454	23.4668	1.472	2.3242	5
DQUA	0.943	-0.0821	0.3754	9.4692	0.3801	9.5889	3.9644	4.0464	14
DRV1	0.9529	-0.1991	0.4881	12.7192	0.4697	12.2413	3.8373	4.0364	10
DSRC	0.9042	0.2229	0.3224	17.3773	0.2443	13.1678	1.8555	1.6325	11
ENG1	0.8968	0.312	0.5423	11.3104	0.4581	9.5545	4.7948	4.4827	16
FBYN	0.7934	-0.1404	0.5802	18.5108	0.5802	18.5133	3.1342	3.2746	17
FST1	0.9048	-0.2521	0.3727	23.1835	0.2893	17.9956	1.6074	1.8595	10
GAL1	0.7036	-0.2321	0.5463	12.863	0.5108	12.0267	4.2471	4.4792	16
GDAC	0.9199	-0.1463	0.3172	13.4942	0.2952	12.5584	2.3509	2.4972	11
GWEN	0.6517	-0.3791	0.5079	34.0274	0.3779	25.3206	1.4926	1.8717	5
HAG1	0.9367	-0.1046	0.2247	11.7971	0.2179	11.4395	1.905	2.0096	6
HBRK	0.9537	-0.0572	0.2754	9.657	0.284	9.9579	2.852	2.9091	10
HDF1	0.9099	0.2703	0.4379	16.0061	0.3559	13.0075	2.736	2.4657	16
HKLO	0.8827	-0.0468	0.4292	12.2675	0.4406	12.5945	3.4984	3.5452	16
HTV1	0.8907	0.3279	0.7311	20.6946	0.6825	19.3194	3.5327	3.2048	12
HVLK	0.7542	-0.1491	0.4412	15.481	0.4377	15.3578	2.85	2.9991	10
JTNT	0.7076	-0.0332	0.5168	15.4786	0.5316	15.922	3.3385	3.3718	17
KYW1	0.7096	-0.2379	0.5822	12.0407	0.5488	11.3496	4.8352	5.0731	16
LMNO	0.8836	-0.2137	0.5129	16.9213	0.4915	16.2146	3.031	3.2447	10
LTHM	0.9961	0.2442	0.4392	17.4002	0.4081	16.1688	2.524	2.2798	5
MBWW	0.7118	0.0154	0.1882	8.6437	0.2055	9.4371	2.1778	2.1625	6
MC01	0.8996	0.2213	0.35	16.1245	0.28	12.9	2.1705	1.9492	16
MCN1	0.9296	0.1086	0.5433	13.2502	0.5498	13.4085	4.1001	3.9915	16
MOB1	0.8728	0.2491	0.5555	11.4749	0.5127	10.5924	4.8407	4.5916	16
MOR1	0.9399	0.0214	0.4517	16.1451	0.466	16.6558	2.798	2.7766	16
MRRN	0.9164	-0.137	0.3587	13.2201	0.3417	12.594	2.713	2.85	17
NDBC	0.8755	0.1965	0.5413	11.2829	0.5199	10.8368	4.7975	4.601	17
NDS1	0.8981	-0.1437	0.4637	14.6347	0.4544	14.3423	3.1682	3.3119	17
NLGN	0.8893	-0.1633	0.4625	14.8316	0.446	14.3028	3.1183	3.2816	17
OKOM	0.8148	0.1789	0.6182	15.8011	0.6125	15.6561	3.9121	3.7332	15
PATT	0.9429	-0.2206	0.3506	8.0717	0.2858	6.5798	4.3432	4.5638	11
PLS1	0.8434	-0.1819	0.2839	18.339	0.2438	15.7455	1.5482	1.7301	5
PLTC	0.9395	-0.1951	0.2481	14.5824	0.1626	9.5558	1.7011	1.8962	9
PNB1	0.8913	-0.2955	0.5235	24.8566	0.4555	21.6289	2.106	2.4015	10
PRCO	0.9186	-0.0093	0.3625	10.4113	0.3736	10.7282	3.4821	3.4915	17
RWDN	0.7414	-0.2361	0.5008	17.4554	0.4552	15.8672	2.8688	3.1049	17
SAV1	0.8384	0.1501	0.65	14.6398	0.6531	14.7112	4.4397	4.2896	16
SEAW	0.6535	-0.1135	0.2631	11.4429	0.2601	11.3095	2.2997	2.4132	6
SHK1	0.9264	-0.0558	0.5046	18.3305	0.518	18.8156	2.7529	2.8087	16
SIO3	0.3974	-0.4666	1.0137	41.968	0.9439	39.0768	2.4155	2.882	11
SLA1	0.5537	-0.0595	0.3509	16.1864	0.3867	17.8353	2.168	2.2275	5
SPN1	0.8976	-0.3012	0.3605	21.9419	0.2214	13.4783	1.643	1.9442	5
SUM1	0.7631	0.2733	0.4855	17.1125	0.4154	14.6396	2.8373	2.5639	15
SYCN	0.8523	0.2455	0.454	18.5988	0.4006	16.4081	2.4413	2.1957	11
TCUN	0.8408	0.1396	0.3302	12.7064	0.3091	11.8927	2.5989	2.4593	16
VCIO	0.8009	-0.1658	0.5064	16.7033	0.4932	16.2686	3.0315	3.1972	17
WDLN	0.6773	-0.282	0.5294	20.7808	0.4628	18.1632	2.5477	2.8298	16
WHN1	0.8337	-0.1245	0.4544	17.3543	0.4513	17.2378	2.6183	2.7427	16
WLCI	0.7789	-0.121	0.4047	16.6451	0.4096	16.8471	2.4314	2.5525	9
WNCI	0.9512	-0.1227	0.3488	13.7696	0.3411	13.4623	2.5334	2.6561	12
WNFL	0.8788	-0.0291	0.3929	9.5258	0.4055	9.833	4.1243	4.1534	15
WSMN	0.8134	0.1568	0.3202	10.1585	0.2985	9.4688	3.1524	2.9956	8
Means	0.8336	-0.0656	0.4589	16.6326	0.4260	14.9847	2.9651	3.0307	12.2576
Mean n>10	0.8544	-0.0351		15.3416		14.4759			14.2857



## Appendix C: Location-Specific Statistics

Table C-2-1. Alaska Statistics: 00 UTC Initialization, 06H Forecast

ID	Correlation	Bias	RMSE	RMSE%	StDev	%Stdev	Mean GPS	Mean MM5	n
CENA	0.8177	-0.0159	0.2649	12.8416	0.2709	13.135	2.0626	2.0785	21
CLGO	0.9775	-0.0707	0.1308	6.0873	0.1137	5.2905	2.1489	2.2195	16
TLKA	0.9248	0.1793	0.2527	10.5	0.1828	7.5928	2.407	2.2277	20
GNAA	0.8369	0.2439	0.3125	14.4388	0.2001	9.2464	2.164	1.9201	21
<b>Means</b>	<b>0.8892</b>	<b>0.0842</b>	<b>0.2402</b>	<b>10.9669</b>	<b>0.1919</b>	<b>8.8162</b>	<b>2.1956</b>	<b>2.1115</b>	<b>19.5000</b>

Table C-2-2. Alaska Statistics: 00 UTC Initialization, 09H Forecast

ID	Correlation	Bias	RMSE	RMSE%	StDev	%Stdev	Mean GPS	Mean MM5	n
CENA	0.85	-0.05	0.25	12.59	0.25	12.58	2.00	2.06	22
CLGO	0.72	-0.27	0.48	24.38	0.41	20.69	1.97	2.24	17
TLKA	0.64	-0.07	0.39	17.97	0.39	18.05	2.18	2.26	22
GNAA	0.29	-0.04	0.40	20.78	0.41	21.15	1.94	1.98	22
<b>Means</b>	<b>0.62</b>	<b>-0.11</b>	<b>0.38</b>	<b>18.93</b>	<b>0.37</b>	<b>18.12</b>	<b>2.02</b>	<b>2.13</b>	<b>20.7500</b>

Table C-2-3. Alaska Statistics: 00 UTC Initialization, 12H Forecast

ID	Correlation	Bias	RMSE	RMSE%	StDev	%Stdev	Mean GPS	Mean MM5	n
CENA	0.87	-0.01	0.20	10.28	0.21	10.50	1.98	2.00	22
CLGO	0.87	-0.25	0.35	18.09	0.26	13.16	1.95	2.20	18
TLKA	0.71	-0.12	0.36	16.34	0.34	15.67	2.18	2.30	23
GNAA	0.55	-0.01	0.31	16.22	0.32	16.58	1.94	1.95	23
<b>Means</b>	<b>0.75</b>	<b>-0.10</b>	<b>0.31</b>	<b>15.23</b>	<b>0.28</b>	<b>13.98</b>	<b>2.01</b>	<b>2.11</b>	<b>21.5000</b>

Table C-2-4. Alaska Statistics: 00 UTC Initialization, 15H Forecast

ID	Correlation	Bias	RMSE	RMSE%	StDev	%Stdev	Mean GPS	Mean MM5	n
CENA	0.87	0.07	0.21	10.18	0.21	9.93	2.07	2.00	19
CLGO	0.72	-0.10	0.39	19.72	0.39	19.73	1.99	2.09	16
TLKA	0.83	-0.03	0.27	11.88	0.27	12.12	2.26	2.29	21
GNAA	0.67	0.07	0.29	14.78	0.29	14.72	1.99	1.92	21
<b>Means</b>	<b>0.77</b>	<b>0.00</b>	<b>0.29</b>	<b>14.14</b>	<b>0.29</b>	<b>14.12</b>	<b>2.08</b>	<b>2.08</b>	<b>19.2500</b>

## Appendix C: Location-Specific Statistics

Table C-2-5. Alaska Statistics: 00 UTC Initialization, 18H Forecast

ID	Correlation	Bias	RMSE	RMSE%	StDev	%Stdev	Mean GPS	Mean MM5	n
CENA	0.77	0.12	0.30	14.57	0.28	13.61	2.06	1.93	21
CLGO	0.88	-0.06	0.24	11.87	0.24	11.83	2.04	2.10	17
TLKA	0.83	0.08	0.25	10.76	0.24	10.43	2.34	2.26	21
GNAA	0.85	0.12	0.23	11.17	0.20	9.78	2.03	1.92	22
<b>Means</b>	<b>0.83</b>	<b>0.07</b>	<b>0.26</b>	<b>12.09</b>	<b>0.24</b>	<b>11.41</b>	<b>2.12</b>	<b>2.05</b>	<b>20.2500</b>

Table C-2-6. Alaska Statistics: 00 UTC Initialization, 21H Forecast

ID	Correlation	Bias	RMSE	RMSE%	StDev	%Stdev	Mean GPS	Mean MM5	n
CENA	0.64	0.11	0.37	18.15	0.37	17.79	2.06	1.95	23
CLGO	0.50	-0.15	0.57	29.98	0.57	29.92	1.92	2.07	15
TLKA	0.59	0.16	0.45	18.57	0.43	17.72	2.43	2.27	23
GNAA	0.67	0.03	0.34	17.57	0.35	17.87	1.96	1.92	23
<b>Means</b>	<b>0.60</b>	<b>0.04</b>	<b>0.44</b>	<b>21.07</b>	<b>0.43</b>	<b>20.83</b>	<b>2.09</b>	<b>2.05</b>	<b>21.0000</b>

Table C-2-7. Alaska Statistics: 00 UTC Initialization, 24H Forecast

ID	Correlation	Bias	RMSE	RMSE%	StDev	%Stdev	Mean GPS	Mean MM5	n
CENA	0.81	0.26	0.36	16.09	0.26	11.50	2.23	1.98	19
CLGO	0.95	0.02	0.17	7.61	0.17	7.82	2.18	2.17	16
TLKA	0.84	0.27	0.35	13.76	0.23	8.90	2.53	2.26	19
GNAA	0.86	0.22	0.27	12.45	0.16	7.52	2.14	1.92	20
<b>Means</b>	<b>0.86</b>	<b>0.19</b>	<b>0.28</b>	<b>12.48</b>	<b>0.20</b>	<b>8.94</b>	<b>2.27</b>	<b>2.08</b>	<b>18.5000</b>

Table C-2-8. Alaska Statistics: 12 UTC Initialization, 06H Forecast

ID	Correlation	Bias	RMSE	RMSE%	StDev	%Stdev	Mean GPS	Mean MM5	n
CENA	0.8397	0.0961	0.2566	12.3606	0.2442	11.7589	2.0764	1.9802	20
CLGO	0.8883	0.0495	0.2246	11.0112	0.2258	11.0704	2.0394	1.9898	17
TLKA	0.8719	0.2444	0.337	14.4228	0.2382	10.1915	2.3368	2.0924	20
GNAA	0.9203	0.2888	0.323	15.9488	0.1483	7.3224	2.0253	1.7365	21
<b>Means</b>	<b>0.8801</b>	<b>0.1697</b>	<b>0.2853</b>	<b>13.4359</b>	<b>0.2141</b>	<b>10.0858</b>	<b>2.1195</b>	<b>1.9497</b>	<b>19.5000</b>

## Appendix C: Location-Specific Statistics

Table C-2-8. Alaska Statistics: 12 UTC Initialization, 09H Forecast

ID	Correlation	Bias	RMSE	RMSE%	StDev	%Stdev	Mean GPS	Mean MM5	n
CENA	0.787	0.115	0.3041	14.6185	0.2882	13.8517	2.0803	1.9653	22
CLGO	0.6069	-0.0891	0.5115	26.6866	0.5214	27.2013	1.9168	2.0059	15
TLKA	0.6803	0.2793	0.4847	20.0708	0.4055	16.7904	2.415	2.1357	22
GNAA	0.6954	0.1042	0.3525	18.1591	0.3446	17.7553	1.9411	1.8369	22
<b>Means</b>	<b>0.6924</b>	<b>0.1024</b>	<b>0.4132</b>	<b>19.8838</b>	<b>0.3899</b>	<b>18.8997</b>	<b>2.0883</b>	<b>1.9860</b>	<b>20.2500</b>

Table C-2-9. Alaska Statistics: 12 UTC Initialization, 12H Forecast

ID	Correlation	Bias	RMSE	RMSE%	StDev	%Stdev	Mean GPS	Mean MM5	n
CENA	0.8136	0.2657	0.3698	16.779	0.2639	11.9745	2.204	1.9383	20
CLGO	0.9357	0.0693	0.1913	8.9577	0.1838	8.6059	2.136	2.0667	17
TLKA	0.9114	0.3115	0.368	14.8229	0.201	8.0958	2.4827	2.1711	20
GNAA	0.8733	0.241	0.2989	14.0964	0.1812	8.5431	2.1206	1.8796	21
<b>Means</b>	<b>0.8835</b>	<b>0.2219</b>	<b>0.3070</b>	<b>13.6640</b>	<b>0.2075</b>	<b>9.3048</b>	<b>2.2358</b>	<b>2.0139</b>	<b>19.5000</b>

Table C-2-11. Alaska Statistics: 12 UTC Initialization, 18H Forecast

ID	Correlation	Bias	RMSE	RMSE%	StDev	%Stdev	Mean GPS	Mean MM5	n
CENA	0.8613	0.1478	0.2669	12.728	0.2278	10.8611	2.0973	1.9495	21
CLGO	0.8962	0.0068	0.2293	10.9638	0.2368	11.3184	2.0919	2.0851	16
TLKA	0.9501	0.1691	0.226	9.278	0.1537	6.3099	2.436	2.2669	21
GNAA	0.7475	0.2401	0.3445	16.0953	0.2532	11.8271	2.1404	1.9003	21
<b>Means</b>	<b>0.8638</b>	<b>0.1410</b>	<b>0.2667</b>	<b>12.2663</b>	<b>0.2179</b>	<b>10.0791</b>	<b>2.1914</b>	<b>2.0505</b>	<b>19.7500</b>

Table C-2-12. Alaska Statistics: 12 UTC Initialization, 21H Forecast

ID	Correlation	Bias	RMSE	RMSE%	StDev	%Stdev	Mean GPS	Mean MM5	n
CENA	0.7476	0.01	0.3132	15.8365	0.3212	16.2397	1.9777	1.9677	20
CLGO	0.8168	-0.0976	0.3314	16.5285	0.3278	16.3491	2.005	2.1026	15
TLKA	0.7791	-0.0386	0.2962	13.5837	0.3013	13.8175	2.1802	2.2189	20
GNAA	0.5849	0.0497	0.3077	15.746	0.3116	15.9428	1.9543	1.9046	20
<b>Means</b>	<b>0.7321</b>	<b>-0.0191</b>	<b>0.3121</b>	<b>15.4237</b>	<b>0.3155</b>	<b>15.5873</b>	<b>2.0293</b>	<b>2.0485</b>	<b>18.7500</b>

## Appendix C: Location-Specific Statistics

Table C-2-13. Alaska Statistics: 12 UTC Initialization, 24H Forecast

<b>ID</b>	<b>Correlation</b>	<b>Bias</b>	<b>RMSE</b>	<b>RMSE%</b>	<b>StDev</b>	<b>%Stdev</b>	<b>Mean GPS</b>	<b>Mean MM5</b>	<b>n</b>
CENA	0.7801	0.0833	0.2891	14.5326	0.2836	14.2592	1.9891	1.9058	21
CLGO	0.8635	-0.1306	0.2909	14.9584	0.2685	13.8042	1.9449	2.0756	16
TLKA	0.8187	-0.0482	0.2662	12.1899	0.2683	12.2845	2.1841	2.2323	21
GNAA	0.6308	0.0223	0.2992	15.294	0.3057	15.6281	1.956	1.9338	21
<b>Means</b>	<b>0.7733</b>	<b>-0.0183</b>	<b>0.2864</b>	<b>14.2437</b>	<b>0.2815</b>	<b>13.9940</b>	<b>2.0185</b>	<b>2.0369</b>	<b>19.7500</b>

## **Vita**

Captain Patricia A. Vollmer graduated from Lake Taylor High School in Norfolk, Virginia in June 1991. She entered undergraduate studies at The Pennsylvania State University in University Park, Pennsylvania where she earned her Bachelor's Degree in Meteorology and was commissioned through the Reserve Officer Training Corps in May 1995.

Her first duty assignment was with the 21<sup>st</sup> Air Support Operations Squadron, Fort Polk, Louisiana and included staff weather officer duties supporting both the Joint Readiness Training Center and 2d Armored Cavalry Regiment. While assigned to Fort Polk, she deployed to Tuzla Air Base, Bosnia-Herzegovina in 1997 in support of Operation JOINT GUARD. In 1998, Captain Vollmer was assigned to the 607<sup>th</sup> Weather Squadron, Yongsan Army Garrison, Seoul, Republic of Korea. There, she was staff weather officer to the 17<sup>th</sup> Aviation Brigade. Also, while with the 607<sup>th</sup> Weather Squadron, she had the opportunity to serve as the combined Plans and Programs officer, in support of joint and multi-national weather operations in the Korean theater of operations. She entered the Graduate School of Engineering and Management, Air Force Institute of Technology in August 2000. Upon graduation, Captain Vollmer's next duty assignment will be with the Air Force Technical Applications Center at Patrick AFB, Florida.

REPORT DOCUMENTATION PAGE				Form Approved OMB No. 074-0188	
<p>The public reporting burden for this collection of information is estimated to average 1 hour per response, including the time for reviewing instructions, searching existing data sources, gathering and maintaining the data needed, and completing and reviewing the collection of information. Send comments regarding this burden estimate or any other aspect of the collection of information, including suggestions for reducing this burden to Department of Defense, Washington Headquarters Services, Directorate for Information Operations and Reports (0704-0188), 1215 Jefferson Davis Highway, Suite 1204, Arlington, VA 22202-4302. Respondents should be aware that notwithstanding any other provision of law, no person shall be subject to a penalty for failing to comply with a collection of information if it does not display a currently valid OMB control number.</p> <p><b>PLEASE DO NOT RETURN YOUR FORM TO THE ABOVE ADDRESS.</b></p>					
1. REPORT DATE (DD-MM-YYYY) 26-03-2002		2. REPORT TYPE Master's Thesis		3. DATES COVERED (From – To) Jun 2001 – Mar 2002	
4. TITLE AND SUBTITLE  GPS-DERIVED PRECIPITABLE WATER COMPARED WITH THE AIR FORCE WEATHER AGENCY'S MM5 MODEL OUTPUT				5a. CONTRACT NUMBER	
				5b. GRANT NUMBER	
				5c. PROGRAM ELEMENT NUMBER	
6. AUTHOR(S)  Vollmer, Patricia A., Captain, USAF				5d. PROJECT NUMBER	
				5e. TASK NUMBER	
				5f. WORK UNIT NUMBER	
7. PERFORMING ORGANIZATION NAMES(S) AND ADDRESS(S) Air Force Institute of Technology Graduate School of Engineering and Management (AFIT/EN) 2950 P Street, Building 640 WPAFB OH 45433-7765				8. PERFORMING ORGANIZATION REPORT NUMBER  AFIT/GM/ENP/02M-11	
9. SPONSORING/MONITORING AGENCY NAME(S) AND ADDRESS(ES) AFWA/DNXT Attn: Bruce Telfeyan 301 Peacekeeper Dr. Offutt AFB, NE  DSN: 271-1690 e-mail: bruce.telfeyan@afwa.af.mil				10. SPONSOR/MONITOR'S ACRONYM(S)	
				11. SPONSOR/MONITOR'S REPORT NUMBER(S)	
12. DISTRIBUTION/AVAILABILITY STATEMENT  APPROVED FOR PUBLIC RELEASE; DISTRIBUTION UNLIMITED.					
13. SUPPLEMENTARY NOTES					
14. ABSTRACT <p>Current moisture initialization sources lack the spatial and temporal resolution required for mesoscale moisture forecast accuracy critical for military operations. The Global Positioning System (GPS) satellite constellation provides an opportunity to extract accurate moisture observations based on the refraction of the GPS signal through the troposphere. GPS-derived precipitable water (PW) from two different research areas was independently compared with the Air Force Weather Agency's (AFWA's) MM5 PW model output. Results were concurrent with similar studies comparing GPS-derived PW with numerical weather models. The mean correlation in CONUS was 92.5%, while in Alaska it was 72.8%. Mean model biases were -1.22 mm in CONUS and 0.69 mm in Alaska, where a negative bias signifies the model having higher PWs. Mean RMSEs were 4.36 mm in CONUS and 2.76 mm in Alaska.</p> <p>The GPS network's superior temporal resolution captured the diurnal variations in PW, while the model consistently failed to take such variations into account as its forecast progressed. This seems it could be the largest source of error between the two data sets. A number of non-meteorological error sources exist that could impact use of GPS-derived PW in operational applications, such as terrain differences between the GPS receiver sites and the model interpolated heights. These error sources need to be further addressed prior to operational assimilation of this data into military weather models.</p>					
15. SUBJECT TERMS Meteorology, Global Positioning System, Numerical Methods and Procedures, Satellites, Atmospheric Moisture Content					
16. SECURITY CLASSIFICATION OF:			17. LIMITATION OF ABSTRACT	18. NUMBER OF PAGES	19a. NAME OF RESPONSIBLE PERSON
a. REPORT	b. ABSTRACT	c. THIS PAGE			Gary R. Huffines, Maj, USAF (AFIT/ENP)
U	U	U	UU	108	19b. TELEPHONE NUMBER (Include area code) (937) 255-3636, x4511; e-mail: gary.huffines@afit.edu